OUKA
Osaka University Knowledge Archive

Title	Studies on the Relationship between the Physical Properties and Internal Structures of Oxygen-Permeable Optically Transparent Materials for Medical Devices
Author(s)	Yokota, Mitsuru
Citation	大阪大学, 2012, 博士論文
Version Type	VoR
URL	https://hdl.handle.net/11094/24730
rights	
Note	

Osaka University Knowledge Archive : OUKA

https://ir.library.osaka-u.ac.jp/

Osaka University

Studies on the Relationship between the Physical Properties and Internal Structures of Oxygen-Permeable Optically Transparent Materials for Medical Devices

MITSURU YOKOTA

2012

To my wife Kikue, and my parents
Haru and Late Inakichi.

Contents

Page

General Introduction 1

References 17

Part I Rigid Gas Permeable Materials

Chapter 1

Relationship between the Physical Properties and Internal Structure of Rigid Gas Permeable Materials

1.1 Relationship among Internal Structure, Gas Permeability and Transparency in Copolymer Networks Composed of Methacrylates and Siloxane Macromers

1.1.1 Introduction 23

1.1.2 Experimental Section 24

1.1.3 Results and Discussion 26

1.1.4 Conclusions 41

1.1.5 References 42

1.2 The Systematic Study of the Microstructure of Crosslinked Copolymers from Siloxane Macromonomers and Methacrylates with Various Composition and Components

1.2.1 Introduction 45

1.2.2 Experimental Section 46

1.2.3 Results and Discussion 47

1.2.4 Conclusions 55

1.2.5 References 55

1.3 Transmission Electron Microscopic Observations of the Multilevel Microstructure of Crosslinked Copolymers with Methacrylates and Siloxane Macromers by a Radically Polymerizable Tuning Approach

1.3.1 Introduction 57

1.3.2 Experimental 58

1.3.3 Results and Discussion 59
1.3.4 Conclusions 68
1.3.5 References 69

Chapter 2
The Effect of Polymer Structure on Durability of Rigid Gas Permeable Materials

2.1 Introduction 71
2.2 Experimental Section 72
2.3 Results 73
2.4 Discussion 74
2.5 Conclusions 79
2.6 References 79

Part II Silicone-Containing Hydrogel Materials

Chapter 3
Creation of Novel Silicone-Containing Monomer and Novel Silicone-Containing Hydrogel

3.1 Synthesis of a Novel Silicone Monomer Bearing Amide Groups to Improve Compatibility with Hydrophilic Vinyl Monomer
3.1.1 Introduction 81
3.1.2 Experimental Section 82
3.1.3 Results and Discussion 85
3.1.4 Conclusions 87
3.1.5 References 87

3.2 The Role of Amide Groups in Vinyl Monomers Containing Siloxane Groups for Highly Oxygen Permeable Hydrogels
3.2.1 Introduction 89
3.2.2 Experimental Section 90

3.2.3 Results and Discussion 94
3.2.4 Conclusions 105
3.2.5 References 106

Chapter 4
Novel Method for Surface Modification of Silicone-Containing Hydrogel Using Addition Reaction

4.1 Introduction 109
4.2 Experimental Section 110
4.3 Results and Discussion 113
4.4 Conclusions 118
4.5 References 119

Concluding Remarks 121

List of Publication 127

Acknowledgements 129

General Introduction

Contact lens has been attracting much attention as one of the means for vision correction after its invention by J. Mullen and T. Obrig in 1936 with poly(methyl methacrylate) (PMMA).[1)] The invention of hydrogel soft contact lens from 2-hydroxyethyl methacrylate (HEMA) by O. Wichterle[2)] led to more popular use because of its wearing comfort. Compared with eyeglasses, contact lens has many characteristics as shown in Table 1.

Table 1. Comparison of the characteristics of contact lens and eye glass

Characteristics	Contact lens	Eye glass
Visual field	wide	narrow
Vision correction		
Irregular astigmatism	compatible	incompatible
Optical aberration	small	large
Cosmetic appearance	compatible	incompatible
Use for sports	compatible	less compatible
Handling	complicated (conventional) easy (disposable)	easy
Wearing comfort	foreign body sensation (hard) good (soft)	—

However, in the course of the popularization of contact lenses, many issues have been found and various researches revealed the importance of oxygen permeability of the contact lens material on a physiological health of the cornea. The main reason was that the cornea had no blood vessel to keep transparency and demanded oxygen was supplied from circumstances such as tear film, eye lid, and inner part of anterior eye such as aqueous humor. The situation is shown in Figure 1.[3)] I. Fatt and co-workers calculated the partial pressure of oxygen and carbon dioxide in the cornea and reported that when eyes were closed, the carbon dioxide partial pressure was about 55 mmHg overall cornea thickness, and higher than oxygen partial pressure which showed 44–55

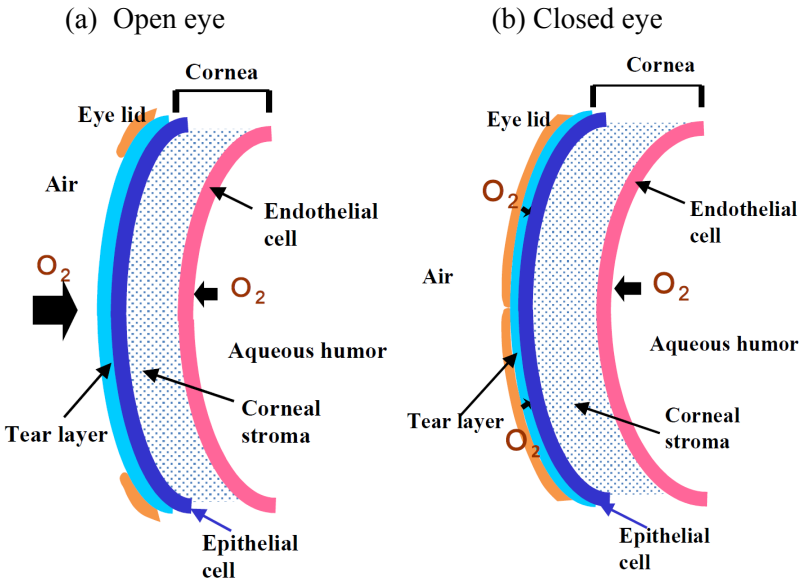

Figure 1. Oxygen supply path to cornea. (a) Open eye, (b) Closed eye.[3)]

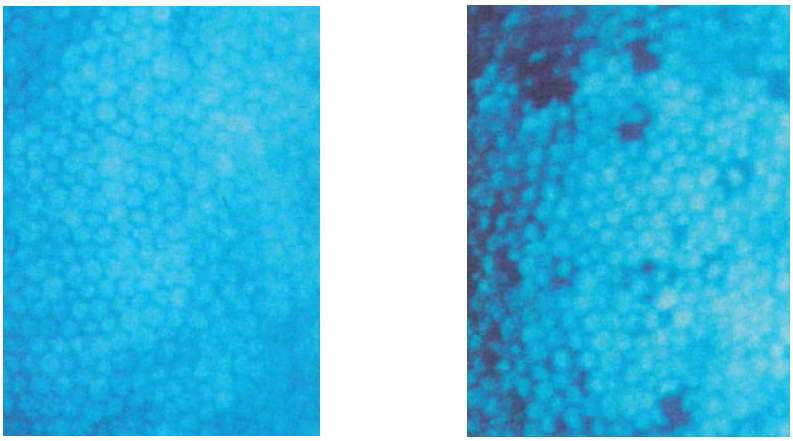

(a) Prior to lens insertion (b) Peak response to stimulus

Figure 2. A typical endothelial bleb response when wore a thick HEMA contact lens at prior to lens insertion (a), and peak response to stimulus (b).[10)]

mmHg.[4)] Inspired by this study, actual oxygen partial pressure under contact lenses has been reported and it was confirmed that oxygen diffusing through the lens material primarily affected the oxygen concentration at the tear layer, when a contact lens was worn.[5–7)] At the same time, various researches revealed the importance of oxygen permeability of contact lens material for the maintenance of corneal healthy functions.

One of the effect of insufficient oxygen permeability is a transient endothelial change (bleb response of corneal endothelial cells),[8–10] and an example is shown in Figure 2.[10] The reason of the response was supposed to be the lactic acid produced by anoxia metabolic cycle and pH change by the formation of carbonic acid (HCO_3^-), according to accumulation of carbon dioxide under contact lens.

Another issue is the corneal swelling from contact lens wear. Many researches were conducted intensively with this issue to find out the necessary and sufficient condition for the safe daily wear and extended wear.[11–13] The examples of overnight corneal swelling with and without contact lens wear are shown in Figure 3.[14] Even in the case of no lens, about 4% swelling was observed because of reduced oxygen partial pressure in closed eye. B. A. Holden and co-workers[14] investigated the critical lens oxygen transmissibilities required to avoid edema, and they found that lenses having an oxygen transmissibility of at least 24.1 ± 2.7×10^{-9} (cm×mlO_2)/(sec×ml×mmHg) did not induce corneal edema at daily wear. They also discovered that the critical contact lens oxygen transmissibility needed to limit overnight corneal edema to 4% (the level experienced without a contact lens in place) was 87.0 ± 3.3×10^{-9} (cm×mlO_2)/

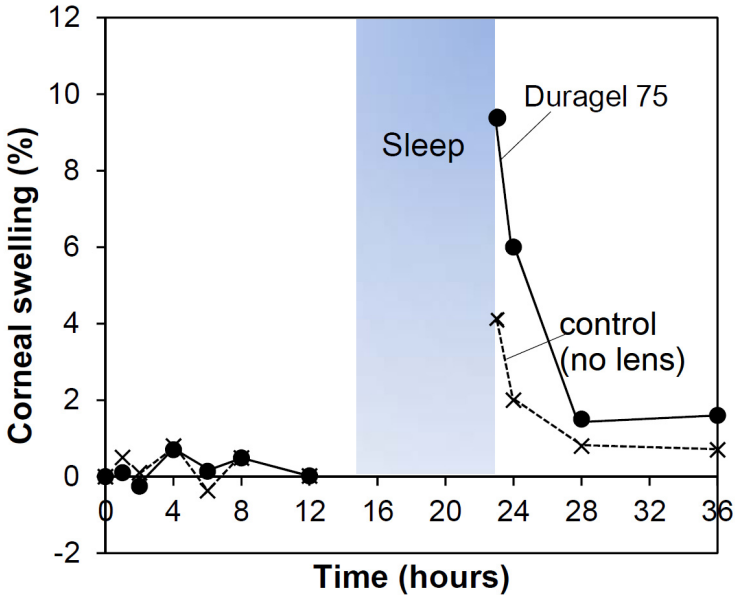

Figure 3. Corneal swelling with contact lens wear.[14]

(sec×ml×mmHg), and these are now regarded as the standard value for safe contact lens wear.

In addition, many researches were carried out on the polymegathism and polypleomorphism in the corneal endothelium.[15–19] An example of observed endothelial cell is shown in Figure 4.[16] K. H. Carlson and co-workers reported that long-term contact lens wear induced morphologic changes in the corneal endothelium, however, these changes did not result in functional abnormalities.[17] Furthermore, it was also reported that lens-induced effects on corneal physiology can be minimized by fitting lenses that possess greater oxygen transmissibility, are more mobile, and more frequently removed.[15]

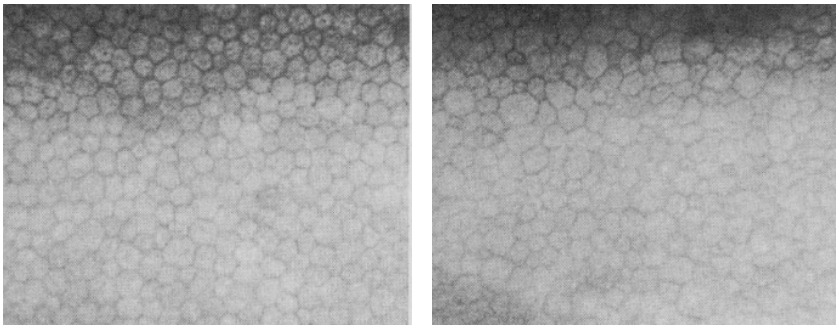

(a) Patient with intra capsular cataract extraction and no contact lens wear.

(b) Patient with intra capsular cataract extraction and contact lens extended wear.

Figure 4. Specular microscope photographs of endothelial cell.[16]

Thus, progress of the research, which revealed the great role of oxygen permeability in the contact lens material, inspired in the gas permeable material development. It is well known that silicone material possesses extremely high gas permeability. As gas permeability coefficient is expressed as following formula, the solubility coefficient and the diffusivity coefficient of various polymers are shown in Table 2.[20]

P (permeability coefficient) = S (solubility coefficient) × D (diffusivity coefficient)

Table 2. Solubility coefficient and diffusivity coefficient of various polymers[20)]

Material	Solubility coefficient ($25^{\circ}C, \times 10^{-5} cm^3(STP)/(cm^3 \cdot Pa)$)			Diffusivity coefficient ($25^{\circ}C, \times 10^{-6} cm^2/sec$)		
	N_2	O_2	CO_2	N_2	O_2	CO_2
Elastomer						
Silicone rubber	0.081	0.126	0.43	15	25	15
Butyl rubber	0.055	0.122	0.68	0.05	0.08	0.06
Natural rubber	0.055	0.112	0.90	1.1	1.6	1.1
Glassy polymer						
Polystyrene	—	0.055	0.65	0.06	0.11	0.06
Poly(vinyl chloride)	0.024	0.029	0.4	0.004	0.012	0.0025
Poly(vinyl acetate)	0.02	0.04	—	0.03	0.05	—
Semicrystalline						
Polyethylene H.D.	0.025	0.047	0.35	0.10	0.17	0.12
Poly(ethylene)	0.039	0.069	1.3	0.0014	0.0036	0.0015

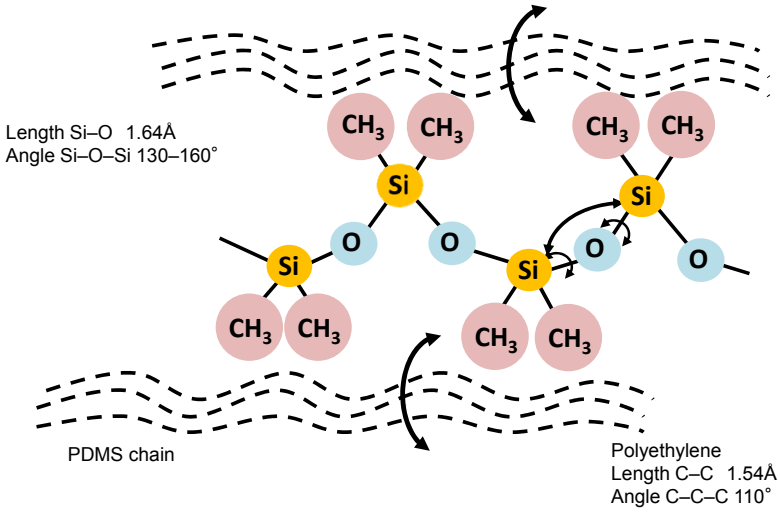

Figure 5. Mechanism of large diffusivity coefficient of silicone.[21)]

It is clear that silicone has 10–100 times larger diffusivity constant than other materials as shown in Table 2. The reason why silicone has large diffusivity coefficient is shown in Figure 5.[21)] Compared with C–C bond length (1.54 Å) and angle made by two C–C bonds (110º) of polyethylene, poly(dimethylsiloxane) (PDMS) has longer Si–O bond length (1.64 Å) and wider angle formed by two Si–O bonds (130–160º). Therefore, silicone has larger volume in which these atoms moves freely and provides the space for

gas molecule diffusion. Moreover, it is noteworthy that carbon dioxide has 3 to 10-folds higher solubility coefficient than oxygen in silicone, although its diffusivity coefficient value is about 60% of oxygen value, thus carbon dioxide permeability is 2 to 6-folds larger than that of oxygen. This gas molecules dependency of gas permeability is very suitable for our purpose and application field, as it clearly shows that higher oxygen permeability coefficient ($P(O_2)$) equivalently means acceptable carbon dioxide permeability coefficient.

Thus introducing silicone group had become the main stream of the material development having high gas permeability. As already stated, there are two main types of materials from the history of contact lens development. One is rigid material developed from PMMA and another one is hydrogel material. Thus, I tried to start my research with rigid gas permeable (RGP) material. The first trial to use the acrylic monomer bearing silicone-containing group had been conducted by N. Gaylord.[22] He newly designed and synthesized silicone-containing acrylic monomer and developed the composition as shown in Figure 6. The typical example of monomer is tris(trimethyl-siloxy)silylpropyl methacrylate (TRIS). This invention triggered a development of

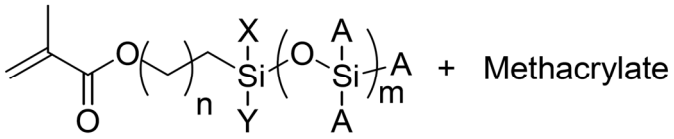

Figure 6. Example of composition and monomer structure developed by N. Gaylord.[22]

silicone acrylate type material and furthermore the development of the silicone acrylate-fluorine group containing acrylate materials. The grouping of these RGP materials by FDA is shown in Table 3.[23] Example of silicone acrylate composition in Group II is, other than the composition by Gaylord, a copolymer of a siloxanyl alkyl ester monomer, an itaconate ester and an ester of acrylic or methacrylic acid,[24] as well

as a copolymer composition of hydroxysilane esters of acrylic or methacrylic acid and alkanol ester of acrylic or methacrylic acid.[25] Examples of fluoro silicone acrylate which bear fluorine containing group are, a copolymer from an organosilane or

Table 3. Lens grouping for hydrophobic plastic contact lenses by FDA[23]

Group	Material	Example (USAN*)
I	PMMA	
	CAB**	cabufocon A, porofocon A
	t-Butylstyrene	arfocon A
II	Silicone	elastofilcon A, demefocon A
	Silicone Acrylate	pasifocon, itafocon, nefocon, telefocon, silafocon
	t-Butylstyrene/Silicone Acrylate	pentasilcon P, synergicon
III	Fluoro Silicone Acrylate	itafluorofocon, itabisfluorofocon, paflufocon, flusilfocon, melafocon, tolofocon
IV	Poly(perfluoroether)	flurofocon

I for materials which do not contain either silicone or fluorine.
II for materials which contain silicone but not fluorine.
III for materials which contain both silicon and fluorine.
IV for materials which contain fluorine but not silicon.
*United States Adopted Name.
**Celluose acetate butyrate.

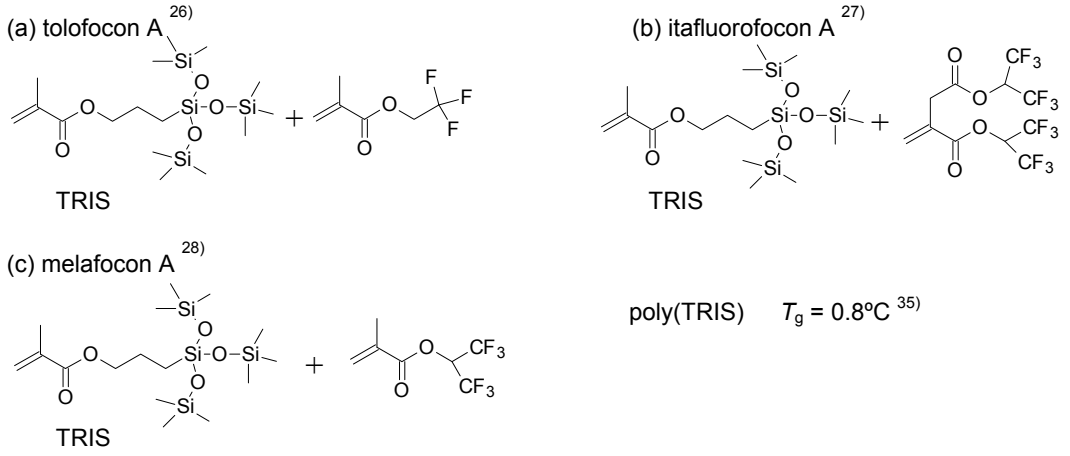

Figure 7. Examples of fluoro silicone acrylate in Group III (main constituents).

organosiloxane methacrylate and fluoroalkylacrylate or methacrylate,[26] a siloxane copolymer incorporated with a fluorine containing mono or diester of itaconic acid,[27] as well as a composition comprising an acrylic silicate of the type having fluorinated siloxanyl group.[28] A part of these fluoro silicone acrylate is shown in Figure 7.

In the course of the development of RGP materials with high $P(O_2)$ which utilize the silicone acrylate monomer, the issue of fragility had arisen compared with PMMA.[29–33] For example, L. Jones and co-workers reported that higher the $P(O_2)$ (or *Dk*), the shorter the lens life calculated from the number of lenses replaced because of loss, breakage, deposition, or poor wettability.[30] Furthermore, I. Tranoudis and co-workers focused on the importance of determining the extent of scratching on the surface of RGP contact lens, and found that this property was related to material oxygen permeability and refractive index of the material.[31] These may be due to the weak intermolecular force between Si–Me groups of silicone which gives the large diffusivity coefficient and resultant large gas permeability coefficient.

To overcome the fragility issue, based on the original Gaylord approach and focusing on the low glass transition temperature (T_g) of poly(TRIS) as shown in Figure 7,[34] the attempts to develop novel silicone monomer possessing high T_g have been conducted. One is a series of the study on siloxanylstyrene compounds by Y. Kawakami and co-workers as shown in Figure 8(a).[35–38] T. Otsu and coworkers developed siloxanyl fumarate[39] with similar approach as shown in Figure 8(b). Siloxanyl maleimide was developed as shown in Figure 8(c).[40] However, as these compounds have also some issues such as copolymerization activity of styrene derivatives with acrylic monomer, poor polymerization activity of siloxanyl fumarate, and some difficulties in synthesis, only one material have been launched having USAN of tisilfocon A which is composed of vinylbenzylmethacrylate, tris(trimethylsiloxy)silyl-styrene, hexafluoroisopropyl methacrylate, ethyleneglycol dimethacrylate, *N*-vinyl-pyrrolidone (NVP) and methacrylic acid to cover the difference of copolymerization

activity.[41] However, it has still relatively low ball impact strength of 32 cm.

(a) Siloxanyl styrene [35–38]

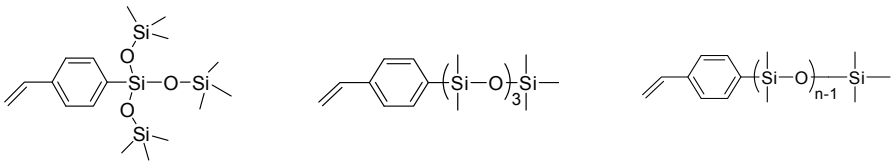

St 4 T_g = 114°C S4 Sn

(b) Siloxanyl fumarate [39]

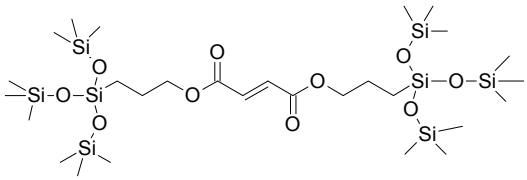

(c) Siloxanyl maleimide [40]

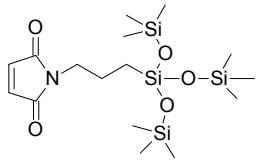

Figure 8. Novel silicone-containing monomer with rigid backbone.

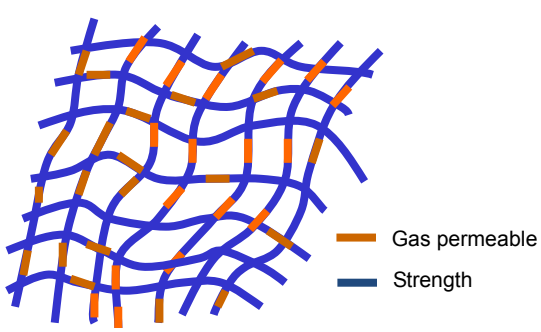

(a) Homogeneous structure. Strength is inconsistent with very high gas permeability.

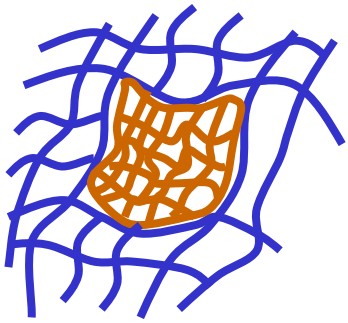

(b) Microheterophase structure. Strength is consistent with very high gas permeability.

Figure 9. Design concept of new rigid material with microheterophase structure.

Herein, to overcome aforementioned incompatibility between high oxygen permeability and breakage strength, I designed a nm-level microheterophase structure to expect the internal structure which enables the consistency among strength, gas permeability and transparency as shown in Figure 9(b). With regard to the method to prepare microheterophase with silicone constituent, two types of approach had been conducted. One of these approaches is the introduction of PDMS chains by

condensation reactions with rigid segments, such as polyamide and polyimide groups, to create multi-block copolymers.[42,43)]

However, the restricted variety of PDMS molecular weight (M_n) and another constituent tend to make difficult to get sufficient information in this approach, which are necessary for detailed design to get expected properties. Another approach is the polymerization induced phase separation (PIPS) method that consists of radical copolymerization of methacrylates with PDMS macromers that contain radically polymerizable groups at the end of the PDMS chain and crosslinkers that have multiple radically polymerizable groups. Eventhough the crosslinked copolymer from PDMS macromers and hydrophobic vinyl monomers has been reported,[44,45)] there was no systematic study, which enables collecting the information for the material design.

In this doctoral thesis, a series of siloxane containing polymers were synthesized with several approaches, such as copolymer, monomer design, and surface modification, in order to investigate the relationship between structural conditions and physical functions systematically. Especially, oxygen permeability and mechanical strength were focused in the view point of contact lens application.

Thus, using the PDMS macromer, various types of methacrylates, and crosslinker which gave the microheterophase structure, the measurements on the crosslinked copolymer T_g, light transmittance, $P(O_2)$, Vickers hardness, solid-state ^{13}C cross polarization magic angle spinning (CP-MAS) NMR and transmission electron microscopy (TEM) were conducted. Furthermore, the relationship between microstructure and physical properties was evaluated and speculated, to determine the guidelines for the design and preparation of my material, and to confirm the material design concept.

Another theme of this thesis is how to achieve highly oxygen permeable hydrogel. While the progress has been made in development of RGP materials, the researches on the hydrogel with high oxygen permeability had been extensively

conducted. The approach to high gas permeability is same as in the case of rigid material, the use of silicone material. The big issue is the hydrophobicity and non-polar properties of silicone. As shown in Figure 10,[46] silicone has low solubility parameter and resultant low compatibility with solvents and materials having large solubility parameter such as water or alcohols. Thus, due to this difference of solubility parameter, incorporation of silicone constituent tends to lead to phase separation between water or

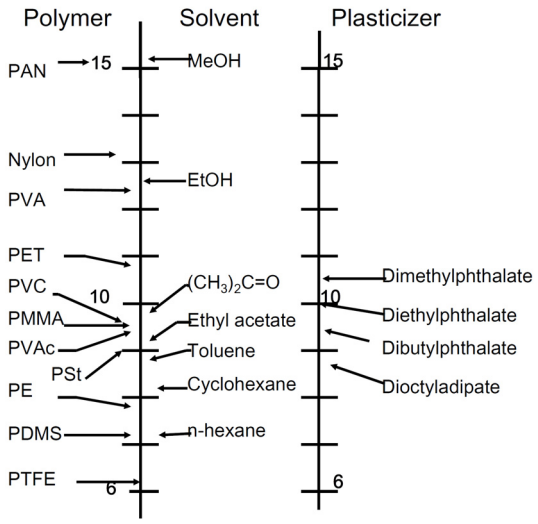

Figure 10. Solubility parameter of various materials and solvents.[46]

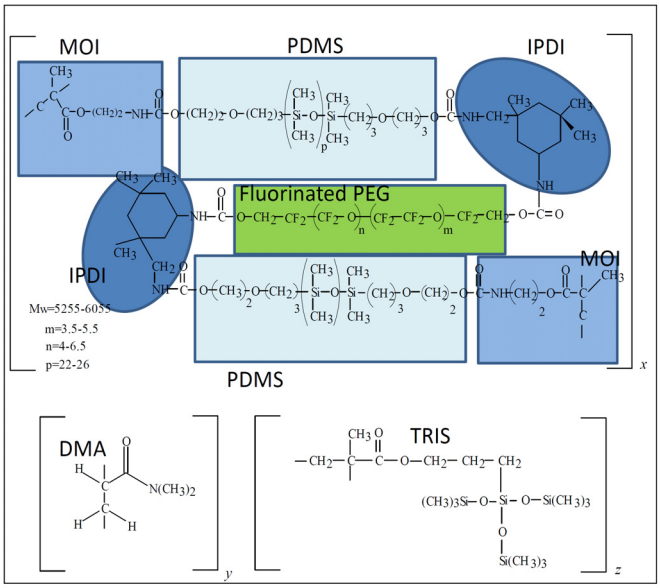

Figure 11. An example of composition of existing silicone hydrogel (Lotrafilcon).[47]

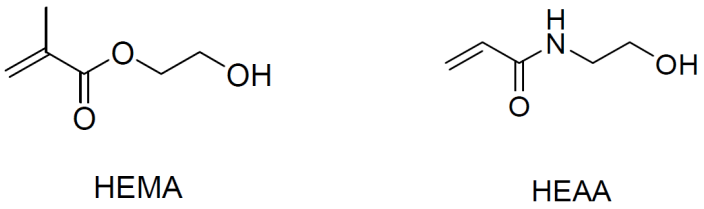

Figure 12. Typical hydroxy group bearing hydrophilic monomer.

hydrophilic phase and silicone phase, and resultant opaqueness of hydrogel. This limitation of the type of hydrophilic constituents to *N*, *N*-dimethylacrylamide (DMA) or NVP for transparent material has been causing the reduced freedom of selection of silicone hydrogel composition and also the reduced control of physical properties. To overcome these issues, the design and synthesis of a silicone-containing acrylic monomer was conducted which had good compatibility with hydroxy group bearing hydrophilic monomer, such as HEMA and 2-hydroxyethyl acrylamide (HEAA) shown in Figure 12. For this purpose, introducing highly hydrophilic group into silicone-containing monomer was planned. As similar approach, T. Itoh and co-workers investigated the two types of amphiphilic monomer, such as dissymmetric fumarate monomers bearing short polyethyleneglycol (PEG) chain (n=1–3) and siloxanyl group,[48] as well as itaconate monomer, which has also ethyleneglycol group (n=1) and siloxanyl group[49] as shown in Figure 13. This introduction of ethyleneglycol chain is

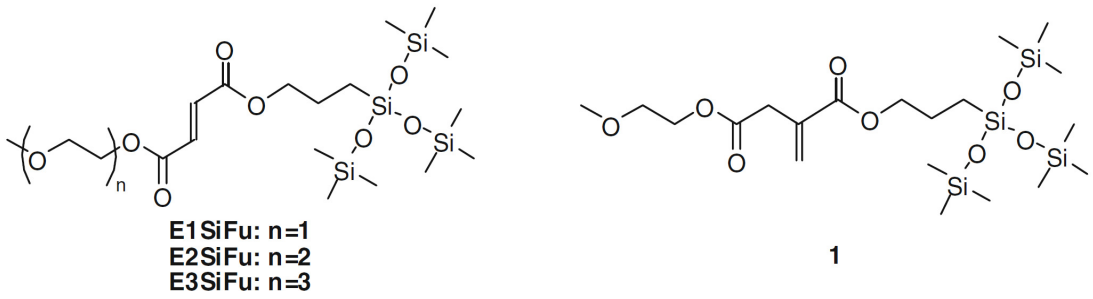

Figure 13. Silicone bearing fumarate monomer[48] and itaconate monomer.[49]

same approach as Lotrafilcon in Figure 11, and they improved transparency of silicone hydrogel with fumarate monomer and NVP or (NVP + HEMA), while only slight improvement with itaconate monomer and NVP or (NVP + HEMA) compared with that of TRIS. However, no information was reported on the only hydroxy group bearing hydrophilic monomer used silicone-containing hydrogel.

Thus, to overcome this issue, considering the high polymerization reactivity, introducing a highly hydrophilic dimethylcarbamoyl group into silicone group containing monomer was performed for the improvement of the compatibility between silicone-containing monomer and hydroxy group containing hydrophilic monomer such as HEMA and HEAA.

As another issue of silicone hydrogel, there is a surface wettability problem. When considering the wettability, surface tension has a great role. It is known that surface tension has strong correlation with solubility parameter as shown in Figure 14.[50] Furthermore, the balance between the surface tension of solid and that of liquid determines that the surface is wettable by the solvent or not as shown in Figure 15. The condition that the surface tension of solid is greater than that of liquid is necessary for wetting.[51] However the low surface tension of silicone compounds and also fluorine containing material causes a poor wettability to water which has large surface tension.

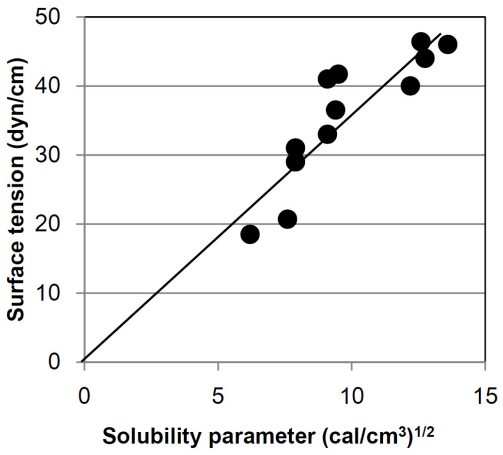

Figure 14. Solubility parameter and surface tension.[50]

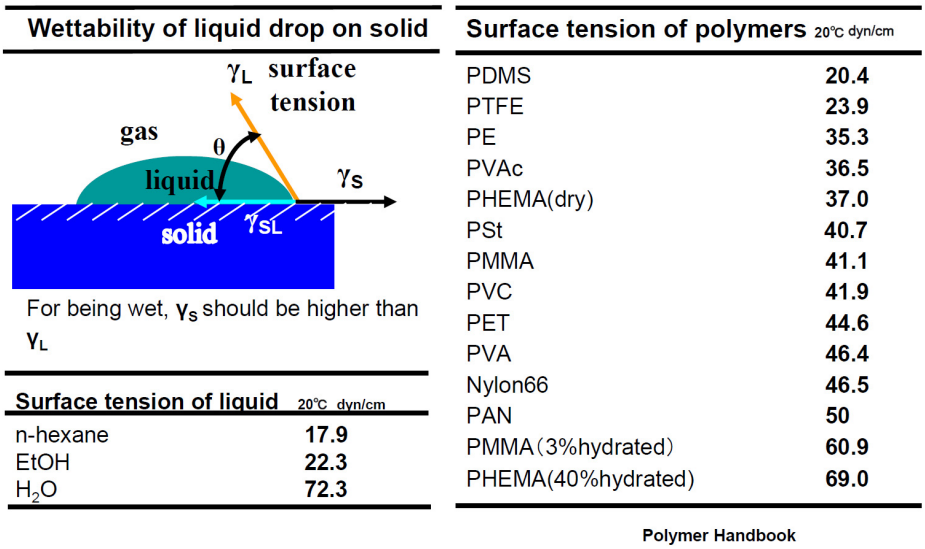

Figure 15. Wettability and surface tension.[51)]

In order to overcome this issue, various researches had been conducted,[52)] for example, oxidative plasma discharge treatment,[53)] low temperature inert gas plasma processing,[54)] plasma polymerization,[55,56] plasma induced polymerization or graft polymerization,[57)] combination of plasma polymerization and graft reaction[58)] and so on.

However, there are still some points to be improved such as durability of wettability.[59)] It is a common approach to combine the introduction of reactive group by plasma polymerization and subsequent reaction between PEG chain and the reactive

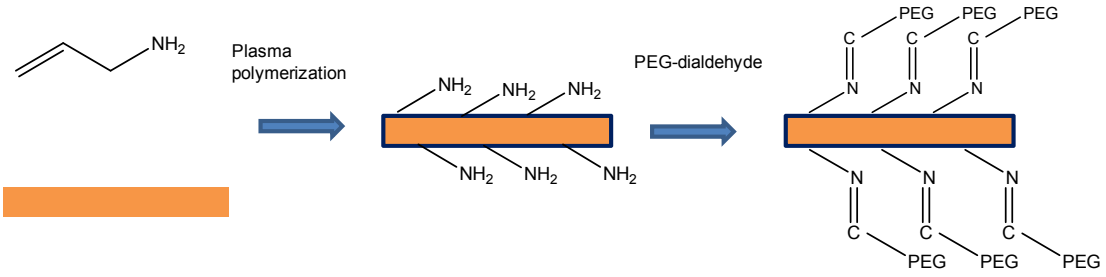

Figure 16. Plasma polymerization of allylamine and subsequent reaction between PEG chain and amino group.[58)]

group.[58] However, as the reactive group exists only on the surface of plasma polymerized film as shown in Figure 16, the density of PEG chain may be insufficient, thus it may lead to unsatisfactory performance. In this thesis, I tried to use the hydrosilylation reaction to make a Si–C linkage with high durability between siloxane group and PEG monoallylether.

Thus, I conducted the researches on the RGP material and silicone-containing hydrogel having high $P(O_2)$ and good biocompatibility in anterior eyes. As I took different approachs to these materials, I made this thesis divided into Part I (RGP material) and Part II (silicone-containing hydrogel material).

In the first section of Chapter 1, I designed a microheterophase structure materials from PDMS macromer and acrylic monomers for novel RGP material possessing both very high $P(O_2)$ and durability such as good breakage strength. In order to clarify the effect of the type of acrylic monomer and the M_n of PDMS on the relationship among the internal structure, $P(O_2)$ and transparency, crosslinked copolymers were prepared with two different acrylic monomers: methyl methacrylate (MMA) and trifluoroethyl methacrylate (TFEMA). PDMS macromers with four types of M_n were used. In the seacrh of the relationship between the composition and results, the calculations on the relationship among the $P(O_2)$, PDMS volume fraction, and morphology model were performed, and it was found that some properties such as solubility parameters should play important roles.

In the second section of Chapter 1, ^{13}C solid-state CP-MAS NMR measurements of the aforementioned copolymers in the first section were conducted, because it provides fine grain information with respect to the molecular mobility or relaxation time, which indicates the internal structure of heterogeneous polymer composites.[60–62] The molecular-level relationship between the physical properties and the composition of copolymers was investigated. Using the data on T_1^H and $T_{1\rho}^H$, the relationship among PDMS M_n value, molecular mobility of $–OSi(CH_3)_2–$, and gas

permeability, as well as the diameter of homogeneously dispersed structure were discussed. Differences of the morphology between MMA copolymers and TFEMA copolymers, suggested from the T_1^H, $T_{1\rho}^H$ and $T_{1\rho}^C$ measured values, were also discussed. The relationship between incorporation of CF_3-group and $T_{1\rho}^C$ value implied that the amplified molecular motion of aforementioned groups is related to the mechanism of increased oxygen permeability in copolymers produced of fluorine-bearing monomers and the PDMS macromonomer.

In the third section of Chapter 1, the morphologies of crosslinked copolymers in the first section were investigated by TEM. The influence of varied PDMS contents, PDMS macromer M_n, and types of methacrylate on morphology, the difference in the observed results between different magnification (a "fundamental domain" due to the M_n of the PDMS macromer, and an aggregated domain. The former was constant under all conditions, but the latter was affected by the co-monomer and its ratio), and factors which determine the morphology and domain size were discussed.

In Chapter 2, using my RGP material design concept, novel RGP contact lens was developed and the verification of the design concept was carried out. For this purpose, new lens strength *in vitro* evaluation test methods, such as ball impact strength and flexural breakage strength, were developed. In addition to the breakage strength tests using these methods, the evaluation of physical properties of various RGP contact lens materials was conducted, such as internal structures from TEM observation. Furthermore, the reported breakage and deposit found in clinical studies were also included in this verification.

In Part II, novel silicone-containing monomer design concept and the demonstration of the validity of the concept for silicone hydrogel, as well as the novel surface modification method of silicone hydrogel were discussed.

At first, in the first section of Chapter 3, novel monomer was designed, which beared one organosiloxanyl group and two amide groups in order to improve its

compatibility with hydrophilic monomer, especially hydroxy group bearing monomer. *N*-2-(*N*', *N*'-dimethylcarbamoyl)ethyl-*N*-[3-tris(trimethylsiloxy)silylpropyl]acrylamide (SiDAAA) was synthesized, and the miscibility with hydrophilic monomer as well as the appearance of silicone hydrogel was evaluated to validate the monomer design concept.

In the second section of Chapter 3, in addition to aforementioned SiDAAA, *N*-2-(*N*', *N*'-dimethylcarbamoyl)ethyl-*N*-{3-[methylbis(trimethylsiloxy)silyl]propyl} acrylamide (SiDAAA2) was synthesized to confirm the influence of the balance between siloxanyl group and amide group on various properties such as radical polymerizability as well as T_g of homopolymer. Furthermore, the silicone hydrogels were prepared using these novel silicone monomers, and various properties such as water content, $P(O_2)$, light transmittance and lysozyme uptake were measured to validate the design concept which provides silicone hydrogels with high freedom to select the composition, high intermolecular force and biocompatibility in anterior eye.

In Chapter 4, a novel surface modification method of shaped articles from silicone-containing hydrogel was designed using hydrosilylation reaction between silicone component and PEG chain in order to improve the surface wettability. For the introduction of –SiH group to hydrogel, in addition to copolymerization of –SiH-containing methacrylate, argon gas plasma treatment was found to be effective. Hydrosilylation reaction between shaped article and PEG easily proceeded in organic solvent, and the resultant hydrogel showed reduced contact angle after the hydration in water. The attenuated total reflection (ATR)-FTIR measurement suggested the validity of my process design concept.

References

1) Mullen, J. and Obrig, T. US Patent 2,129,305, September 6, **1938**.

2) Wichterle, O. and Lim, D. US Patent 3,220,960, November 30, **1965**.

Wichterle, O. US Patent 3,408,429, October 29, **1968**.

Wichterle, O. US Patent 3,496,251, February 17, **1970**.

3) "Practice in Ophthalmology, 27, Contact Lens Examination", Tsubota, K., Tano, Y., Negi, A., Ohga, T., Eds.; Bunkodo; Tokyo ; **2009**. pp37–40.

4) Fatt, I. and Bieber, M.T. *Exptl. Eye Res.* **1968**, *7*, 103.

5) Fatt, I. and St. Helen, R. *Am. J. Optom. Arch. Am. Acad. Optom.* **1971**, *48*, 545.

6) Fatt, I and Lin, D. *Am. J. Optom. Physiol. Opt.* **1976**, *53*, 104.

7) Polse, K. A. *Invest. Ophthalmol. Vis. Sci.* **1979**, *18*. 409.

8) Zantos, S.G. and Holden, B.A. *Am. J. Optom. Physiol. Opt*. **1977**, *54*, 856.

9) Vannas, A., Jukka, K., Jukka, S., Reijo, A. and Esko, J. *Acta Ophthalmol.* **1981**, *59*, 552.

10) Holden, B.A., Williams, L. and Zantos, S.G. *Invest. Ophthalmol. Vis. Sci.* **1985**, *26*, 1354.

11) Polse, K.A. and Mandell, R.B. *Arch. Ophthalmol.* **1970**, *84*, 505.

12) Mandell, R.B. and Farrel, R. *Invest. Ophthalmol. Vis. Sci.* **1984**, *25*, 476.

13) Holden, B.A., Sweeney, D.F. and Sanderson, G. *Invest. Ophthalmol. Vis. Sci.* **1983**, *24*, 218.

14) Holden, B.A. and Mertz, G.W. *Invest. Ophthalmol. Vis. Sci.* **1984**, *25*, 1161.

15) Holden, B.A., Sweeney, D.F., Vannas, A., Nilsson, K.T. and Efron, N. *Invest. Ophthalmol. Vis. Sci*. **1985**, *26*, 1489.

16) Matsuda, M., Inaba, M., Suda, T. and MacRae, S.M. *Arch. Ophthalmol.* **1988**, *106*, 70.

17) Carlson, K.H., Bourne, W.M. and Brubaker, R.F. *Invest. Ophthalmol. Vis. Sci.* **1988**, *29*, 185.

18) Carlson, K.H. and Bourne, W.M. *Arch. Ophthalmol*. **1988**, *106*, 1677.

19) Speaker, M.G., Cohen, E.J., Edelhauser, H.F., Clemens, C.S., Arentsen, J.J., Laibson, P.R. and Raskin, E.M. *Arch. Ophthalmol*. **1991**, *109*, 1703.

20) Van Krevelen, D.W. “Properties of Polymers”. 3rd Ed., Elsevier: Amsterdam, **1990**; p539, pp544–545.

21) “Silicone Materials Handbook” edited by Toray Dow Corning Silicone Inc., Tokyo.

22) Gaylord, N.G. US Patent 3,808,178, April 30, **1974**.

23) “Premarket Notification (510(k)) Guidance Document for Daily Wear Contact Lenses” prepared by Contact Lens Branch, Division of Ophthalmic Devices, Office of Device Evaluation, Center for Devices and Radiological Health, FDA (May, **1994**).

24) Ellis E.J. and Salamone, J.C. US Patent 4,152,508, May 1, **1979**.

25) Ratkowski D.J. and Lue, P-C. US Patent 4,419,505, December 6, **1983**.

26) Ichinohe, S., Takahashi, K. and Tanaka, Y. U.S. Patent 4,433,125, February 21, **1984**.

27) Ellis, E.J. and Ellis, J.Y. US Patent 4,686,267, August 11, **1987**.

28) Chapman, D.R. US Patent 4,709,066, November 24, **1987**.

29) Woods, C.A. and Efron, N. *CLAO J*. **1996**, *22*, 172.

30) Jones, L., Woods, C.A. and Efron, N. *CLAO J*. **1996**, *22*, 258.

31) Tranoudis, I. and Efron, N. *Ophthal. Physiol. Optics*. **1996**, *16*, 303.

32) Ichikawa, T., Itoh, N., Ohya, S., Momose, T., Magatani, H., Fujiki, K. and Kanai, A. *J. Jpn. Contact Lens Soc.* **1995**, *37*, 131.

33) Kanai, A. *J. Jpn. Contact Lens Soc.* **1997**, *39*, 271.

34) Yokota, M., Ajiro, H. and Akashi, M. *Bull. Chem. Soc. Jpn.* **2012***, 85,* 584.

35) Kawakami, Y., Karasawa, H., Aoki, T., Yamamura, Y., Hisada, H. and Yamashita, Y. *Polym. J.* **1985**, *17*, 1159.

36) Kawakami, Y., Karasawa, H., Kamiya, H., Aoki, T. and Yamashita, Y. *Polym. J.* **1986**, *18*, 237.

37) Kawakami, Y., Kamiya, H., Toda, H. and Yamashita, Y. *J. Polym. Sci. Part A: Polym. Chem.* **1987**, *25*, 3191.

38) Kawakami, Y. and Sugisaka, T. *J. Membr. Sci.* **1990**, *50*, 189.

39) Otsu, T. and Yoshioka, Y. *Makromol. Chem.* **1992**, *193*, 2283.

40) Kawano, T. and Yokota, M. US Patent 5,393,803, February 28, **1995**.

41) Takahashi, K., Tanaka, Y., Isobe, K. and S. Ichinohe. US Patent 4,594,401.

42) Matsumoto, T., Koinuma, Y., Waki, K., Kishida, A., Furuzono, T., Maruyama, I. and Akashi, M. *J. Appl. Polym. Sci*. **1996**, *59*, 1067.

43) Ha, S.Y., Park, H.B. and Lee, Y.M. *Macromolecules* **1999**, *32*, 2394.

44) Yu, X., Nagarajan, M.R., Li, C., Speckhard, T.A. and Cooper, S.L. *J. Appl. Polym. Sci.* **1985**, *30*, 2115.

45) Mazurek, M., Kinning, D.J. and Kinoshita, T. *J. Appl. Polym. Sci.* **2001**, *80*, 159.

46) Plastics Processing Technology Handbook Editorial Committee Ed. "Plastics Processing Technology Handbook" **1969**, THE NIKKAN KOGYO SHIMBUN, LTD., Tokyo.

47) Nicolson, P.C. and Vogt, J. *Biomaterials* **2001**, *22*, 3273.

48) Ohnishi, M., Uno, T., Kubo, M. and Itoh, T. *J. Polym. Sci. Part A: Polym .Chem*. **2009**, *47*, 420.

49) Ohnishi, M., Taguchi, N., Gotoh, J., Uno, T., Kubo, K. and Itoh, T. *Polym. Bull*. **2009**, *62*, 761.

50) Okitsu, T. *Technology on Adhesion & Sealing (Settyaku),* **1996,** *40*, 294.

51) Pauly S. In "Polymer Handbook"; Brandrup, J.; Immergut, E.H.; Grulke, E.A.; Eds., 4th ed. Wiley: New York: **1999**; pVI/558.

52) Lee, J.H., Kopecek, J. and Andrade, J.D. *J. Biomed. Mater. Res.* **1989**, *23*, 351.

53) Newton, J.M., Watts, J.F. and Edgell, M.J. *Surf. Interface Anal*. **1987**, *10*, 416.

54) Tin, S., Weng, Y., Ren, L., Zhao, L., Kuang, T., Chen, H. and Qu, J. *Appl. Surf. Sci.* **2008**, *255*, 483.

55) Ho, C.P. and Yasuda, H. *Polym. Mater. Sci. Eng.* **1987**, *56*, 705.

56) Yasuda, H. and Matsuzawa, T. *Plasma Process Polymer* **2005**, *2*, 507.

57) Yao, K., Huang, X-D., Huang, X-J. and Xu, Z-K. *J. Biomed. Mater. Res. Part A* **2006**, *78A*, 684.

58) Kingshott, P., Thissen, H. and Griesser, H. *Biomaterials* **2002**, *23*, 2043.

59) Thissen, H. Gengenbach, T., du Toit, R., Sweeney, D.F., Kingshott, P., Griesser, H.J. and Meagher, L. *Biomaterials* **2010**, *31*, 5510.

60) Havens, J.R. and VanderHart, D.L. *Macromolecules* **1985**, *18*, 1663.

61) Clauss, J., Schmidt-Rohr, K. and Spiess, H.W. *Acta Polymer.* **1993**, *44*, 1.

62) Cho, G., Natansohn, A., Ho, T. and Wynne, K.J. *Macromolecules* **1996**, *29*, 2563.

Part I Rigid Gas Permeable Materials

Chapter 1
Relationship between the Physical Properties and Internal Structure of Rigid Gas Permeable Materials

1.1 Relationship among Internal Structure, Gas Permeability and Transparency in Copolymer Networks Composed of Methacrylates and Siloxane Macromers

1.1.1 Introduction

Silicone compounds[1–9] possess superior properties in terms of gas permeability, and have been employed for medical applications such as contact lenses. However, short Si–O–Si chains bearing silicone monomers lead to various undesired properties, such as the fragility and hydrophobicity due to their weak intermolecular forces and strong hydrophobicity. To overcome the abovementioned issues, the introduction of silicone compounds having long Si–O–Si chains such as PDMS into the polymer backbone have been developed. Polycondensation was one approach for the introduction of a PDMS chain with a rigid segment, such as polyamide and polyimide groups, as multi-block copolymers.[10–13] The resultant copolymer had improved mechanical strength and solubility, but the polycondensation approach limited the monomer type and composition ratio, based on the esterification and amidation.

Another approach is the radical copolymerization with an acrylic monomer and a PDMS macromer bearing vinyl groups at the PDMS chain ends. This approach enables the usage of a variety of characteristics of the acrylic monomers. Moreover, the composition ratio between the PDMS and acrylic monomers can be controlled by the feed conditions, and this allows a systematic study on the relationship between the physical properties and the copolymer composition, which is important for medical

applications. However, there are very few articles describing the aforementioned crosslinked copolymers[14,15] and no reports were found on the relationship among the transparency, oxygen permeability, internal structure, and the type of acrylic monomers.

In this study, I fabricated crosslinked copolymers composed of PDMS macromers and acrylic monomers at varied composition ratios by the radical polymerization approach, to examine the effects of the composition on the physical properties. TFEMA, which possesses a low refractive index comparable with silicone compounds, and MMA, which is used as an optical material with a relatively high T_g were selected as acrylic monomers.

1.1.2 Experimental Section

Materials

PDMS macromer was purchased from Shin-Etsu Chemical Co., Ltd., and was used without further purification. M_n measurements by ^1H NMR were performed with a JEOL ECS400 spectrometer using $CDCl_3$ as the solvent, and the SEC measurements were performed with a HLC-8120 SEC system by the TOSOH Corporation (Japan). MMA (Wako Pure Chemical Industries), TFEMA (Osaka Organic Chemical Industry Ltd.), *tert*-butyl methacrylate (*t*-BuMA) (Wako Pure Chemical Industries), hexafluoroisopropyl methacrylate (HFIPMA) (Synquest Labs., Inc., USA), ethyleneglycol dimethacrylate (1G) (Shin-Nakamura Chemical Co., Ltd.), 2, 2'-azobis (2,4-dimethyl-valeronitrile)(V-65) (Wako), and 1,1'-azobis (cyclohexane-1-carbonitrile) (V-40) (Wako) were used without further purification. The chemical structures of the monomers and crosslinker are shown in Figure 1-1-1.

Preparation of the crosslinked copolymer from acrylic monomer and PDMS macromer

The preparation of the crosslinked copolymer was performed by bulk

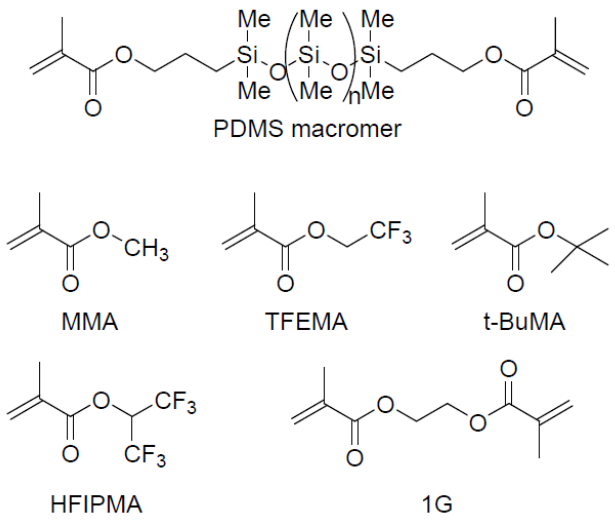

Figure 1-1-1. Chemical structures of monomers in this study.

polymerization in a sheet shape. PDMS macromers with four different M_n values, MMA, TFEMA, *t*-BuMA, and HFIPMA as methacrylates, 1G as the crosslinker (added at 1 wt% of the methacrylates) plus V-65 and V40 as the initiators, were combined according to the required balance and degassed by five repeated freeze-thaw cycles under nitrogen atmosphere. The mixtures were injected between a glass plate and a poly(tetrafluoroethylene) (PTFE) film separated with a silicone elastomer gasket (0.2–0.5 mm thickness) under a nitrogen atmosphere. The polymerization was then performed by keeping the temperature at 50 ºC for 16 h, followed by elevating the temperature to 110 ºC using steps of 20 ºC and 2 h. After polymerization, the PTFE film and silicone gasket were removed, and then the crosslinked copolymer sheet was removed from the glass plate. For the annealing of the copolymers, obtained crosslinked copolymer sheets were kept at 115 ºC for 16 h *in vacuo*. The properties of the crosslinked copolymer were evaluated after annealing. ATR-FTIR spectra of some samples were recorded to monitor the residual methacryloyl groups.

Evaluation of crosslinked copolymers

Light transmittance was measured by a SM-5 color computer (Suga Test Instruments Co., Ltd.). The $P(O_2)$ was measured with a GTR-10XACT gas transmissibility measurement apparatus (GTR Tec Corporation) at 35 ºC. The T_g was measured by a SEIKO Instruments Exstar 6000. The Vickers hardness was measured with an AKASHI hardness tester MVK-G1.

1.1.3 Results and Discussion

Molecular weight of PDMS macromers

The M_ns from the manufacturer and the results from the ^{1}H NMR and SEC measurements of the PDMS macromer are shown in Table 1-1-1. As the results from the ^{1}H NMR and SEC measurements showed similar values as those from the manufacturer, the M_n from the manufacturer was used in the following analysis.

Table 1-1-1. Molecular weight of PDMS macromer

Code	M_n from Manufacturer	M_n from NMR	Results from SEC		
			M_n	M_w	M_w/M_n
A	1,720	1,700	N.D.[a]	*	*
B	3,260	3,300	3,700	6,700	1.81
C	4,740	4,500	4,600	8,300	1.80
D	7,800	7,300	6,300	10,000	1.59

[a] Not determined.

Preparation of crosslinked copolymers

The comparison of the ATR-FTIR spectra between a monomer mixture from MMA and 3,300 g/mol M_n PDMS macromer at a 20/80 weight ratio (Figure 1-1-2a), and the two types of crosslinked copolymers are shown in Figure 1-1-2. The composition of one of the crosslinked copolymers was MMA plus a 3,300 g/mol M_n PDMS macromer at a 80/20 weight ratio (Figure 1-1-2b), and the other one was MMA and a PDMS (M_n = 4,700 g/mol) macromer at a 70/30 weight ratio (Figure 1-1-2c). The

peak signal at 1638 cm^{-1}, which corresponded to the double bond from the methacryloyl group, could not be detected in the crosslinked copolymer due to the polymerization. Furthermore, any influence of the PDMS M_n on the polymerization was not observed. An example of the FT-IR peak list of the crosslinked copolymer composed of MMA and a PDMS (M_n = 3,300 g/mol) macromer at a weight ratio of 80/20 is as follows: 2,950cm^{-1}(C–H stretching), 1,723cm^{-1} (C=O of ester stretching), 1,435cm^{-1} (Si–CH_3 deformation), 1,261cm^{-1} (Si–CH_3 deformation), 1,143cm^{-1} (Si–O–Si stretching), 804cm^{-1} (Si–CH_3 stretching).

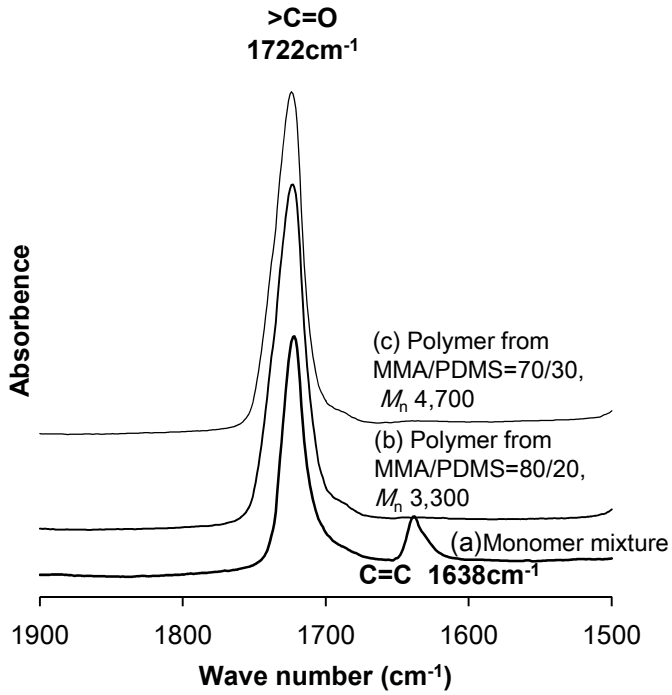

Fgure 1-1-2. ATR-FTIR spectra of monomer mixture and crosslinked copolymers. The composition of monomer mixture of (a) is MMA and 3,300 g/mol M_n PDMS macromer at a 20/80 weight ratio. The composition of crosslinked copolymer is (b) MMA and 3,300 g/mol M_n PDMS macromer at a 80/20 weight ratio, and (c) MMA and 4,700 g/mol M_n PDMS macromer at a 70/30 weight ratio.

DSC measurements

The results from DSC measurements of the crosslinked copolymer formed from MMA and PDMS macromers with different M_ns (1,700, and 4,700 g/mol) are shown in Figure 1-1-3 (A). In these crosslinked copolymers, two different T_gs were

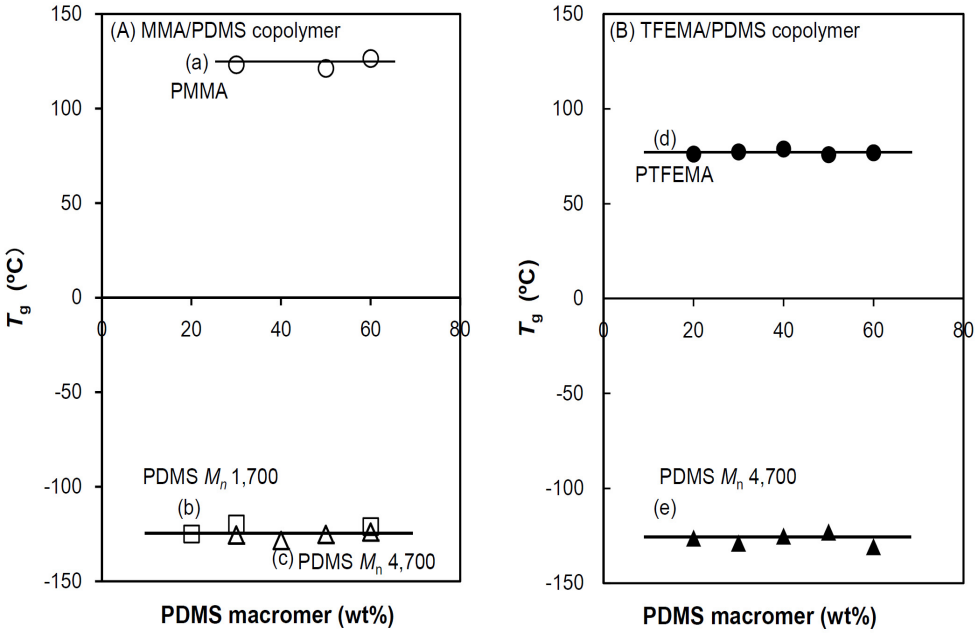

Figure 1-1-3. Plot of T_g of the crosslinked copolymer from methacrylate and PDMS macromer versus PDMS macromer content (wt%). (A) MMA/PDMS crosslinked copolymer. Phase of measured T_g and M_n of PDMS macromer are (a) PMMA phase and 4,700 g/mol (open circle), (b) PDMS phase and 1,700 g/mol (open square), (c) PDMS phase and 4,700 g/mol (open triangle). (B) TFEMA/4,700 g/mol M_n PDMS crosslinked copolymer. Phase is (d) PTFEMA phase (closed circle), and (e) PDMS phase (closed triangle).

recognized. These T_gs showed constant values, which may correspond to the PMMA phase (around 124 ºC) and PDMS phase (around –125 ºC), whereas the compositions of PMMA and PDMS were varied in the crosslinked copolymer.

The results from the crosslinked copolymer of TFEMA/PDMS macromer with a M_n of 4,700 g/mol are shown in Figure 1-1-3(B). As seen in the MMA/PDMS macromer crosslinked copolymer, two different T_gs were recognized, and showed constant values, which may correspond to the PTFEMA phase (around 77 ºC), and the PDMS phase (around –125 ºC) at varied compositions.

These results imply that PMMA, PTFEMA and PDMS are insoluble in each other over the PDMS M_n range used, and that they have phase separated internal structures.

Light transmittance and crosslinked copolymer composition

The relationship among the light transmittance of the crosslinked copolymer from MMA and PDMS macromer of 0.5 mm thickness, the PDMS volume fraction, the PDMS M_n, and the acrylic monomer is shown in Figure 1-1-4(A). The PDMS volume fraction was estimated assuming a density value of 0.98 and 1.19 for PDMS and PMMA including poly(1G), respectively.

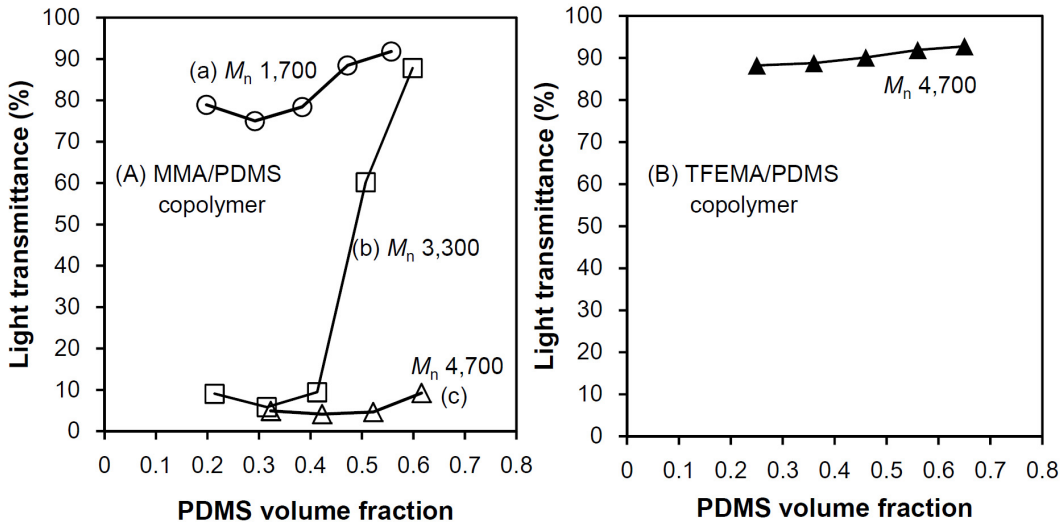

Figure 1-1-4. Light transmittance and crosslinked copolymer composition. (A) MMA and PDMS macromer. (a), (b), and (c) represent PDMS M_n of 1,700 g/mol (open circle), 3,300 g/mol (open square), and 4,700 g/mol (open triangle), respectively. (B) TFEMA and 4,700 g/mol M_n PDMS macromer.

Although the monomer mixture before polymerization was uniform and transparent, the light transmittance of the crosslinked copolymer composed of MMA and PDMS macromer depended on the M_n and volume fraction of PDMS. A PDMS macromer of 1,700 g/mol gives an almost transparent crosslinked copolymer for the measured volume fraction range (Figure 1-1-4 (A) (a)). This suggests that the size of the phase separation is sufficiently small for low light scattering, and the resultant high transparency. The crosslinked copolymer composed of a PDMS macromer at 3,300

g/mol shows a drastic transmittance change according to the change in the volume fraction (Figure 1-1-4(A) (b)). Over the region where the PDMS volume fraction was less than 0.4, the appearance of the copolymer network was opaque. In contrast, a higher light transmittance was observed at a PDMS volume fraction more than 0.4. This suggests a change in morphology according to the variations of the PDMS volume fraction. In addition, crosslinked copolymers with a higher M_n PDMS (Figure 1-1-4(A) (c)) have an opaque appearance over the measured PDMS volume fraction range. This implies that a higher M_n PDMS causes a greater phase separation, resulting in light scattering even though a morphology change occurred.

In contrast to the results from the crosslinked copolymer composed of MMA and PDMS macromer, TFEMA caused a drastic improvement in light transmittance, as shown in Figure 1-1-4(B). The PDMS volume fraction was estimated assuming density values of 0.98, 1.41, and 1.19 for PDMS, PTFEMA, and poly(1G) respectively. The reason why TFEMA gave good transparency may be: (a) reduced light scattering at the domain boundary because of the small difference in refractive index between TFEMA and PDMS; or (b) a different morphology from the MMA/PDMS macromer composition. With regard to the former reason, crosslinked copolymer with *t*-BuMA instead of TFEMA was prepared, because *t*-BuMA shows an intermediate refractive index between MMA and TFEMA as shown in Table 1-1-2. The appearance of the crosslinked copolymer using MMA, TFEMA and *t*-BuMA is shown in Figure 1-1-5, and supports the important role of the refractive index of the polymer used on the crosslinked copolymer transparency, and the advantage of fluorine containing acrylic

Table 1-1-2. Refractive index of some polymers

Polymer	Refractive index
Methacryloyl capped polydimethylsiloxane(M_n = 4,700)	1.408
PMMA	1.4893
PTFEMA	1.437
poly(*tert*-butyl methacrylate) (P-*t*-BuMA)	1.4638

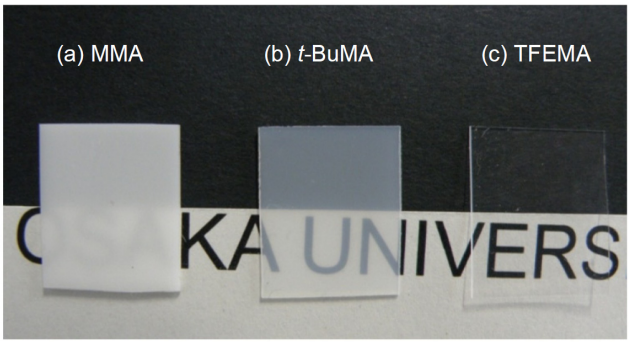

Figure 1-1-5. The appearance of crosslinked copolymer. M_n of PDMS macromer is 4,700 g/mol and the used comonomers are MMA (a), *t*-BuMA (b), and TFEMA (c).

monomers.

Oxygen permeability coefficient and crosslinked copolymer composition

The results of $P(O_2)$ measurements on crosslinked copolymers composed of MMA and PDMS macromer are shown in Figure 1-1-6(A).

At first, the contribution of the PDMS M_n to the $P(O_2)$ was studied. With regards to the domain size of the block copolymer, T. Hashimoto and co-workers reported that the domain identity period (D) and sphere domain radius (R) were proportional to the $[M_n]^{2/3}$ in styrene-isoprene block copolymers.[16,17] As the $P(O_2)$ is mainly related to the PDMS domain size in the crosslinked copolymer composed of MMA/PDMS macromer, a simple proportional calculation of the $P(O_2)$ and a comparison between those oxygen permeability data would be useful for the estimation of the microheterophase structure of crosslinked copolymers of various PDMS M_ns. Referring to the results from T. Hashimoto and co-workers, a calculation on the basis of the 2/3 power of the PDMS M_n between 1,700 and 3,300 g/mol, and also between 1,700 and 4,700 g/mol, was performed and the results are also shown in Figure 1-1-6(A).

There was good agreement between the measured and calculated values for crosslinked copolymers composed of MMA and PDMS (M_n = 3,300 g/mol) macromer

for PDMS volume fractions less than about 0.45 (Figure 1-1-6(A), (b) and (e)). In the combination between a M_n of 1,700 and 4,700 g/mol, there was some difference between the calculated and measured values (Figure 1-1-6(A), (c) and (d)). This suggests that the applicable range of this $[M_n]^{2/3}$ theory was restricted in a sphere morphology.

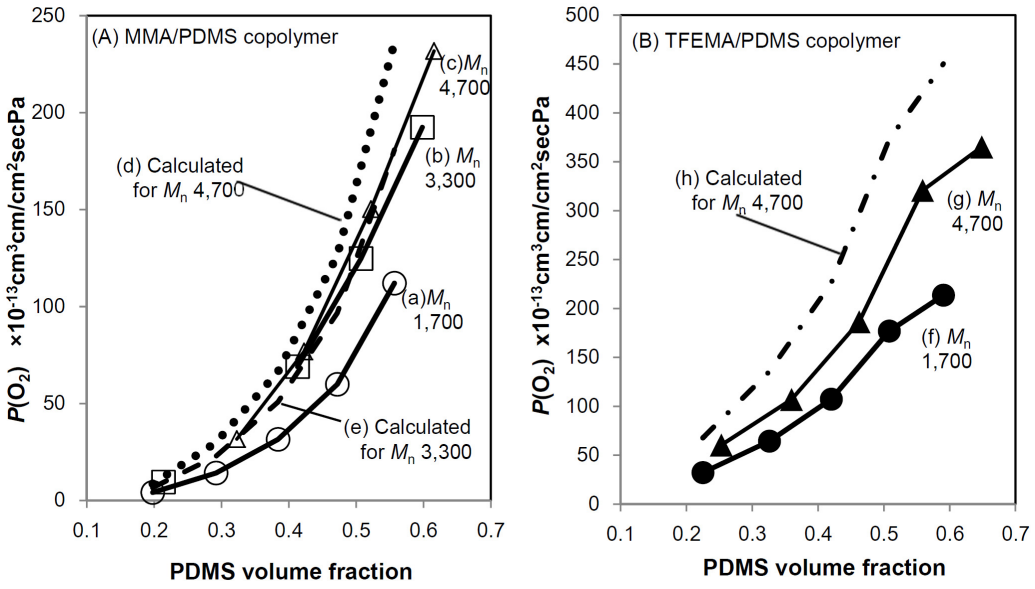

Figure 1-1-6. Oxygen permeability coefficient ($P(O_2)$) versus crosslinked copolymer composition. (A) Crosslinked copolymer from MMA and PDMS macromer. (a), (b), and (c) represent the crosslinked copolymer from PDMS macromer with M_n of 1,700 g/mol (open circle), 3,300 g/mol (open square) and 4,700 g/mol (open triangle), respectively. (d) (dotted line) and (e) (broken line) represent calculated $P(O_2)$ value according to $[M_n]^{2/3}$ model for composition (c) based on (a), and for composition (b) based on (a), respectively. (B) Crosslinked copolymer from TFEMA and PDMS macromer. (f) and (g) represent the crosslinked copolymer from PDMS macromer with M_n of 1,700 g/mol (closed circle) and 4,700 g/mol (closed triangle), respectively. (h) (dashed line) represents calculated $P(O_2)$ value according to $[M_n]^{2/3}$ model for composition (g) based on (f).

The copolymerization of TFEMA instead of MMA led to drastic increases in the $P(O_2)$ as shown in Figure 1-1-6(B). The measured data shows about a 2- or 3-fold higher value as compared with the value from the MMA crosslinked copolymer (Figure 1-1-6 (a) versus (f), (c) versus (g)). In the case of the copolymerization of TFEMA with

a PDMS macromer, the influence of the M_n on the $P(O_2)$ and the applicability of the $[M_n]^{2/3}$ rule were studied. There was no applicability of this rule implying that this region did not correspond to sphere type morphology (Figure 1-1-6(B), (g) and (h)). With regard to the influence of fluorine bearing compounds on the $P(O_2)$ increase, blending the polymer from a fluorine containing vinyl monomer to PDMS or the copolymerization of a fluorine containing vinyl monomer, MMA, and a relatively small quantity of PDMS macromer has been reported.[18,19] However, one issue relates to the surface modification and the other related to the material and the condition where phase separation does not occur. For my purpose, I tried to study the relationship between copolymer morphology and the $P(O_2)$ using model calculations.

Calculation of P (O_2) of crosslinked copolymer by morphology model

Many studies have been carried out on the relationship between morphology and gas transport in block copolymers.[20–26] Among the many models in this study, I noticed the method by J. Sax and J. M. Ottino[20] because of its wide applicability. As this model was developed for block copolymers without crosslinking, there may be some differences between our crosslinked material and block copolymers. However, I believe it is effective for comparative studies on the effects of morphology on bulk copolymer properties. In this method, the diffusion constant for each morphology was calculated using the following formulae.[20]

a. Sphere model

$$D_{eff} = D_c(1+3\Phi_d(\frac{\bar{s}\bar{x}+2}{\bar{s}\bar{x}-1}-\Phi_d)^{-1})/[\bar{s}(1+\Phi_c(1-\bar{s})/\bar{s})]$$

b. Cylinder model

$$D_{eff} = [\bar{s}(1+\Phi_c(1-\bar{s})/\bar{s})]^{-1}D_c$$
$$\times\left\{(\frac{1}{3})[(1-\Phi_d)+\Phi_d\bar{x}\bar{s}]+(\frac{2}{3})\left[1+2\Phi_d(\frac{\bar{s}\bar{x}+1}{\bar{s}\bar{x}-1}-\Phi_d+0.3\frac{\bar{s}\bar{x}-1}{\bar{s}\bar{x}+1}\Phi_d{}^4+0.013\frac{\bar{s}\bar{x}-1}{\bar{s}\bar{x}+1}\Phi_d{}^8)^{-1}\right]\right\}$$

c. Lamellar model

$$D_{eff} = D_c((1/3)[(\frac{1-\Phi_c}{Sx}) + \Phi_c]^{-1} + (2/3)[(1-\Phi_c)Sx + \Phi_c])/S(1+\Phi_c(1-S)/S)$$

where, D_{eff} is the effective diffusion coefficient, $_c$ shows the continuous phase, $_d$ shows the dispersed phase, $\bar{s}$ and S represent the solubility ratio (S_d/S_c), $\bar{x}$ is the diffusivity ratio (D_d/D_c), and Φ is the volume fraction.

The solubility coefficient was also calculated. S_{eff} (effective solubility) was calculated from following formula because E. L. Thomas and co-workers[21] reported good agreement between the predicted and measured values with it:

$$S_{eff} = S_A\Phi_A + S_B\Phi_B$$

where, Φ is the volume fraction, S is the solubility and $_A$, $_B$ are the constituents. The oxygen permeability coefficient of the sphere, cylinder and lamellar models were calculated as follows,

$$P = D_{eff}\,S_{eff}$$

d. Calculation of P with the parallel model

The oxygen permeability coefficient of the parallel model was calculated by the following formula:

$$P = P_A\Phi_A + P_B\Phi_B$$

where P, P_A, P_B represent the oxygen permeability coefficients.

The diffusion coefficients and solubility coefficients of PDMS, PMMA, PTFEMA, and P(*t*-BuMA) for the calculations were summarized in Table 1-1-3. The calculated results using these values are shown in Figure 1-1-7(A), (B), and (C).

With regard to the crosslinked copolymer composed of MMA and PDMS macromer, it is recognized from Figure 1-1-7(A) that the $P(O_2)$ values of the crosslinked copolymer with PDMS (M_n = 1,700 g/mol) macromer were intermediate between the sphere and cylinder models. On the other hand, the $P(O_2)$ values of crosslinked copolymers at 3,300 and 4,700 g/mol M_n were intermediate between the sphere and lamellar models. This may correlate with the aforementioned results, which showed that the $P(O_2)$ of the crosslinked copolymer with a 3,300 g/mol M_n could be

predicted from that of the 1,700 g/mol crosslinked copolymer, but that of the crosslinked copolymer with a 4,700 g/mol could not be predicted.

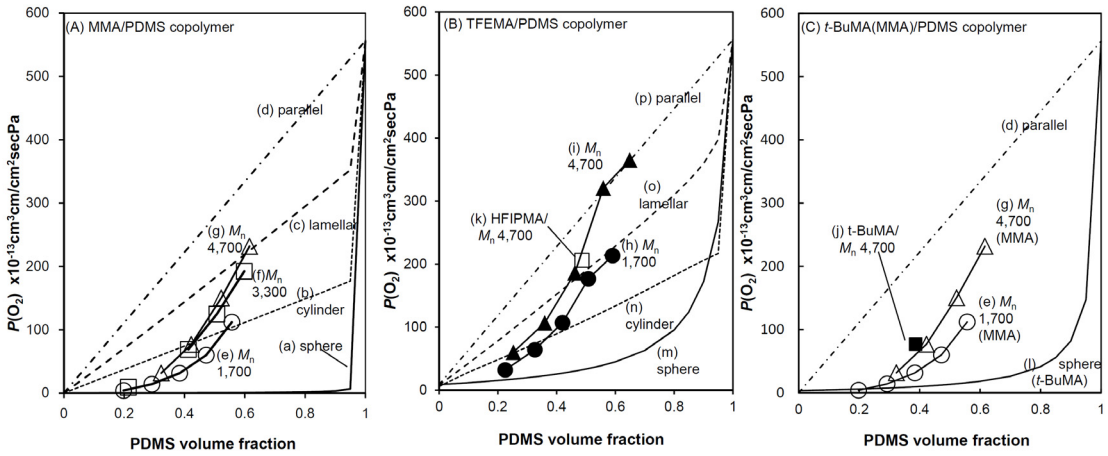

Figure 1-1-7. Results from calculation of $P(O_2)$ for various morphology according to the method by Sax and Ottino.[20] (A) The results for MMA/PDMS crosslinked copolymer. (a), (b), (c), and (d) represent sphere model, cylinder model, lamellar model, and parallel model, respectively. PDMS M_n is (e) 1,700 g/mol (open circle), (f) 3,300 g/mol (open square), and (g) 4,700 g/mol (open triangle). (B) The results for PTFEMA/PDMS crosslinked copolymer. (m), (n), (o) and (p) represent sphere model, cylinder model, lamellar model, and parallel model, respectively. PDMS M_n is (h) 1,700 g/mol (closed circle), and (i) 4,700 g/mol (closed triangle). The composition of (k) is HFIPA and 4,700 g/mol M_n (open square). (C) The results for additional data from *t*-BuMA/PDMS crosslinked copolymer. The composition of (j) is *t*-BuMA and PDMS with 4,700 g/mol M_n (closed square). (l) is calculated $P(O_2)$ of sphere model for *t*-BuMA and PDMS macromer.

Similarly, the calculated results of the crosslinked copolymer composed of TFEMA and PDMS macromer are shown in Figure 1-1-7(B). Comparing the results from the crosslinked copolymer of MMA/PDMS macromer (Figure 1-1-7(A)) with that of the PTFEMA/PDMS macromer (Figure 1-1-7(B)), it is clear that the $P(O_2)$ of the PTFEMA/PDMS macromer already has the parallel model structure at less than a 0.6 PDMS volume fraction (Figure 1-1-7(B), (i) versus (p)). This may be related to following factors. One may be the oxygen permeable properties of PTFEMA, even

though the $P(O_2)$ of PTFEMA is only 9×10^{-13}cm^{3}cm/(cm^{2}secPa), and low when compared with the 556×10^{-13}cm^{3}cm/(cm^{2}secPa) value of PDMS. In contrast to the $P(O_2)$ of almost zero of the MMA/PDMS crosslinked copolymer at a PDMS volume fraction of 0.2, the TFEMA/PDMS crosslinked copolymer showed a $P(O_2)$ around 30×10^{-13}cm^{3}cm/(cm^{2}secPa), even in the case of PDMS macromer with M_n of 1,700 g/mol. This situation is clearly shown in Figure 1-1-7(A) (a) versus (B) (m). Another factor may be the mutual solubility or miscibility between PTFEMA, poly(TFEMA-*co*-PDMS) copolymer and PDMS, which are the constituents of the TFEMA/PDMS crosslinked copolymer, or similarly the solubility among PMMA, poly (MMA-*co*-PDMS) copolymer and PDMS. In my study, according to the progress of the polymerization, a phase separation between those constituents may occur, and thus the aforementioned solubility may affect the morphology to form a parallel model structure. Furthermore, since the fluorine-containing PTFEMA has a larger specific density than PMMA, the resultant PDMS volume fraction in the crosslinked copolymer was larger in the TFEMA/PDMS crosslinked copolymer with the same PDMS macromer content on a weight basis, and this may be correlated to the difference in the relationship between the morphology and the PDMS volume fraction.

To confirm these points, $P(O_2)$ measurements were carried out on the following samples. One sample contained *t*-BuMA as a comonomer which had a low specific density of 1.022, a somewhat low refractive index of 1.4638, and a Hildebrand solubility parameter of 18 MPa$^{1/2}$ which is comparable to that of PMMA,[27] as the solubility parameters of PMMA, PDMS, and PTFEMA have been reported as 18.0–23.1,[28] 14.9,[29] and 16.4–17.3 (the values for trifluoroethyl acrylate are reported) [30] MPa$^{1/2}$, respectively. Another sample had HFIPMA as a comonomer, and this one had a high specific density (assumed to be 1.56), a low refractive index (1.39), and a low Hildebrand solubility parameter (assumed to be low from the data for hexafluoropropylene of 10.4–14.4 MPa$^{1/2}$ or heptafluorobutyl acrylate of 15.8

Table 1-1-3. Used constants for the estimation of coefficients in this study

(a) PDMS

Constant	value	source
O_2 Diffusion coefficient at 25 ºC	16×10^{-6} cm^2/s	33
Solubility coefficient at 25 ºC	3.1×10^{-6} cm^3/cm^3Pa	33
Activation Energy	E_D = 9.0kJ/mol	34
	E_S= –0.3kJ/mol	34

*Value at 35ºC was obtained using $D=D_0\exp(-E_D/RT)$ or $E=E_0\exp(-E_S/RT)$ as 18×10^{-6} $cm^2/$, 3.09×10^{-6} cm^3/cm^3Pa respectively.

(b) Polyethylmethacrylate(PEMA) and PMMA

Constant	Material	Value	source
Diffusion coefficient at 25 ºC	PEMA	0.106×10^{-6} cm^2/s	35
Solubility coefficient at 25 ºC		0.839×10^{-6} cm^3/cm^3Pa	35
Activation Energy	PEMA	E_D=31.8kJ	35
		E_S= 4.6kJ	35
Oxygen permeability coefficient at 34 ºC	PMMA	0.116×10^{-13} $cm^3\times cm/(cm^2\times sec\times Pa)$	35

*Value at 35 ºC for PEMA was obtained using $D=D_0\exp(-E_D/RT)$ or $E=E_0\exp(-E_S/RT)$ as 0.161×10^{-6} cm^2/s, 0.891×10^{-6} cm^3/cm^3Pa respectively. Ignoring the difference between 34 ºC and 35 ºC, and assuming the solubility coefficient is the same as both PMMA and PEMA, the diffusion coefficient for PMMA was obtained by dividing the oxygen permeability coefficient of PMMA by solubility coefficient of PEMA as 0.013×10^{-6} cm^2/s.

*With regard to the constants for PTFEMA, following assumption was made for calculation. From the similarity of the molecular structure between EMA and TFEMA, solubility coefficient was considered to be the same value. The diffusion coefficient was calculated by dividing the oxygen permeability coefficient of PTFEMA (9×10^{-13} $cm^3\times cm/(cm^2\times sec\times Pa)$) by the solubility coefficient.

(c) Obtained diffusion and solubility coefficient for calculation

Material	Coefficient		Source
PDMS	diffusion	18×10^{-6} cm^2/s	
	solubility	3.09×10^{-6} cm^3/cm^3Pa	
PMMA	diffusion	0.013×10^{-6} cm^2/s	
	solubility	0.891×10^{-6} cm^3/cm^3Pa	
PTFEMA	diffusion	1.01×10^{-6} cm^2/s	
	solubility	0.891×10^{-6} cm^3/cm^3Pa	
P-*t*-BuMA	diffusion	0.108×10^{-6} cm^2/s	36
	solubility	3.2×10^{-6} cm^3/cm^3Pa	36

$MPa^{1/2}$).[31] Furthermore, as this PHFIPMA has a higher fluorine content than PTFEMA, its $P(O_2)$ was expected to be higher than that of PTFEMA. The results from measurements are plotted in Figure 1-1-7 as (j) and (k). It is clear that the $P(O_2)$ from the composition containing HFIPMA is on the line from the composition containing TFEMA (Figure 1-1-7(B), (i) and (k)). Similarly, the $P(O_2)$ from the composition containing *t*-BuMA is almost on the line from the composition containing MMA (Figure 1-1-7(C), (g) and (j)). The calculated $P(O_2)$ from a sphere model of copolymer composed of *t*-BuMA and PDMS macromer is also shown (Figure 1-1-7(C), (l)). There was only a small difference in the measured $P(O_2)$ of the crosslinked copolymer composed of *t*-BuMA and PDMS macromer compared with MMA/PDMS crosslinked copolymer (Figure 1-1-7(C), (g) and (j)), although P-*t*-BuMA had higher calculated $P(O_2)$ value for a sphere model than PMMA and similar one to PTFEMA as shown in Figure 1-1-7(a), (m) and (l). This implies that there is only a weak correlation between the morphology control and comonomer oxygen permeability, but rather some correlation between the crosslinked copolymer constituent's compatibility or solubility, and the copolymer morphology.

Thus, this systematic study of the composition change of crosslinked copolymers composed of PDMS macromers and methacrylates revealed that the method by Sax and Ottino[20] was effective in understanding the great influence of the methacrylate type on the change in morphology with the PDMS volume fraction from the measured oxygen permeability. Furthermore, this supports the importance of the solubility or miscibility of methacrylates and PDMS on the morphology change and resultant oxygen permeability change.

$P(O_2)$ and estimation of the domain size with the $[M_n]^{2/3}$ model

There are very few reports describing the PDMS domain size. Akashi and co-workers[32] reported 6–8 nm or 10–15 nm as the domain size in Aramid-PDMS

block copolymers by TEM observation. However, this result was from only one PDMS (M_n = 1,680 g/mol). More information on the PDMS domain size has been reported by M. Mazurek and co-workers[15] on the crosslinked copolymer composed of isobornyl acrylate and both end acrylamidoamidos capped PDMS. They reported 10 nm and 500 nm as the domain size of the copolymer from PDMSs (M_n = 5,000 and 10,000 g/mol, respectively), but this is somewhat peculiar from the viewpoint of $[M_n]^{2/3}$ theory. Therefore, I tried to compare the PDMS domain sizes with different M_n values.

As stated above, the $P(O_2)$ of crosslinked copolymer composed of PDMS with a M_n of 1,700 and 3,300 g/mol was proportional to $[M_n]^{2/3}$. Assuming that the PDMS domain shape is a sphere with a radius of R, I tried to calculate the domain size ratio. Considering that the surface of a sphere is resistance to the diffusion of oxygen, the surface area for any unit volume of a sphere is expressed as:

$$4\pi R^2 / [(4/3)\ \pi R^3] = 3/R$$

Therefore, the ratio of resistance to gas permeation through spheres with a radius of R_1 and R_2 is expressed as follows:

$$3/R_1 : 3/R_2 = R_2 : R_1$$

where R_1 and R_2 are the radii of domains with different PDMS M_n values.

Because the permeability coefficient is the reciprocal of the resistance to permeation, the ratio of $P(O_2)$ from PDMS domain radii of R_1 and R_2 can be calculated from the ratio of the observed $P(O_2)$ (the ratio between Figure 1-1-6(A), (a) and (b)) as follows:

$$1/R_2 : 1/R_1 = R_1 : R_2 = 1 : 1.6$$

Thus, the PDMS domain size for a M_n of 3,300 g/mol is expected to be 1.6 times larger than that of PDMS with a M_n of 1,700 g/mol.

Morphology change of the copolymer network and light transmittance

The relationship obtained between the PDMS volume fraction and the $P(O_2)$

may be applicable to the relationship between the morphology and the transparency. Comparing Figures 1-1-4 and 1-1-7, there is good coincidence between the light transmittance change and the morphology change. At a PDMS volume fraction of 0.43 or so, the $P(O_2)$ line from PDMS with a M_n of 3,300 g/mol crosses the cylinder model line (Figure 1-1-7(A), (f) and (b)), and this may correspond to the morphology change. Conversely, Figure 1-1-4(A)(b) shows the drastic improvement in transparency at a PDMS volume fraction of around 0.43, as already described. Thus, this clearly shows the usefulness of this model calculation to understand the internal structure of copolymers.

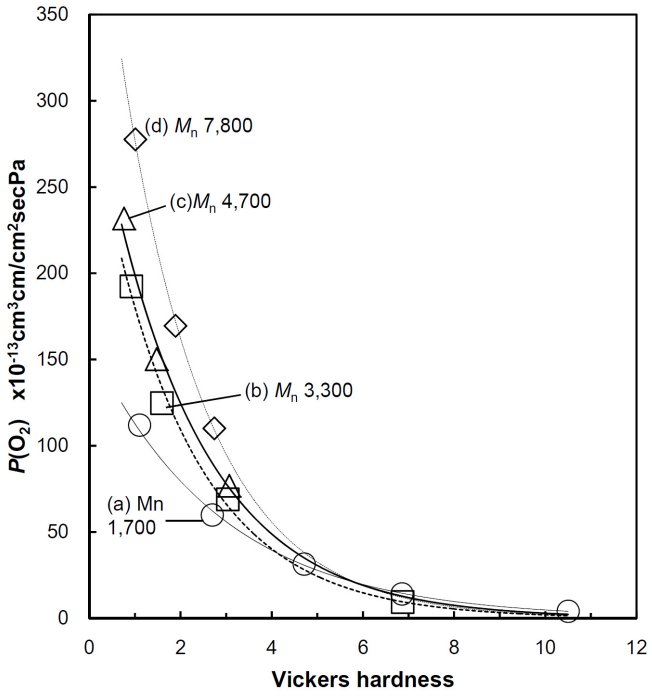

Figure 1-1-8. Plot of the measured $P(O_2)$ versus Vickers hardness of crosslinked copolymer from MMA and PDMS macromer. The regression curve is shown as exponential function. PDMS macromer M_n is (a) 1,700 g/mol (open circle), (b) 3,300 g/mol (open square), (c) 4,700 g/mol (open triangle), and (d) 7,800 g/mol (open diamond).

Vickers hardness of crosslinked copolymers composed of MMA and the PDMS macromers and PDMS M_n

As a measure of the practical performance of a rigid material, the Vickers hardness measurement was performed, and a plot of the $P(O_2)$ versus the Vickers hardness is shown in Figure 1-1-8. It was observed that the higher the molecular weight of the PDMS macromer used, the higher the $P(O_2)$ for the same Vickers hardness. The soft crosslinked copolymer tended to possess a higher $P(O_2)$, which is in agreement with the higher content of PDMS macromer. Conversely, a longer Si–O–Si chain of the PDMS macromer resulted in higher gas permeability, even if it was the same hardness, suggesting a different micro phase separation.

1.1.4 Conclusions

Crosslinked copolymers with various PDMS chain lengths and two types of acrylic monomer were prepared from MMA or TFEMA, PDMS macromer and 1G. DSC measurements of the T_g showed that PMMA or PTFEMA and PDMS were insoluble in each other. The transparency of the crosslinked copolymer composed of MMA and PDMS macromer depended on the PDMS M_n; a higher M_n (partly 3,300 g/mol, 4,700 g/mol and 7,800 g/mol) caused an opaque appearance, but copolymerizing with TFEMA instead of MMA induced a drastic improvement in transparency. This could be the result of reduced light scattering due to a reduced difference in refractive index, and the copolymerization of *t*-BuMA supported this hypothesis.

In the low PDMS M_n range (1,700 g/mol and 3,300 g/mol), the $P(O_2)$ was proportional to $[M_n]^{2/3}$, and from this relationship the domain size ratio between a M_n of 1,700 g/mol and 3,300 g/mol was calculated, and the ratio was found to be 1.6. This is the first proof of the relationship between domain size and the PDMS $[M_n]$ in a crosslinked copolymer.

Copolymerization with TFEMA instead of MMA gave a surprisingly large

increase in the $P(O_2)$ of the crosslinked copolymer. To clarify the mechanism of this drastic change, a calculation of the relationship among the morphology model, PDMS volume fraction, and $P(O_2)$ was performed. This implied that a morphology change to the parallel model occurred at a low PDMS volume fraction, and was caused by some properties such as the solubility parameter and so on. This was supported by the additional measurements with *t*-BuMA and HFIPMA.

Thus, the copolymerization of a fluorine-containing acrylic monomer was found to lead to a transparency improvement, a $P(O_2)$ increase, and therefore, fluorine-containing monomers could be expected to develop further applications in various fields.

1.1.5 References

1) Napp, D.J., Yang, W-H.M. and Peppas, N.A. *J. Appl. Polym. Sci.* **1983**, *28*, 2793.
2) Kang, Y-J., Aiba, N., Iwamoto, K. and Senô, M. *Kobunshi Ronbunsyu* **1985**, *42*, 345.
3) Kawakami, Y., Karasawa, H., Aoki, T., Yamamura, Y., Hisada, H. and Yamashita, Y. *Polym. J.* **1985**, *17*, 1159.
4) Kawakami, Y., Kamiya, H. and Yamashita, Y. *J. Polym. Sci. Polym. Symp.* **1986**, *74*, 291.
5) Kawakami, Y., Karasawa, H., Kamiya, H. Aoki, T. and Yamashita, Y. *Polym. J.* **1986**, *18*, 237.
6) Kawakami, Y., Kamiya, H., Toda, H. and Yamashita, Y. *J. Polym. Sci. Part A: Polym. Chem.* **1987**, *25*, 3191.
7) Kawakami, Y. and Sugisaka, T. *J. Membr. Sci.***1990**, *50*, 189.
8) Otsu, T. and Yoshioka, Y. *Makromol. Chem.* **1992**, *193*, 2283.
9) Ohnishi, M., Uno, T., Kubo, M. and Itoh, T. *J. Polym. Sci. Part A: Polym. Chem.* **2009**, *47*, 420.

10) Matsumoto, T., Koinuma, Y., Waki, K., Kishida, A., Furuzono,T., Maruyama, I. and Akashi, M. *J. Appl. Polym. Sci.* **1996**, *59*, 1067.

11) Chen, S-H., Lee, M-H. and Lai, J-Y. *Eur. Polym. J.* **1996**, *32*, 1403.

12) Ha, S.Y., Park, H.B. and Lee Y.M. *Macromolecules* **1999**, *32*, 2394.

13) Ghosh, A., Sen, K.S., Dasgupta B., Banerjee, S. and Voit, B. *J. Membr. Sci*. **2010**, *364*, 211.

14) Yu, X., Nagarajan, M.R., Li, C., Speckhard, T.A. and Cooper, S.L. *J. Appl. Polym. Sci*. **1985**, *30*, 2115.

15) Mazurek, M., Kinning, D.J. and Kinoshita, T. *J. Appl. Polym. Sci.* **2001**, *80*, 159.

16) Hashimoto, T., Shibayama, M. and Kawai, H. *Macromolecules* **1980**, *13*, 1237.

17) Hashimoto, T., Fujimura, M. and Kawai, H. *Macromolecules* **1980**, *13*, 1660.

18) Kawakami, Y., Aoki, T. and Yamashita, Y. *Polym. Bull.* **1987**, *17*, 293.

19) Koßmehl, G., Fluthwedel, A. and Schäfer, H. *Makromol. Chem.* **1992**, *193*, 157.

20) Sax, J. and Ottino J.M. *Polym. Eng. Sci.* **1983**, *23*, 165.

21) Kinning, D.J., Thomas, E.L. and Ottino, J.M. *Macromolecules* **1987**, *20*, 1129.

22) Rein, D.H., Baddour, R.F. and Cohen, R.E. *J. Appl. Polym. Sci.* **1992**, *45*, 1223.

23) Okamoto, K., Fujii, M., Okamyo, S., Suzuki, H., Tanaka, K. and Kita, H. *Macromolecules* **1995**, *28*, 6950.

24) Patel, N.P. and Spontak, R.J. *Macromolecules* **2004**, *37*, 2829.

25) Wang, J., DeRocher, J.P., Wu, L., Bates, F.S. and Cussler, E.L. *J. Membr. Sci.* **2006**, *270*, 13.

26) Lin, G., Aucoin, D., Giotto, M., Canfield, A., Wen, W-Y. and Jones, A.A. *Macromolecules* **2007**, 40, 1521.

27) Barton, A.F.M.; "CRC Handbook of Polymer-Liquid Interaction Parameters and Solubility Parameters"; CRC Press, Inc; Boca Raton, **1990**; p 462.

28) Barton, A.F.M.; "CRC Handbook of Polymer-Liquid Interaction Parameters and Solubility Parameters"; CRC Press, Inc; Boca Raton, **1990**; p 259.

29) Barton, A.F.M.; “CRC Handbook of Polymer-Liquid Interaction Parameters and Solubility Parameters”; CRC Press, Inc; Boca Raton, **1990**; p 125.

30) Barton, A.F.M.; “CRC Handbook of Polymer-Liquid Interaction Parameters and Solubility Parameters”; CRC Press, Inc; Boca Raton, **1990**; p 678.

31) Barton, A.F.M.; “CRC Handbook of Polymer-Liquid Interaction Parameters and Solubility Parameters”; CRC Press, Inc; Boca Raton, **1990**; pp 540-541.

32) Furuzono, T., Senshu. K., Kishida, A. Matsumoto, T. and Akashi M. *Polym. J.* **1997**, *29*, 201.

33) “Polymer Data Handbook”; Mark, J.E. Ed.; Oxford University Press: New York, **1999**; p 424.

34) Pauly S. In “Polymer Handbook”; Brandrup, J.; Immergut, E.H.; Grulke, E.A.; Eds., 4th ed. Wiley: New York: **1999**; pVI/558.

35) Pauly S. In “Polymer Handbook”; Brandrup, J.; Immergut, E.H.; Grulke, E.A.; Eds., 4th ed. Wiley: New York: **1999**; p VI/548.

36) Wright, C.T. and Paul, D.R. *Polymer* **1997**, *38*, 1871.

1.2 The Systematic Study of the Microstructure of Crosslinked Copolymers from Siloxane Macromonomers and Methacrylates with Various Composition and Components

1.2.1 Introduction

As stated in Section 1.1, the relationship among internal structure, gas permeability and transparency in copolymer networks, which were composed of methacrylates and siloxane macromers had been studied. The effects of the solubility parameter of methacrylate on the gas permeability and the possible morphology were observed. This type of copolymerization is considered to be PIPS.[1)] An amphiphilic co-network created from the combination of PDMS macromonomer and hydrophilic vinyl monomer[2,3)] has been reported, as has been the crosslinked copolymer from PDMS macromers and hydrophobic vinyl monomers.[4,5)] Previous research on the amphiphilic network focused on analysis of the structure or dynamics for a specific polymer composition. Research on hydrophobic crosslinked copolymers focused on the properties of various polymerizable groups at the PDMS tail end. As far as we know, no articles have been published that investigated the microstructure of PDMS-bearing copolymers at the molecular level with solid-state NMR.

In the radical copolymerization approach, a systematic study is useful to investigate the relationship between composition and physical properties as a function of the various monomers and PDMS macromonomers of various M_n. However, no articles using such an approach were found. Moreover, further analysis of microstructures of the copolymers is required at the molecular level to develop a copolymer material with superior characteristics.

In this study, ^{13}C solid-state CP-MAS NMR measurements of the aforementioned copolymers were conducted, because it provides fine grain information with respect to the molecular mobility or relaxation time, which enables analysis of the internal structure of heterogeneous polymer composites.[6–8)] MMA and TFEMA were

selected as the methacrylates, because they have been used as optical materials in medical materials, such as contact lenses, due to their high glass transition temperature (T_g) and transparency. TFEMA also has a low refractive index, similar to that of PDMS, and oxygen permeability was also considered. I believe that my approach to investigate the relationship between copolymer compositions and their physical properties with solid-state NMR will contribute greatly to the new field of the study of polymerization-induced phase separation products.

1.2.2 Experimental Section

Materials and Preparation of crosslinked copolymer

PDMS macromer was purchased from Shin-Etsu Chemical Co., Ltd. and used without further purification. MMA (Wako Pure Chemical Industries), TFEMA (Osaka Organic Chemical Industry Ltd.), 1G (Shin-Nakamura Chemical Co., Ltd.), V-65 (Wako) and V-40 (Wako) were used without further purification.

Molecular weight measurements of PDMS macromers by ^{1}H NMR and SEC method as well as the preparation of crosslinked copolymer were carried out in the same way as aforementioned in Section 1.1.2. Measured PDMS macromer molecular weights are shown in Table 1-1-1 and chemical structures of the monomers and crosslinker are shown in Figure 1-1-1.

CP-MAS NMR measurement

Specimens for NMR measurements were cut into 0.5–1 mm width and length rectangular piece from 0.2 mm thickness sheet of crosslinked copolymer. ^{13}C NMR spectra were recorded on a Chemagnetics CMX 300 NMR infinity spectrometer operating at 7.05 T at room temperature by CP-MAS methods. Magic angle frequency was set to 10.5 kHz. The 90° pulse, contact time, and recycle time were 4.2 μsec, 1.5 msec, and 5 sec, respectively. Pulse mode was CP/MAS. The ^{1}H spin-lattice relaxation

time in the laboratory frame (T_1^H) was indirectly measured from ^{13}C signals enhanced by CP of 1.5 msec applied after the ^1H π pulse. Similarly, indirect measurement was applied for detecting the ^1H spin-lattice relaxation time in the rotating frame ($T_{1\rho}^H$) combined use of CP and spin locking of ^1H nuclei. The irradiation power and spin-locking power were 55.6 kHz. The compositions of the samples are shown in Table 1-2-1.

Table 1-2-1. Composition[a] of the specimens employed in this study

Specimen	Acrylic monomer		PDMS macromer		PDMS fraction [b]		Appearance
	Type	Weight	M_n	Weight	Weight	Volume	
M129	MMA	70	1,700	30	0.25	0.29	transparent
M147	MMA	50	1,700	50	0.42	0.47	transparent
M432	MMA	70	4,700	30	0.23	0.32	opaque
M442	MMA	60	4,700	40	0.38	0.42	opaque
T436	TFEMA	70	4,700	30	0.28	0.36	transparent
T446	TFEMA	60	4,700	40	0.38	0.46	transparent

[a] Parts of weight for 1G is acrylic monomer×(1/100) for all specimens.

[b] PDMS weight fraction and volume fraction were calculated using PDMS weight which was obtained from the subtraction of the weight of methacryloyloxypropyl group from PDMS macromer.

1.2.3 Results and Discussion

CP-MAS Spectra

Typical CP-MAS spectra and assignments of the signals are shown in Figure 1-2-1. The peak patterns differ depending on the chemical structure of the monomers. In addition, the intensity at 1.5 ppm (a) of specimen M147, with a PDMS M_n of 1,700, was higher than those of specimens M442 and T446, with a PDMS M_n of 4,700. It is reported that a higher intensity signal corresponds to a lower mobility in the CP-MAS spectrum because the efficiency of cross-polarization inversely depends on mobility.[8)]

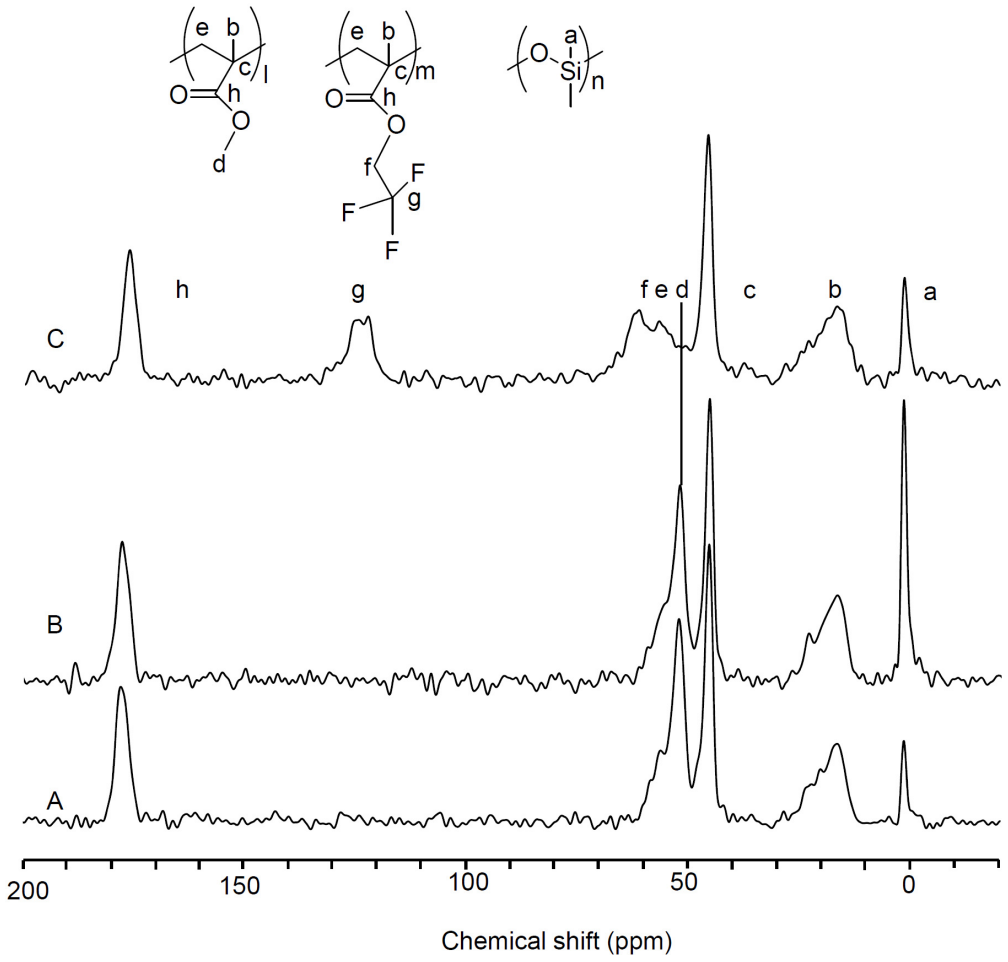

Figure 1-2-1. ^{13}C CP-MAS NMR spectra of crosslinked copolymers from methacrylates and the PDMS macromonomer. A, B, and C correspond to the following compositions. A : M442 (MMA/PDMS macromonomer with M_n = 4,700, PDMS = 38 wt%), B: M147 (MMA/PDMS macromonomer with M_n = 1,700, PDMS = 42 wt%), C : T446 (TFEMA/PDMS macromonomer with M_n = 4,700, PDMS = 38 wt%).

Because the PDMS content is almost the same for all specimens (PDMS is 38–42 wt%), it was recognized from the signal at 1.5 ppm (Figure 1-2-1a) that the larger PDMS segment (M_n = 4,700) is more mobile than the PDMS segment with a M_n of 1,700. These results suggest that a higher PDMS M_n allows a higher diffusivity of gas molecules and results in a higher gas permeability coefficient. This shows good correspondence to our previous report that described a material with a microheterophase structure with a high M_n.[9] The results showed higher oxygen permeability than a

material made from a low-molecular-weight silicone constituent.

Comparison of T_1 values from the copolymer and pristine polymer

The measured T_1^H, $T_{1\rho}^H$, T_1^C, and $T_{1\rho}^C$ values of pristine PDMS (I), PMMA (I) and PTFEMA (II) are shown with those of the copolymer in Figure 1-2-2. The T_1^H, $T_{1\rho}^H$, T_1^C, and $T_{1\rho}^C$ values of pristine PDMS are clearly different from those of copolymerized PDMS. Furthermore, comparing the T_1 values of pristine PMMA and PTFEMA with those of copolymerized PMMA and PTFEMA, it is possible to observe the composition dependency of the T_1 values. Thus, it was recognized that the copolymerization of the PDMS macromonomer with MMA or TFEMA resulted in a finely dispersed microstructure that is dependent on the composition and PDMS M_n value.

T_1^H vs PDMS M_n, PDMS volume fraction, and co-monomer

The proton spin-lattice relaxation time T_1^H is used to elucidate the parts that have a relatively high mobility on the order of MHz, and T_1^H measurements have been performed to obtain information with respect to the size of the domains in polymers.[10–13] The measured T_1^H values for all specimens, including pristine PDMS, PMMA, and PTFEMA, are shown in Figure 1-2-2A. In addition, the T_1^H values for the PDMS macromonomer with M_n = 1,700 and 4,700 were 1.16 sec and 1.25 sec, respectively.

Specimen M129 (MMA copolymer and 1,700 M_n PDMS) had almost the same T_1^H values at all peaks (average value is 0.60 sec), implying effective spin diffusion due to the low molecular mobility and implying a homogeneous dispersion structure. The diameter of the homogeneously distributed area (domain size) was calculated using the following formula[11] and average T_1^H value:

$$L = (6Dt)^{1/2} \qquad (1)$$

where L represents the domain size, D is $\sim 10^{-12}$ cm^2/sec (spin diffusion coefficient),

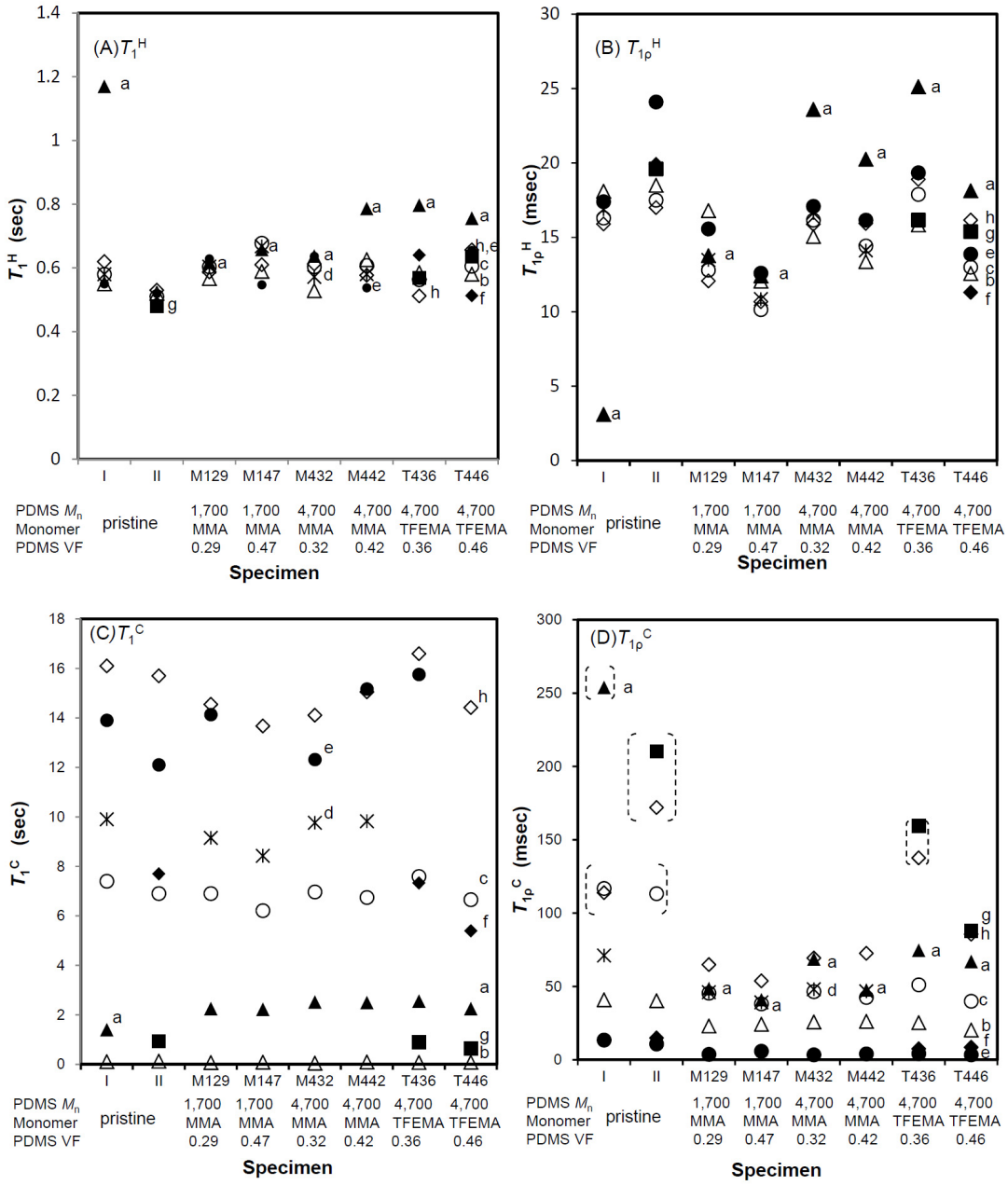

Figure 1-2-2. Measured T_1^H, $T_{1\rho}^H$, T_1^C and $T_{1\rho}^C$ values. a, b, c, d, e, f, g, and h correspond to the peak signals in Figure 2. PDMS VF indicates the PDMS volume fraction. The dotted-line brackets in (D) show only the trends in the measured values and not the exact values. I and II indicate pristine PDMS (M_n = 4,700) combined with pristine PMMA, and pristine PTFEMA, respectively.

and t represents T_1^H.

Thus, this implies that in M129, PDMS and PMMA are dispersed homogeneously within regions that are 19 nm in diameter. Similarly, the specimens M147 and M432, which had different PDMS M_n values, showed T_1^H values with relatively small dispersion, and both were determined to have a similar diameter of homogeneously dispersed range.

Alternatively, T_1^H values at peak (a) for the specimens M442, T436, and T446, all with an M_n of 4,700, showed higher values than those of M129, M147 and M432. Because the longer T_1^H values correspond to higher degrees of molecular motion, this implies that a larger PDMS M_n results in more molecular motion, a higher diffusivity of gas molecules and a higher gas permeability, similar to the observation using the CP-MAS spectra. A longer T_1^H value also corresponds to inefficient spin diffusion and results in phase separation of PDMS and PMMA or PTFEMA. Therefore, these results correspond well with my previous report.[9)]

MMA copolymers with a higher PDMS content showed higher values of T_1^H at peak (a), as shown in Figure 1-2-2A. Alternatively, TFEMA copolymers with a higher PDMS content, T446, showed lower T_1^H values. At the same time, the dispersion of the T_1^H values of all peaks of T446 was smaller than that of T436, suggesting differences in the microstructure among T446 and other copolymers. Previously, different morphologies have been reported from copolymers with different ratios of constituents or different M_n values using TEM observations of the acrylate/PDMS macromonomer copolymer.[5)] Therefore, the aforementioned results suggest that a similar morphology in the TFEMA copolymer may appear at a lower PDMS content than that in the MMA copolymer. Furthermore, the smaller dispersion of T_1^H values of all peaks from T446 implies the finer structure or more continuous structure in T446 than that in T436 or M442. Thus, resulting differences in gas permeability for MMA copolymers and TFEMA copolymers can be expected. Therefore, the reported oxygen permeability

increase[14] can be supported by the possible differences in morphology.

These observations with respect to the correlation between morphology and dispersion of T_1^H values could explain the T_1^H value at peak (a) in M432.

$T_{1\rho}^H$ vs PDMS M_n, PDMS volume fraction, and co-monomer

The $T_{1\rho}^H$ value reflects motion modes of the order of several kHz, which appear primarily in the main chain of the polymer. The relationship between the spin-diffusion phenomenon and molecular mobility is the same as with T_1^H.

As shown in Figure 1-2-2B, specimen M147, with a PDMS M_n of 1,700 and a PDMS volume fraction of 0.47, showed minimum dispersion among all $T_{1\rho}^H$ values. Because this implies effective spin diffusion, the diameter of the homogeneously distributed area (domain size) was calculated to be 2.6 nm by the equation (1). This suggests that in M147, PDMS and PMMA are dispersed homogeneously in an area with a diameter of 2.6 nm. Similarly, the dispersion structure of M129 is considered to be the same as that of specimen M147, suggesting that the 1,700 M_n PDMS macromonomer did not influence the microphase separation when the PDMS volume fraction ranged from 0.29 to 0.47. This suggests that a smaller M_n results in a transparent copolymer and could explain the results related to copolymer transparency shown in Table 1-2-1.

Comparison of the $T_{1\rho}^H$ values of specimens with different PDMS M_n values suggested that a larger PDMS M_n value caused higher $T_{1\rho}^H$ values at peak (a) from 13.8 and 12.4 msec to 23.6, 20.2, 25.1, and 18.1 msec. Specifically, the influence of $–OSi(CH_3)_2–$ chain length on the molecular mobility and gas permeability can be observed using the $T_{1\rho}^H$ value and the T_1^H value.

As shown in Figure 1-2-2B, a comparison of the $T_{1\rho}^H$ values at peak (a) of the specimens with different PDMS volume fractions showed that higher PDMS volume fractions resulted in lower $T_{1\rho}^H$ values. The magnitude of change in the $T_{1\rho}^H$ value depended on the PDMS M_n and co-monomer type. It is interesting that the nature of the

$T_{1\rho}^{H}$ dependency on PDMS content is opposite to that of T_1^{H}.

Furthermore, T446 displayed a somewhat reduced dispersion of all $T_{1\rho}^{H}$ values when compared with the distinct separation of $T_{1\rho}^{H}$ values among peak (a) and the other peaks (b), (c), (e), (f), (g), and (h) in T436. In addition, it is interesting that the $T_{1\rho}^{H}$ values at peak (g) (C in CF_3 group) and peak (h) (C in C=O group) are close in value to those of peak (a) in T446. A comparison of $T_{1\rho}^{H}$ for T446 and M442 led to the same result. These results can be correlated to the possible existence of domain dispersion of the order of several nm or another morphology with finer structures or more continuous structures in T446 than those in T436 or M442. These differences in morphology could lead to the observed difference in gas permeability and support the previously reported results.[14)]

T_1^{C} Values

Results from the T_1^{C} measurements are shown in Figure 1-2-2C. Because the spin-diffusion phenomenon does not occur in the ^{13}C nucleus, independent T_1^{C} values for each C atom were available. This relaxation time also reflects the molecular motion at a frequency of several MHz. Comparing the T_1^{C} data from M129 and M147, both with a PDMS M_n of 1,700, it was determined that the T_1^{C} values of peaks (c), (d), and (h) decreased with an increase in PDMS content. Differences between M432 and M442, both with a PDMS M_n of 4,700, could not be found. However, the decrease in T_1^{C} from peaks (c), (f), and (h) for specimens T436 and T446, both with a PDMS M_n of 4,700, and the PTFEMA copolymer, was recognized with an increase in PDMS content. The decrease in T_1^{C} means an increase in the molecular mobility because these peaks result from PMMA or PTFEMA that have a high T_g value and the applicability of the relationship $\omega_c\tau \gg 1$, where ω_c is angular velocity of the ^{13}C nucleus and τ is the correlation time. Therefore, these T_1^{C} values suggest a difference in the mobility of PMMA or PTFEMA when comparing the M129 and M147, as well as T436 and T446.

$T_{1\rho}^{C}$ vs the PDMS M_n value, the PDMS volume fraction, and the co-monomer

$T_{1\rho}^{C}$ yields information with respect to molecular motion on the order of several kHz, similar to $T_{1\rho}^{H}$, and independent $T_{1\rho}^{C}$ values are available. Results from the measurements are shown in Figure 1-2-2D. $T_{1\rho}^{C}$ values from peak (a) for pristine PDMS, peaks (c) and (h) for pristine PMMA and PTFEMA, peak (g) for pristine PTFEMA, and peaks (g) and (h) for T436 are plotted only to demonstrate the trends in the measured values and are not exact values because of the possible measurement errors.

From Figure 1-2-2D, it was suggested that a higher $T_{1\rho}^{C}$ value at peak (a) was obtained in specimens with a larger PDMS M_n when the PDMS volume fraction ranged from 0.29 to 0.36. In other words, it is suggested that the longer –$OSi(CH_3)_2$– chain resulted in higher molecular mobility and in higher gas molecule permeability, as was also observed in the T_1^{H} and $T_{1\rho}^{H}$ measurements. Moreover, it is interesting that the $T_{1\rho}^{C}$ value at peak (a) in the TFEMA/PDMS copolymer is larger than that of the MMA/PDMS copolymer and that the $T_{1\rho}^{C}$ values at peak (g) and (h) are larger than that at peak (a). This implies amplified molecular motion in the –$OSi(CH_3)_2$– chain, –CF_3 group, and –C=O group and results in a large contribution from the fluorine-containing group to the oxygen permeability, as has been previously reported.[14)]

Phase size and phase separation estimation

Specimens containing PDMS with an M_n of 1,700 exhibited a homogeneously dispersed structure with a diameter of 2.6 nm. When PDMS with a M_n of 4,700 was employed, some samples showed a homogeneously dispersed structure with a diameter of approximately 20 nm; therefore, from the viewpoint of a scale on the order of several nm, all specimens had a phase-separated structure.

1.2.4 Conclusions

^{13}C solid-state NMR measurements were conducted to investigate the molecular-level relationship between the physical properties and the composition of copolymers produced from methacrylates, PDMS macromonomers, and crosslinkers. Using the data from T_1^H and $T_{1\rho}^H$, it was suggested that a larger PDMS M_n value resulted in a higher molecular mobility of –$OSi(CH_3)_2$–, and the high mobility could be correlated to a higher gas permeability. In addition, the copolymer with a M_n of PDMS of 1,700 was found to have a homogeneously dispersed structure with a diameter of approximately 3 nm. PDMS with higher values of M_n, such as 4,700 M_n PDMS, resulted in a phase-separated structure on the order of several nm and eventually resulted in a homogeneously dispersed structure with a diameter of tens of nm. This result could be correlated to the appearance of the copolymer.

Differences in the morphology of MMA copolymers and TFEMA copolymers were suggested from the T_1^H, $T_{1\rho}^H$, and $T_{1\rho}^C$ measurements. Copolymerization of CF_3-bearing TFEMA resulted in a larger $T_{1\rho}^C$ value at peak (a), and the –CF_3 (g) and –C=O (h) groups showed higher $T_{1\rho}^C$ values than that of the –$OSi(CH_3)_2$– chain. The described results implied that the amplified molecular motion of aforementioned groups is related to the mechanism of increased oxygen permeability in copolymers produced from fluorine-bearing monomers and the PDMS macromonomer.

1.2.5 References

1) Yamanaka, K. and Inoue, T. *Polymer* **1989**, *30*, 662.
2) Bruns, N., Scherble, J., Hartmann, L., Thomann, R., Iván, B., Muellhaupt, R. and Tiller, J.C. *Macromolecules* **2005**, *38*, 2431.
3) Yamamoto, K., Ito, E., Fukaya, S. and Takagi, H. *Macromolecules* **2009**, *42*, 9561.
4) Yu, X., Nagarajan, M.R., Li, C., Speckhard, T.A. and Cooper, S.L. *J. Appl. Polym.*

Sci. **1985**, *30*, 2115.

5) Mazurek, M., Kinning, D.J. and Kinoshita, T. *J. Appl. Polym. Sci.* **2001***, 80*, 159.

6) Havens, J.R. and VanderHart, D.L. *Macromolecules* **1985**, *18*, 1663.

7) Clauss, J., Schmidt-Rohr, K. and Spiess, H.W. *Acta Polymer.* 1993, *44*, 1.

8) Cho, G., Natansohn, A., Ho, T. and Wynne, K.J. *Macromolecules* **1996,** *29*, 2563.

9) Yokota, M., Goshima,T. and Itoh, S. *J. Brit. Contact Lens Assoc.***1992**, *15*, 125.

10) Asano, A. Takegoshi, K. and Hikichi, K. *Polymer* **1994**, *35*, 5630.

11) McBrierty, V.J. and Douglass, D.C. *J. Polym. Sci. Macromol. Rev.* **1981**, *16*, 295.

12) Demco, D.E., Utitu, L., Tilmann, W., Blümich, B. and Popescu, C. *Chem. Phys. Lett.* **2011**, *509*, 62.

13) Asano, A., Eguchi, M., Shimizu, M. and Kurotsu, T. *Macromolecules* **2002**, *35,* 8819.

14) Koßmehl, G., Fluthwedel, A. and Schäfer, H. *Makromol. Chem.* **1992**, *193*, 157.

1.3 Transmission Electron Microscopic Observations of the Multilevel Microstructure of Crosslinked Copolymers with Methacrylates and Siloxane Macromers by a Radically Polymerizable Tuning Approach

1.3.1 Introduction

The relationship among internal structure, gas permeability, and transparency in copolymer networks, which were composed of methacrylates and siloxane macromers, have been studied. The effects of the solubility parameter of methacrylate on the gas permeability and possibly the morphology were observed as stated in Section 1.1.[1)] Furthermore, the study on the microstructure of those copolymers with solid state CP-MAS NMR have been also carried out, and it was found that molecular mobility of not only PDMS but also the substituted group of methacrylates was affected by polymer composition such as PDMS M_n, PDMS content and methacrylate type as stated in Section 1.2.[2)] Thus, the correlation between the molecular mobility and the copolymer composition dependency of oxygen permeability, is strongly suggested.

The copolymer material had been prepared using PIPS,[3,4)] which is a convenient method to prepare microheterophases from a homogeneous solution of reactive monomeric compounds and polymeric compounds. This technique has been reported in many fields, such as the polymerizations of monomer/polymer mixtures[5–7)] and hydrogels.[8)] PIPS technology using radically polymerizable PDMS macromers has been applied to copolymers with hydrophilic vinyl monomers[9–11)] and hydrophobic vinyl monomers.[12,13)] Studies on PIPS with hydrophilic vinyl monomers usually focus on the structure and dynamics of the resultant amphiphilic network, and PIPS examples of hydrophobic vinyl monomers show the effect of the monomer structures and the polymerizable groups of PDMS. It is one of the merits of radical copolymerization with vinyl monomers that the composition ratio and M_n of PDMS macromer can be controlled. Thus, it is possible to perform a systematic study on the relationship between

physical properties and copolymer compositions, although there have been no reports on the PIPS microstructures generated from PDMS macromers, with systematic tuning of the composition and components, to our best knowledge.

In this work, I focused on the internal microstructures observed by TEM for crosslinked copolymers composed of methacrylate monomers and PDMS macromers, and the relationship between the morphologies and their compositions was discussed. The TEM observation in this study could give some insight into the properties such as oxygen permeability and light transmittance.

1.3.2 Experimental Section

Materials and Preparation of the crosslinked copolymers composed of methacrylate monomer/PDMS macromer

PDMS macromer was purchased from Shin-Etsu Chemical Co., Ltd. and used without further purification. MMA (Wako Pure Chemical Industries), TFEMA (Osaka Organic Chemical Industry Ltd.), 1G (Shin-Nakamura Chemical Co., Ltd.), V-65 (Wako) and V-40 (Wako) were used without further purification.

M_n measurements of PDMS macromers by ^{1}H NMR and SEC method as well as the preparation of crosslinked copolymer were carried out in the same way as aforementioned in Section 1.1.2. Measured PDMS macromer molecular weights are shown in Table 1-1-1 and chemical structures of the monomers and crosslinker are shown in Figure 1-1-1.

TEM observation

The test specimens were cut from the crosslinked copolymer of 0.2 mm thickness, vacuum dried, and embedded in epoxy resin Quetol 812 (NISSHIN EM Co., Ltd., Tokyo, Japan) without any staining. Ultrathin sections were cut with a diamond knife on an ultramicrotome, ULTRACUT E (Reichert-Jung Optishe Werke AG,

Austria). The TEM observations were performed with a JEM 1200-EX transmission electron microscope (JEOL Ltd., Tokyo, Japan) at an accelerating voltage of 80kV. The composition and other parameters of the test specimens are shown in Table 1-3-1.

Table 1-3-1. Composition[a] of the specimens employed in this study

Code	Acrylic monomer		PDMS macromer		PDMS fraction[b]	
	Type	Weight	PDMS M_n	Weight	Weight	Volume
A	MMA	80	1,700	20	0.17	0.20
B	MMA	50	1,700	50	0.42	0.47
C	MMA	40	1,700	60	0.51	0.56
D	MMA	70	4,700	30	0.28	0.32
E	MMA	60	4,700	40	0.38	0.42
F	MMA	40	4,700	60	0.57	0.62
G	TFEMA	70	4,700	30	0.28	0.36
H	TFEMA	60	4,700	40	0.38	0.46
I	TFEMA	50	4,700	50	0.47	0.56

[a] Parts of weight for 1G is acrylic monomer×(1/100) for all code.
[b] PDMS weight fraction and volume fraction were calculated using PDMS weight which was obtained from the subtraction of the weight of methacryloyloxypropyl group from PDMS macromer. Volume fraction was estimated with feed composition assuming that all constituents are not miscible, the density value is 0.98, 1.41, 1.19 for PDMS, PTFEMA, and PMMA including poly(1G) respectively.

1.3.3 Results and Discussion

Observations at low magnifications

Without any staining of the specimens, all observations were carried out successfully as sufficient contrast was obtained for all specimens because of their electron density difference. Volume fraction was estimated with feed composition assuming that all constituents are not miscible, the density value is 0.98, 1.41, 1.19 for PDMS, PTFEMA, and PMMA including poly(1G) respectively.

Figure 1-3-1 shows TEM images of all of the specimens listed in Table 1-3-1 at 20,000-fold magnifications. Figures 1-3-1a, 1-3-1b, and 1-3-1c are the results from

specimens A, B, and C bearing 1,700 g/mol M_n PDMS. According to the increase of PDMS content, which PDMS volume fraction is 0.2, 0.47, and 0.56 for specimen A, B, and C respectively, the domain size was decreased from 300 nm or more (Figure 1-3-1a), to 100–300 nm (Figure 1-3-1b), and to several 10 nm (Figure 1-3-1c), generating finer structures.

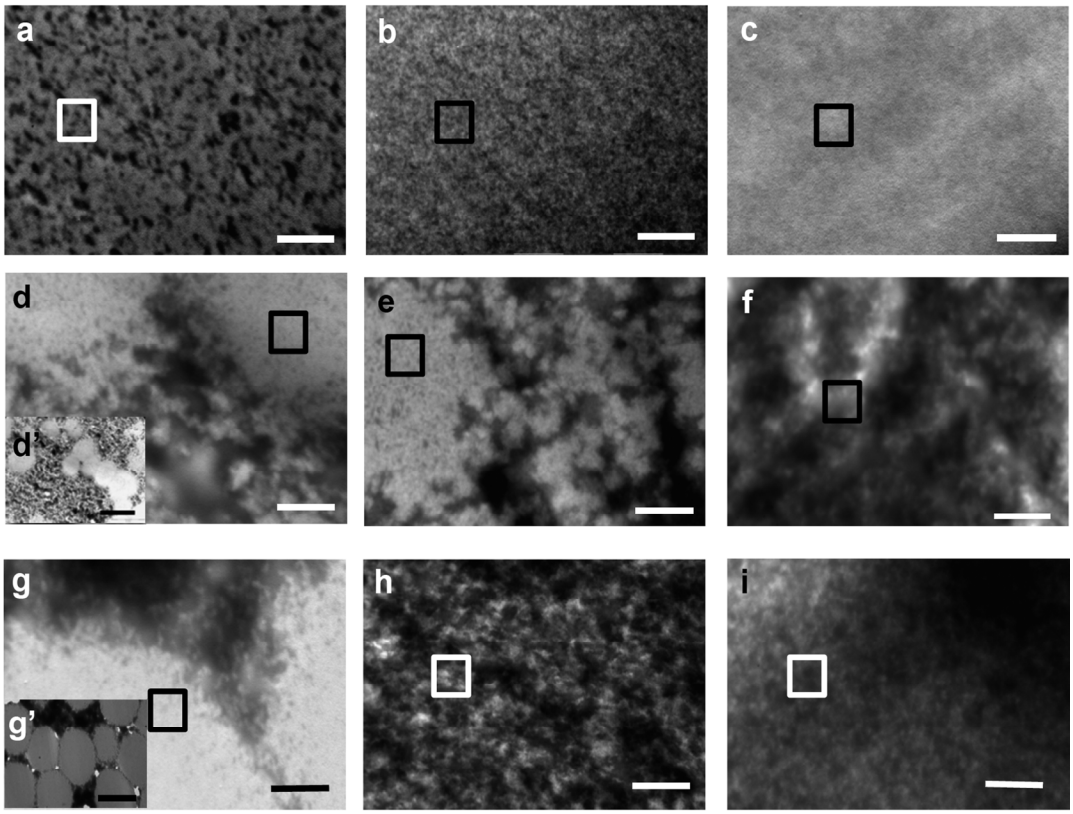

Figure 1-3-1. TEM images at 20,000-fold magnification of specimen A (a), specimen B (b), Specimen C (c), specimen D (d), specimen E (e), specimen F (f), specimen G (g), specimen H (h), and specimen I (i). Scale bar indicates 500 nm. Brighter and darker parts correspond to PMMA or PTFEMA rich phase and PDMS rich phase respectively. Inset images d' and g' were obtained at 10,000-fold magnification. Scale bar in inset indicates 5 μm. Square means observed position at 100,000-fold magnification in Figure 1-3-2.

The PMMA enriched island possessing domain sizes of several μm was observed in specimens D (4,700 g/mol of M_n) (Figure 1-3-1d and 1-3-1d'), which is quite different from specimen A (Figure 1-3-1a) with a similar volume fraction using

the short PDMS chains. Comparing the results from specimen D with those from specimen E and F, with increase of PDMS content (PDMS volume fraction is 0.32, 0.42 and 0.62 for specimen D, E, and F respectively), the domain size reduction of PDMS phase was found from several μm (Figure 1-3-1d) to 1–2 μm (Figure 1-3-1e) and sub-μm to μm size (Figure 1-3-1f).

With regards to specimen G (Figure 1-3-1g), in which TFEMA was copolymerized with PDMS (M_n = 4,700 g/mol), the PTFEMA enriched island structure possessing several μm was also observed, which was clearly observed by inset pictures with 10,000-fold magnification (Figure 1-3-1g'). The contrast between the two phases was clearer than the aforementioned specimen D (Figure 1-3-1d), probably due to the composition of phases. The domain size in specimen G is larger than that of specimen D. Furthermore, most of the spaces between the islands seemed to consist of PDMS domains (dark parts), and the PDMS domains existed also in the PTFEMA islands at 20,000 -fold magnification (Figure 1-3-1g).

In addition, with increase of PDMS content (PDMS volume fraction is 0.36, 0.46, and 0.56 for specimen G, H, and I respectively), the domain size reduction of PDMS phase was also found from several μm (specimen G) to 500 nm (specimen H) and 200–300 nm size (specimen I) (Figures 1-3-1g, 1-3-1h, and 1-3-1i).

TEM observation at high magnification and PDMS domain size measurement

The TEM observation results at a high magnification (100,000-fold magnification) from all specimens are shown in Figure 1-3-2. Comparisons between Figure 1-3-1 and Figure 1-3-2 with the same alphabetical letter suggested that, for example, the observation of specimens A at higher magnification (100,000-fold magnification) demonstrated that a microstructure appeared (Figure 1-3-2a) which was not observed in Figure 1-3-1a. It is suggested that the new structure appearing *de novo* (dark part) was the coagulated small PDMS domain. Figure 1-3-1b (specimen B) and

Figure 1-3-1c (specimen C) also showed fine structures and distributed PDMS domains, whereas Figure 1-3-2b and Figure 1-3-2c showed the finer microstructure.

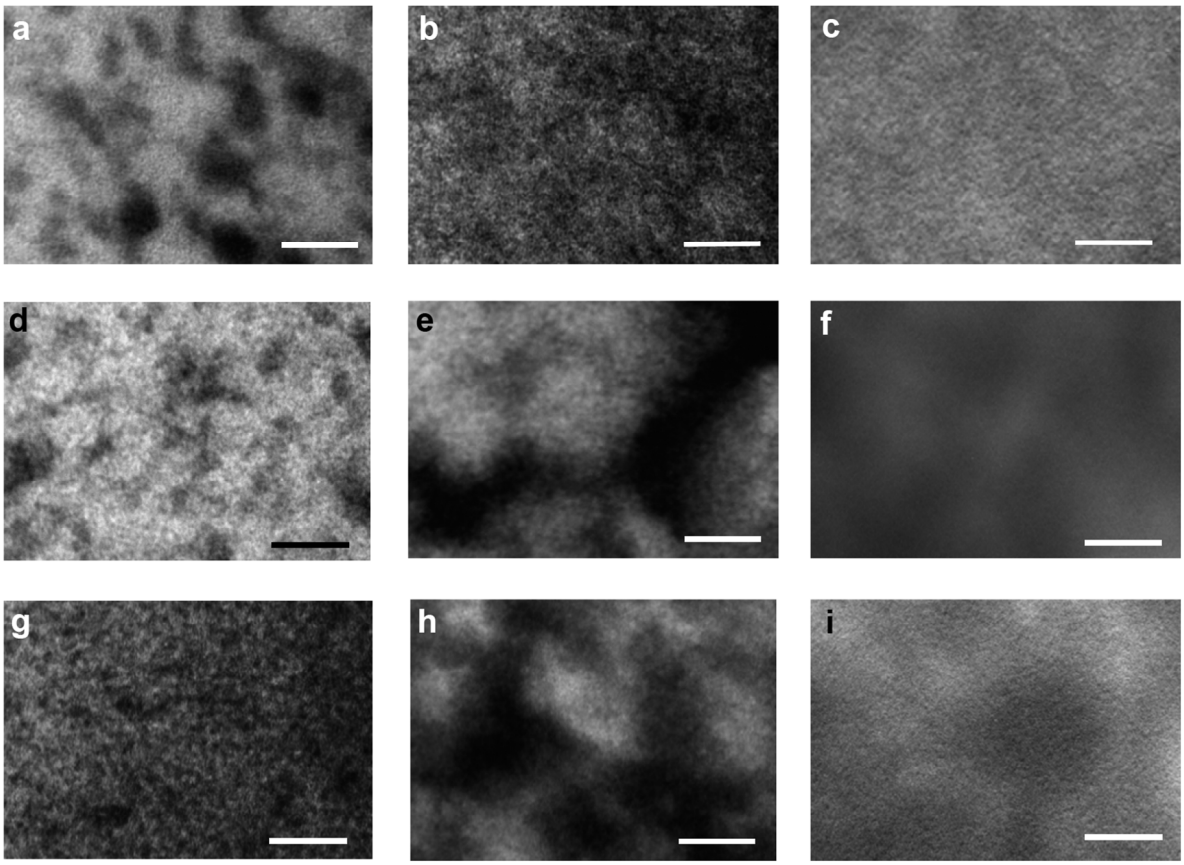

Figure 1-3-2. TEM images at 100,000-fold magnification of specimen A (a), specimen B (b), specimen C (c), specimen D (d), specimen E (e), specimen F (f), specimen G (g), specimen H (h), and specimen I (i). Brighter and darker parts correspond to PMMA or PTFEMA rich phase and PDMS rich phase. Scale bar indicates 100 nm. Observed locations correspond to marked area in Figure 1-3-1.

It is interesting that the similar microstructures which have fine structure and coagulated PDMS domains of 100–200 nm size, were seen in specimens D and G (Figures 1-3-2d and 1-3-2g), although difference in island/sea area ratio and that in dark/bright area ratio in the sea phase were seen between Figure 1-3-1d (or Figure 1-3-1d') and Figure 1-3-1g (or Figure 1-3-1g'). In addition, while difference in the domain size and pattern between Figures 1-3-1e and 1-3-1h was seen, specimen E and

specimen H showed similar fine microstructure which consisted of fine structure and coagulated PDMS domains of 100–200 nm size at 100,000-fold magnifications (Figures 1-3-2e and 1-3-2h). Similarly, while difference in the domain structure and domain size between Figures 1-3-1f and 1-3-1i was seen, specimens F and I also showed similar fine microstructure which consisted of fine structure and coagulated PDMS domains of 100–200 nm size at 100,000-fold magnification (Figures 1-3-2f and 1-3-2i). Thus, it is apparent that all of the observation results in Figure 1-3-2 at 100,000-fold magnification showed the minimum domain size or microstructure, which can be interpreted as them having almost the same "fundamental domain size".

To confirm this assumption, I measured the domain size on the TEM images using the loupe with 10 times greater magnification (n = 30). As shown in Table 1-3-2, the domain sizes of the 1,700 g/mol M_n PDMS were 4.3 nm (specimen A) and 4.4 nm (specimen B), whereas those of the 4,700 g/mol M_n PDMS were 5.5 nm (specimen D), 5.1 nm (specimen E), 5.4 nm (specimen G), and 4.8 nm (specimen H), respectively. These values are appropriately correlated to the M_n of PDMS macromer when they were compared to the results of ca.13.3 nm for the characteristic periodicity from the copolymer of PDMS diacrylate with 6,500 g/mol M_n and the dimethylacrylamide reported by K. Yamamoto and co-workers.[11] Therefore, it is suggested that the bulk properties are influenced by two types of microstructure at different magnification level; one of which is the microstructure consisting of the "fundamental domains" and the other is the microstructure consisting of the aggregation of "fundamental domains". For example, the oxygen permeability could be influenced not only by the "fundamental domain size", but also by the microstructure due to the aggregation of fundamental domains as suggested by Figures 1-3-2d and 1-3-2g. On the other hand, the transparency could be influenced only by the microstructure from the aggregation of the fundamental domains.

This unique different type microstructure at different magnification level could

Table 1-3-2. PDMS measured domain size in crosslinked copolymers [a]

Code	Acrylic monomer	PDMS		Measured domain size
		M_n	Volume fraction	(nm)
A	MMA	1,700	0.20	4.3±0.4
B	MMA	1,700	0.47	4.3±0.4
D	MMA	4,700	0.32	5.5±0.5
E	MMA	4,700	0.42	5.1±0.4
G	TFEMA	4,700	0.36	5.4±0.5
H	TFEMA	4,700	0.46	4.8±0.6

[a] n=30.

be formed by the PIPS process as follow: in the first stage of PIPS process, due to the existence of large quantity of methacrylate monomer as solvent, fine structure (fundamental domain) in nm scale could be formed. While the progress in polymerization causes the reduction of methacrylate monomer as solvent, and this could lead to the phase separation or coagulation of fundamental domains in μm to sub-μm scales which are shown in Figure 1-3-1. The polymer properties such as miscibility and solubility parameter could affect the morphology of phase separation. Similar coexistence of μm scale structure and nm scale structure in spinodal decomposition of sol-gel process with various surfactant concentrations has been reported.[14] Thus, it is suggested that PIPS is very important method to design and prepare the copolymer microstructure and resultant physical properties.

Correlation of the morphology between the results from low maginification level and high magnification level

For further understanding of this specific correlation of morphology, I conducted the TEM observation of islands phase and sea phase from specimen D which showed highly phase separated internal structure from the copolymer of PDMS macromer (M_n = 4,700 g/mol) with MMA at a 0.32 PDMS volume fraction. The observation results are shown in Figure 1-3-3.

It is noteworthy that many large (several μm) domains were observed in Figure 1-3-3a at 10,000-fold magnification. The PMMA enriched phase (bright part) existed as "islands" (isolated domains) at several μm order size, and the other composition phase in the spaces around the PMMA enriched islands showed the presence of both PDMS (dark part) and PMMA. At a higher 100,000-fold magnification (Figure 1-3-3b), in PMMA island, fine dark PDMS domains having several nm to 10 nm size and small amount of large PDMS domains (50–60 nm) were found in the bright continuous PMMA phase. On the contrary, in PDMS rich phase, fine dark PDMS domains having several nm to 10 nm size and large amount of more large PDMS

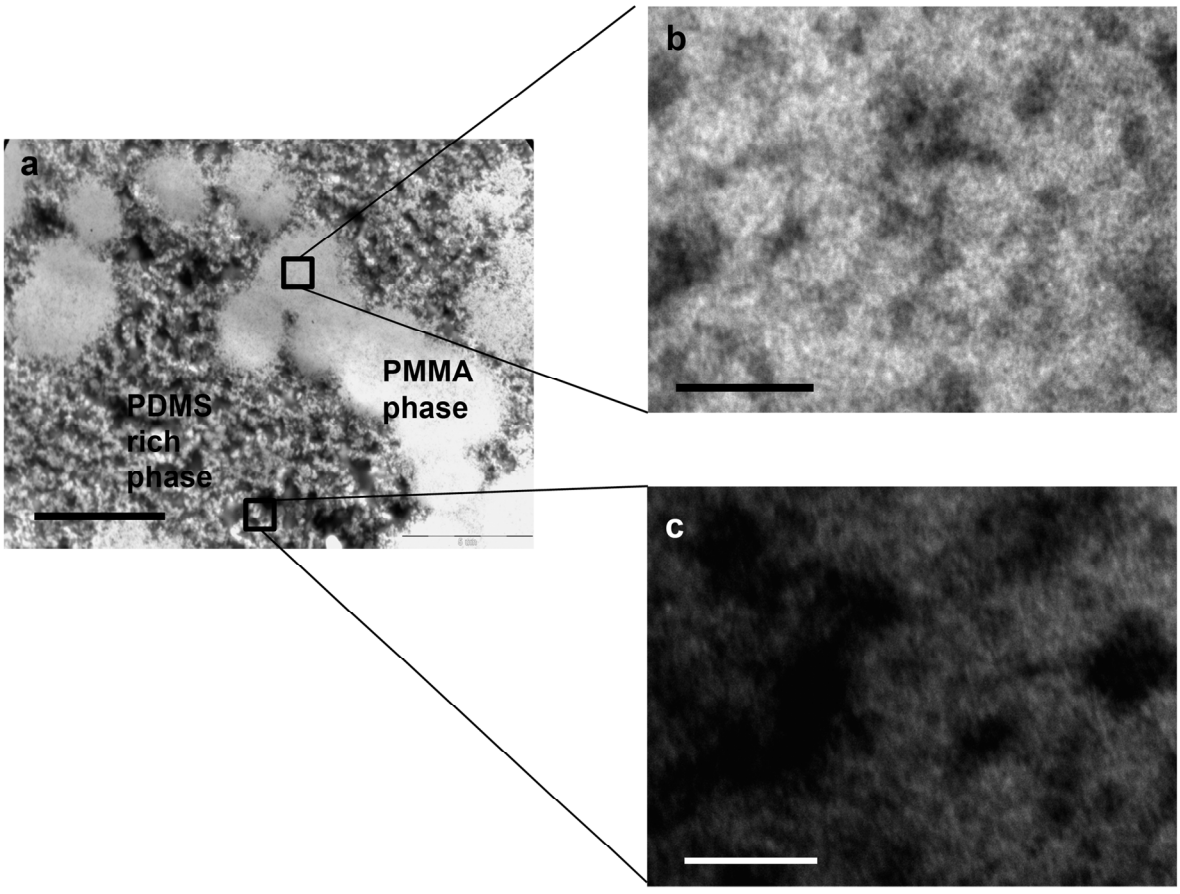

Figure 1-3-3. Correlation of the morphology between different magnification levels of specimen D. (a) was obtained from 10,000-fold magnification. (b) and (c) are PMMA phase and PDMS rich phase respectively, and obtained from 100,000-fold magnification observation. Scale bar shows 5 μm (a), 100 nm (b, c). Bright phase is PMMA and dark phase is PDMS.

domains having about 50–60 nm size were found. Thus, it was found that the present crosslinked copolymers possessed two types of phase separations with μm and nm orders in any composition, and the composition influenced the size of PDMS domain at the larger phase separation level. It was also demonstrated that the two phases possessed different PMMA/PDMS ratios, one of which was greater than 1.0 (the island part), and the other was near 1.0 (the sea part).

PDMS M_n, PDMS content and morphology at low magnification level

As aforementioned, the PDMS M_n effect was clearly observed between the 1,700 g/mol M_n and 4,700 g/mol M_n PDMS. Lower M_n gave finer domain structure suggesting that the miscibility between PMMA or PTFEMA and PDMS affected the morphology.

It is natural that the transparency of the specimen appearance was related to its morphology. Specimens A, B, and C bearing 1,700 g/mol M_n PDMS were transparent, and had small domain sizes of 300 nm or more (Figure 1-3-1a), 100–300nm (Figure 1-3-1b), and several 10 nm (Figure 1-3-1c). In contrast, specimens D, E and F with a 4,700 g/mol M_n showed an opaque appearance due to light scattering at the domain boundaries of the several μm order size (Figures 1-3-1d, 1-3-1e, and 1-3-1f). Thus, it is important to understand the morphologies for the preparation of transparent samples, which is mostly due to the PDMS polymer chain length (PDMS M_n).

In addition, it was clear that a low PDMS content in the range of 0.2 to 0.36 volume fractions (specimens D and G) caused the island shape of the methacrylate polymer phase (Figures 1-3-1d(1-3-1d') and 1-3-1g(1-3-1g')), although the island sizes were different. On the other hand, the middle PDMS content over the range of 0.56 to 0.62 volume fractions (Figures 1-3-1c, 1-3-1f, and 1-3-1i) caused a domain size reduction, and a further continuous phase of the methacrylate polymer. Thus, by changing the composition or PDMS content systematically, the effect of the PDMS

content on the morphology was clarified. The present results gave us essential information on the microstructure, because the morphology is closely associated with the bulk properties.

The importance of the polymerization mixture viscosity in the morphology formation of 2-chlorostyrene/polystyrene PIPS system has been reported by M. Okada and co-workers.[5] It was reported that high viscosity caused the reduced polymer diffusion and this determined the degree of continuous phase formation. Thus island microstructure which was found in specimen D and G (Figures 1-3-1d and 1-3-1g) could result from low viscosity with high monomer content (70 wt%), and the domain size reduction with increased PDMS content could result from high viscosity due to the PDMS M_n and two polymerizable groups in PDMS macromer in polymerization process.

Effects of the methacrylate monomer type on morphology

Next, the influence of the monomer type on the microheterophase structure was examined in detail using specimen D (Figure 1-3-4a) and specimen G (Figure 1-3-4b). I first noticed that specimen D, which was copolymerized with MMA, left relatively small “island” shaped spheres that were rather scattered (Figure 1-3-4a). In contrast, specimen G with TFEMA resulted in larger ovals for the PTFEMA domains, and showed closely packed islands with small dark phases mostly composed of PDMS in the spaces between islands.

To consider the differences in the microphase separation by monomer type, I tried to estimate the area fraction of each “island” part from Figures 1-3-4a and 1-3-4b by calculating the percentages of the oval parts against the total area (n = 3). In spite of the same PDMS weight fractions (0.28), the values differed greatly, showing a 37% ratio for the PMMA islands in specimen D and a 68% ratio for the PTFEMA islands in specimen G. This implied that there were different components ratios in the other “sea”

parts. In addition, PDMS phase (dark) of Figure 1-3-4b shows almost continuous one. Furthermore, comparison between specimens F and I (Figures 1-3-1f and 1-3-1i) which have increased PDMS content than specimen D and G, revealed that the morphology of specimen I correspond to the formation of the component's continuous phase. This formation of the continuous phase means a reduction in the barrier to oxygen permeation. Therefore, the copolymerization of PDMS macromer and TFEMA (specimen I, Figure 1-3-1i) instead of MMA (specimen F, Figure 1-3-1f) could lead to the formation of a morphology having more continuous phase. The oxygen permeability of the TFEMA copolymer would increase based on the phase separation difference, in addition to the original TFEMA character due to the fluoroalkyl groups. Thus, the higher oxygen permeability of the TFEMA copolymer than the MMA copolymer could be predicted from the TEM observations.[1)]

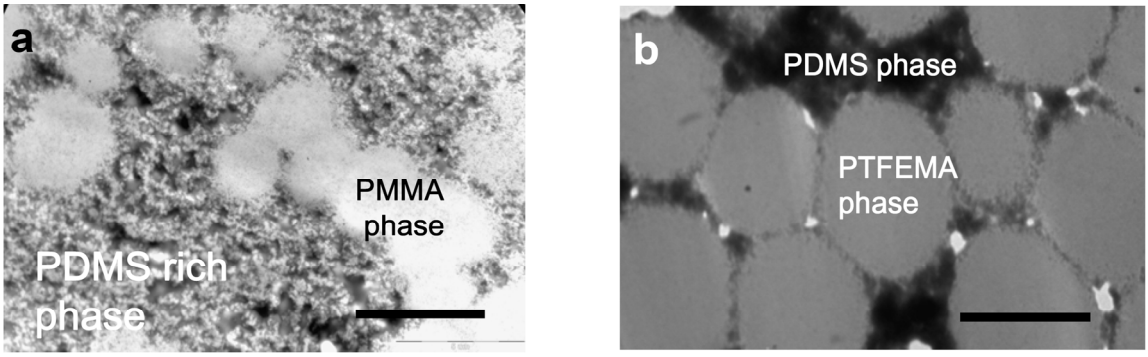

Figure 1-3-4. TEM images at 10,000-fold magnification for the comparison between specimen D (a) and specimen G (b). Scale bar indicates 5 μm. Small white area is due to the specimen defect from ultrathin sample preparation.

1.3.4 Conclusions

TEM observation of crosslinked copolymers prepared from methacrylate monomers, PDMS macromers with M_ns of 1,700 g/mol or 4,700 g/mol, and 1G were carried out. The microstructure of these copolymers depended on the PDMS content, the PDMS M_n, and the type of methacrylate co-monomer.

First, at low PDMS content, the specimens possessing 4,700 g/mol PDMS M_n

showed an “isolated domain” morphology with “islands” or isolated domains of methacrylate polymer dispersed throughout a “sea” like surrounding area. On the other hand, the specimens possessing 1,700 g/mol PDMS M_n showed finer microstructures. At higher PDMS contents, a different morphology was observed, which consisted of a continuous phase of methacrylate polymer and more homogeneously dispersed PDMS domains.

Second, in addition to the PDMS M_n, the employment of TFEMA instead of MMA affected the morphology, such as a different island surrounding area phase composition or structure, and a more homogeneous structure suggestive of better solubility or compatibility between the TFEMA or PTFEMA and the other components.

Third, observations at 100,000-fold magnification revealed that the specimens had a “fundamental” common morphology, and it was a co-continuous one. From measurements of this domain size, the PDMS M_n was concluded to influence this PDMS “fundamental” domain size. Thus, studies using the observation of two microstructures could be a novel tool for evaluating the relationship between morphology and physical properties.

On the basis of those findings, many bulk properties are expected to be predicted by morphology, such as T_g, transparency, and oxygen permeability.

1.3.5 References

1) Yokota, M., Ajiro, H. and Akashi, M. *J. Appl. Polym. Sci.* in press.
2) Yokota, M., Miwa, Y., Ajiro, H. and Akashi, M. *Polym. J.* **2012**, *44*, 301.
3) Yamanaka, K. and Inoue, T. *Polymer* **1989**, *30*, 662.
4) Inoue, T. *Prog. Polym. Sci*. **1995**, *20*, 119.
5) Wang, X. Okada, M. and Han, C.C. *Macromolecules* **2007**, *40*, 4378.
6) Okada, M., Inoue, G., Ikegami, T., Kimura, K. and Furukawa, H. *Polymer* **2004**, *45*, 4315.

7) Okada, M., Fujimoto, K. and Nose, T. *Macromolecules*, **1995**, *28*, 1795.

8) Kwok, A.Y., Prime, E.L., Qiao, G.G. and Solomon, D.H. *Polymer* **2003**, *44*, 7335.

9) Bruns, N., Scherble, J., Hartmann, L., Thomann, R., Iván, B., Muellhaupt, R. and Tiller, J. C. *Macromolecules* **2005**, *38*, 2431.

10) Hanko, M., Bruns, N., Rentmeister, S., Tiller. J.C. and Heinze, J. *Anal. Chem.* **2006**, *78*, 6376.

11) Yamamoto, K., Ito, E., Fukaya, S. and Takagi, H. *Macromolecules* **2009**, *42*, 9561.

12) Yu, X., Nagarajan, M.R., Li, C., Speckhard, T.A. and Cooper, S.L. *J. Appl. Polym. Sci.* **1985**, *30*, 2115.

13) Mazurek, M., Kinning, D.J. and Kinoshita, T. *J. Appl. Polym. Sci.* **2001**, *80*, 159.

14) Kanamori, K., Kodera, Y., Hayase, G., Nakanishi, K. and Hanada, T. *J. Colloid Interface Sci.* **2011**, *357*, 336.

Chapter 2

The Effect of Polymer Structure on Durability of Rigid Gas Permeable Materials

2.1 Introduction

Accompanying the development of many RGP materials with high oxygen permeability coefficient ($P(O_2)$ or Dk) over recent years, has been concern that these lenses tend to be more fragile and attract more deposits than do lower $P(O_2)$ having RGPs. Since the value of fluoroalkyl methacrylates and siloxanylalkyl methacrylates was revealed, most RGP materials have contained these two constituent monomers. Their chemical formulas are shown in Figure 2-1.

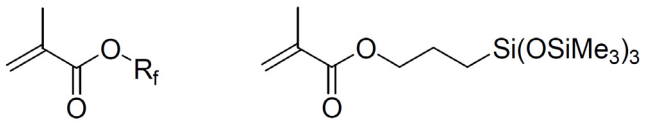

(a) (b)

Figure 2-1. The chemical formula of (a) fluoroalkyl methacrylate (R_f, fluorine containing group) and (b) typical example of siloxanylalkyl methacrylate, TRIS.

In order to prepare a high $P(O_2)$ in lens materials, increased use was made of these constituents. However, siloxanylalkyl methacrylate produces lower interchain forces than do PMMA, which has led to concern about fragility of higher $P(O_2)$ materials. To examine this problem, we have developed new methods of evaluating the physical properties of RGP materials in order to achieve the prediction of clinical performance. Tests of ball impact breakage strength and flexural breakage strength were made, in addition to the study of the physical microstructure of various RGP materials. The relationship between physical microstructure of materials and the breakage test results was examined. Furthermore, correlations between all three laboratory results and

published clinical data were also examined.

2.2 Experimental Section

Methods

Ball Impact Breakage Strength Test

The principle of the ball impact breakage test is shown in Figure 2-2. Test lenses were mounted onto the lower steel ball (of diameter 16.0 mm) and the upper ball (of diameter 11 mm and weight 5.4 g) was dropped from various heights. The height at which the breakage of each lens occurred was recorded. The parameters of the lenses used are shown in Table 2-1.

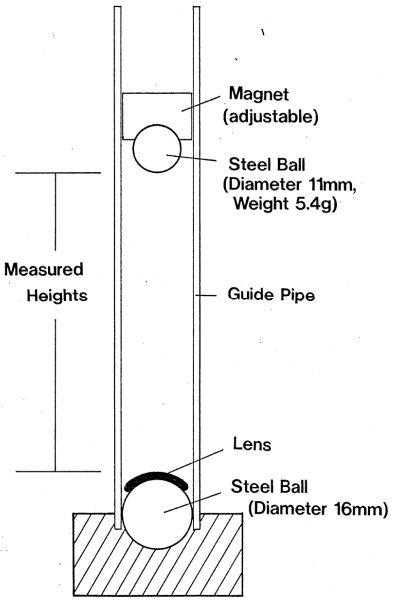

Figure 2-2. The principle of the ball impact breakage strength test.

Table 2-1. Parameters [a] of lenses used in the ball impact and flexural breakage strength tests

Material	Dk[b] by manufacturer	Center thickness nominal (mm)	Diameter nominal (mm)
A	150	0.17	9.0
B	105	0.16	8.8
C	92	0.17	8.8
D	71	0.17	8.9
E	52	0.15	8.8
F	26.3	0.16	8.8
G	12	0.11	9.0

[a] : Back surface radius (nominal) is 8.00mm, and power (nominal) is -3.00 diopter(D).
[b] : $\times 10^{-11}$ml(O_2)cm/cm^2·sec·mmHg.

Flexural Breakage Strength Test

The micro-spring tester (Fujii Seiki, FSP-55D) was used to compress the lens

vertically, i.e., to reduce the lens diameter. The minimum resolution of displacement was 0.01 mm and that of load was 0.1 gf. The percentage change in diameter at breakage was recorded. The parameters of the lenses used are shown in Table 2-1.

Observation of the Physical Microstructure of RGP Materials

Transmission electron microscopy (JEOL JEM-1200) was used to examine the microstructure of materials A–E (Table 2-1), as well as that of PMMA. The samples were prepared by an ultra-thin sectioning technique and observations were carried out using an acceleration voltage of 100kV.

2.3 Results

Ball Impact and Flexural Breakage Strength Tests

The results from the ball impact breakage strength test and flexural breakage strength test are shown in Figures 2-3 and 2-4. The breakage strength was not found to be correlated with the $P(O_2)$ of the material. Furthermore, the results from the two tests did not show good correlation.

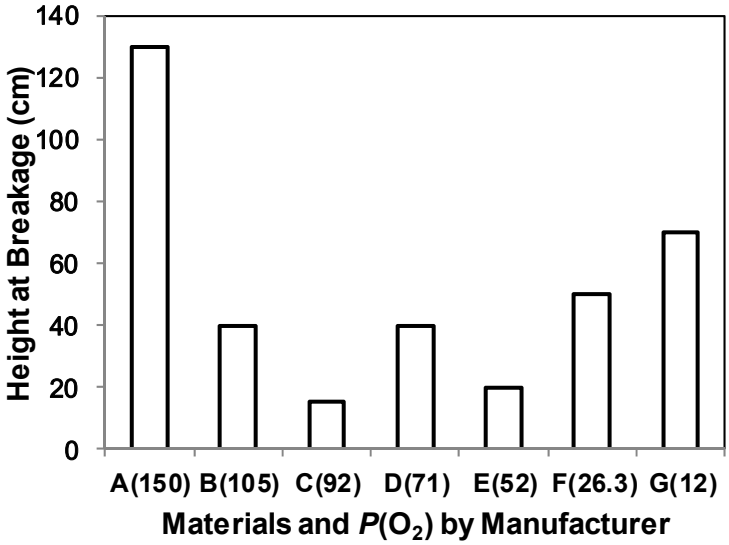

Figure 2-3. The results from the ball impact breakage strength test.

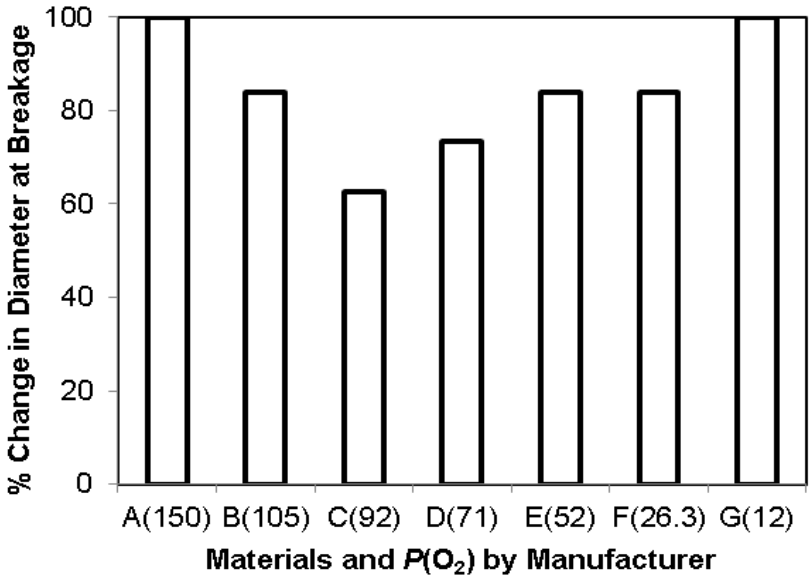

Figure 2-4. The results from the flexural breakage strength test.

Physical Microstructure of the RGP Materials

The TEM physical microstructures of the RGP materials are shown in Figures 2-5(a)–(e), and that of PMMA is also shown (Figure 2-5(f)) as a control. PMMA and RGP materials B–E (Figures 2-5(b)–(e), respectively) showed very similar homogeneous microstructures. Material A, on the other hand, showed microheterophase structure.

2.4 Discussion

There have been many reports that to maintain the healthiness of the cornea while wearing a contact lens, a sufficient oxygen supply, i.e., a high oxygen transmissibility (*Dk/L),* through the lens is required. To satisfy this need, many high $P(O_2)$ RGP materials have been developed. From the viewpoint of the polymer chemistry seeking to design a high $P(O_2)$ polymer composition, hydrogel lenses, in which water is the main constituent for the permeation of oxygen, are not advantageous because of the relatively low $P(O_2)$ (80–90) of water. Even if we could develop a 99% water content hydrogel contact lens materials, the $P(O_2)$ of this material cannot exceed

that of water. On the other hand, as silicone rubber has a $P(O_2)$ value of 600, the use of silicone make possible to formulate a material that has a $P(O_2)$ value of more than 100. However, silicone rubber materials are prepared with different method from those of

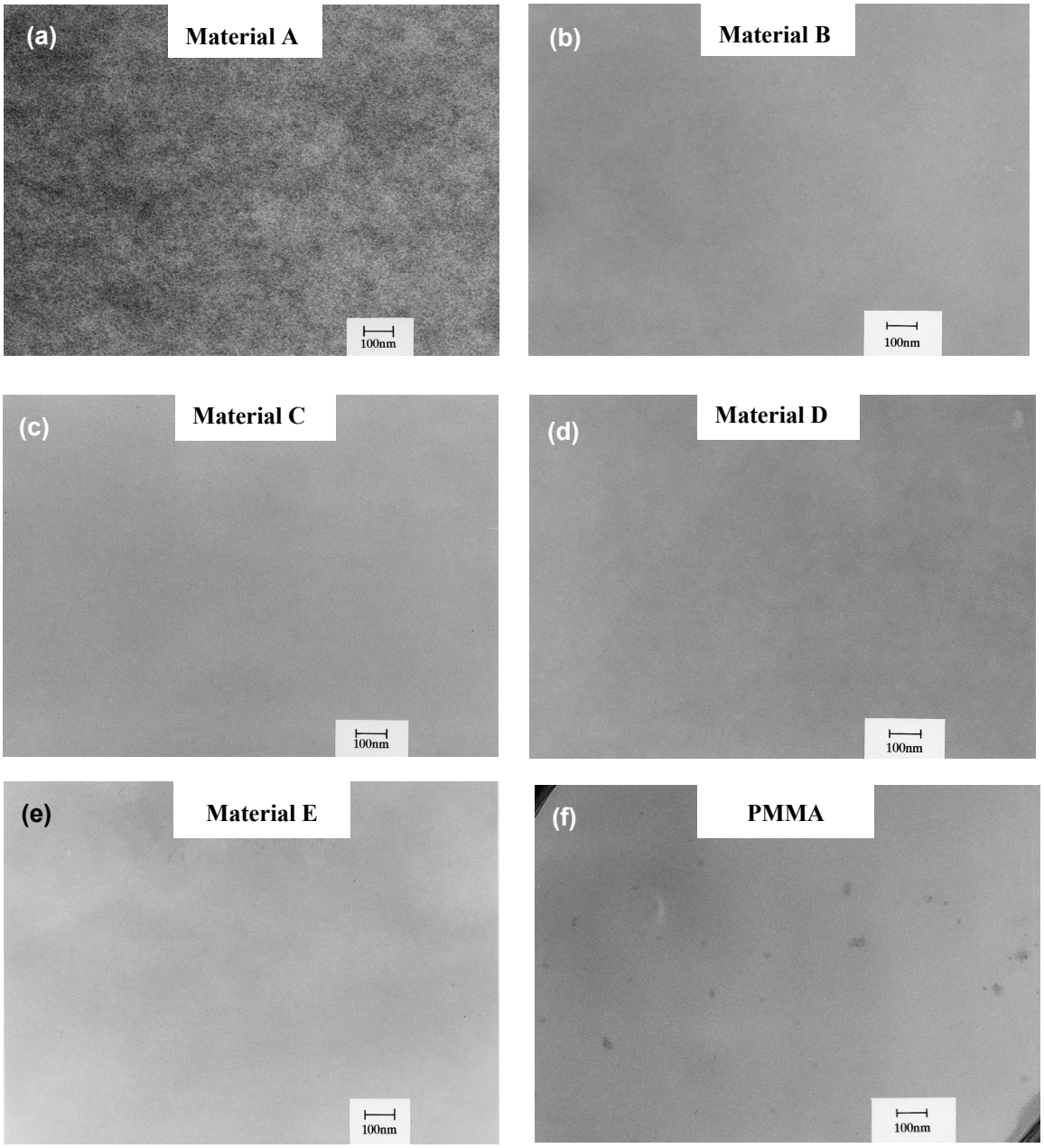

Figure 2-5. TEM photgraphs of materials. (a) Material A. Some dark domains are scattered randomly across the surface which correspond to oxygen permeable constituents. All of (b) Material B, (c) Material C, (d) Material D and (e) Material E, have the uniform structure which resembles to PMMA.

polymeric rigid contact lens materials, such as PMMA, which are generally obtained by radical polymerization. Thus it was the challenge to incorporate the oxygen permeable property of silicone into conventional contact lens material.

Overcoming this difficulty and introducing fluoroalkyl methacrylate or siloxanylalkyl methacrylate into contact lens materials was a great breakthrough, giving high oxygen permeability to contact lens materials as stated in General Introduction. This invention began the age of the RGP lens, and many high $P(O_2)$ RGP materials have been developed from this concept. We can demonstrate the following explanation by observing the microstructure of polymers using TEM. Based on the TEM photograph of PMMA (Figure 2-5(f)), the microstructure of PMMA is shown schematically in

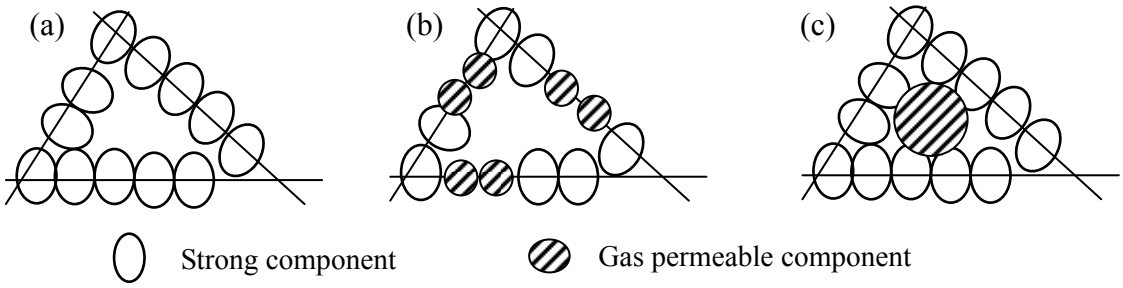

Scheme 2-1. Illustrative scheme of microstructure. (a) PMMA, (b) Materials B–E, (c) Material A.

Scheme 2-1(a). PMMA can be considered as a very strong polymer network, consisting of MMA and a crosslinking agent which provides PMMA with its well-known strength.

The similarity of the microstructures of the RGP materials B–E to that of PMMA suggests that the basic chemical framework of all these materials is similar, and that their polymer compositions are similarly built. The oxygen permeable components in these materials (such as siloxanylalkyl methacrylate) are introduced into the MMA network. This is shown schematically in Scheme 2-1(b). It is known that siloxanylalkyl methacrylate has a rather low intermolecular force and, therefore, the larger the proportion of this gas permeable constituent that is introduced into the polymer network

to increase $P(O_2)$, the more the polymer network will be weakened. The fragility of the material will then increase. RGP lenses of this physical microstructure may be responsible for the anecdotal reports of increased lens fragility with increased $P(O_2)$, although variations in the network structure are equally important in this respect.

Material A did not have the same physical microstructure as PMMA or materials B–E. It showed non-uniform microheterophase structure. The microstructure of material A can be modeled as shown in Scheme 2-1(c). In this case, the strong polymer network is retained while the oxygen permeable constituents are linked internally to the network. These oxygen permeable constituents, surrounded by the walls of the polymer network, are thought to correspond to the dark patches in the TEM photograph. In this structure, each component can maintain its specific role. The crosslinked polymer network sustains strength and the oxygen permeable component, which is independent of the polymer backbone, contributes high oxygen permeability. Therefore, the durability of the material is not as dependent on the proportion of oxygen permeable constituents. This form of polymer structure has the added advantage that the gas permeable component within the network can absorb impact applied to the material.

These structural considerations can be demonstrated in the results from the strength tests and the incidence of lens breakage reported in the literature (Table 2-2). The RGP materials B, D, and E showed relatively low impact strength. Material A showed excellent impact strength, possibly because of the impact absorbing gas permeable component within the polymer backbone of the material.

The flexural strength test did not reflect the difference in physical microstructure as much as did the impact strength test. Material A was still more resistant to breakage than were the RGP materials B, D and E, and was comparable with a much lower $P(O_2)$ (12) material, as shown in Figure 2-4.

The significance of these differences is reflected in the clinical performance. It appears that if we consider the impact or flexural resistance of the material alone, we

Table 2-2. Comparison of the physical microstructures of the various materials with the results from the strength tests and the incidence of lens breakage reported in the literature

Material	Microstructure	Impact strength (cm)	Flexural strength (% change in diameter at breakage)	Clinical data for incidence of breakage (Lens/eye/year)	References
A	microheterophase	130	100	0.015	1–3
B	homogeneous	40	85	0.055	4, 5
D	homogeneous	40	74	0.073	6, 7
E	homogeneous	20	85	0.082	8–11

cannot adequately predict the level of lens breakage during clinical use. However, when the data are combined, the results of clinical performance do agree with those from the laboratory tests.

On the issue of deposit resistance, the microheterophase structure is said to show good biocompatibility and good antithrombogenecity.[12)] The incidence of lens replacement due to deposits damage as reported in the literature is summarized in Table 2-3. Comparing the materials for which similar care regimen were used (an abrasive cleaner), it is seen that polymer morphology may be important in contributing to the minimization of lens replacement due to deposit problems. Further research is needed

Table 2-3. Comparison of the microstructure of various materials with the incidence of lens replacement due to deposit damage reported in the literature

Material	Microstructure	Clinical data for lens replacement due to deposit or damage (Lens/eye/year)	Care Regimen	References
A	microheterophase	0	Abrasive cleaner	1–3
B	homogeneous	0.066	Abrasive cleaner	4, 5
D	homogeneous	0.049	Abrasive cleaner	6, 7
E	homogeneous	0.102	Surfactant cleaner (treated lens surface)	8–11

on this question.

2.5 Conclusions

The breakage resistance of various RGP materials was evaluated and it was revealed that it was not correlated with the $P(O_2)$ value of the material. In addition, by combining the impact and flexural strength test results, the incidence of lens breakages found in clinical studies could be predicted from these combined results. Furthermore, from observation of the physical microstructure of RGP materials by TEM, we could understand why breakage resistance did not depend on the $P(O_2)$ of the material. In other words, breakage strength depends on the type of physical microstructure of the material. In addition, a relationship between the physical microstructure of RGP materials and their deposit resistance is suggested.

2.6 References

1) Ara, F., Yokotani, A., Nakayasu, K., Nemoto, T., Okisaka, S., Ohtsuka, H. and Kenjyo, H. *J. Jpn Contact Lens Soc.***1988***, 30,* 280.
2) Betto, K., Kamiya, M., Fukami, H. and Majima, Y. *J. Jpn Contact Lens Soc.* **1989***, 31*, 20.
3) Momose, T., Itoh, N., Ohkoshi, K., Magatani, H., Nakajima, A., Adachi, Y., Kenjo, H. and Ohtsuka, H. *J. Jpn Contact Lens Soc.* **1989**, *31*, 26.
4) Miyamoto, T., Ohara, K., Okubo, A., Okubo, Y., Takayanagi, Y. and Suzuki, T. *J. Jpn Contact Lens Soc.* **1988***, 30*, 214.
5) Yasuda, N., Itoh, N., Shibata, H., Magatani, H., Kanai, A., Nakajima, A., Nakajima, M. and Nishihira, M. *J. Jpn. Contact Lens Soc*. **1989**, *31*, 1.
6) Hara, C., Kawasaki, S., Tada, M., Kobashi, T., Nunode, Y., Kurihara, E., Nakajima, M., Nakakura, H. and Azuma, I. *J. Jpn. Contact Lens Soc.* **1988***, 30*, 33.
7) Yagasaki, T., Mori, R. and Asakura, K. *J. Jpn. Contact Lens Soc.* **1987***, 29*, 193.

8) Amano, H., Iwase, A., Hirose, S. and Kamiya, C. *J. Jpn. Contact Lens Soc.* **1983***, 25*, 234.

9) Hirano, J., Tanabe, S. and Tabuchi, Y. *J. Jpn. Contact Lens Soc.* **1983**, *25*, 240.

10) Tamura, Y., Yano, M., Murakami, T. and Tokoro, T. *J. Jpn. Contact Lens Soc*. **1986***, 28*, 11.

11) Nishimura, S. and Nagata, M. *J. Jpn. Contact Lens Soc.* **1986**, *28*, 26.

12) Nyilas, E. *Proc.23rd Ann. Conf. Eng. Med. Biol.* **1970***, 12*, 147.

Part II Silicone-Containing Hydrogel Materials

Chapter 3

Creation of Novel Silicone-Containing Monomer and Novel Silicone-Containing Hydrogel

3.1 Synthesis of a Novel Silicone Monomer Bearing Amide Groups to Improve Compatibility with Hydrophilic Vinyl Monomer

3.1.1 Introduction

Silicone material has been attracting much interest due to its extremely high gas permeability. Therefore, it is widely used in medical devices, such as artificial lungs[1,2] and silicone elastomer contact lenses.[3,4] Such applications have been achieved by the modification of the hydrophobic nature of silicone into hydrophilic character. Thus, hydrophilicity is important for medical use of siloxane compounds. In fact, hydrophilic material like hydrogel[5–9] is abundantly applied. So, the silicone-containing hydrogel (silicone hydrogel) has received much attention for decades, possibly improving the poor gas permeability of the original hydrogels. For this purpose, small modifications of PDMS are commonly carried out with PEG chains to transform the hydrophobic and lipophilic silicone character, in addition to the introduction of radically polymerizable groups into PDMS.[10–12] The reason for small modification is that there are only a few methods to connect hydrocarbon groups and silicon atom, such as hydrosilylation reaction.

However this type of siloxane constituent (PDMS macromer) is compatible with only a limited number of hydrophilic monomers. This can lead to insufficient balance among the physical properties of silicone hydrogel. In order to overcome the problems of PDMS macromers, some efforts have been focused on the synthesis of novel silicone-containing monomers which bear both organosiloxanyl and hydrophilic

groups.[13,14] However, the copolymerization reactivity of these monomers has still room for improvement. Considering the wide application of silicone hydrogels however, copolymerization with commercialized vinyl monomers could be an important approach, such as DMA and HEMA. From this point of view, taking advantage of the high hydrophilicity of the amide group, and high activity for vinyl polymerization of the acrylamide group, a novel silicone-containing vinyl monomer was designed, which has one organosiloxanyl group and two amide groups, and then the characteristics of the resulting silicone hydrogel using this novel monomer was examined.

3.1.2 Experimental Section

Materials

DMA and HEAA, both from KOHJIN (Japan), acryloyl chloride and sodium hydroxide (NaOH), both from WAKO (Japan) were used without further purification. Ethyl acetate, ethyl alcohol, sodium sulfate anhydride, all from Kishida Chemical was also used without further purification. 3-Aminopropyltris(trimethylsiloxy)silane (SiPAm) from Gellest (USA) and TRIS from Shin-Etsu Chemical (Japan) were used as received. Triethyleneglycol dimethacrylate (3G) from Shin-Nakamura Chemical Co., Ltd. (Japan) and HEMA from WAKO were also used as received. V-65 and V-40, both from WAKO were used without further purification.

Measurement

^{1}H NMR spectra were measured by JEOL (Japan) ECS400 spectrometer using $CDCl_3$ as a solvent. ATR-FTIR spectrum was obtained with a Spectrum 100 FT-IR spectrometer (Perkin-Elmer). Mass spectra were taken on a JEOL JSM-700 mass spectrometer.

Monomer synthesis

The novel monomer, *N*-2-(*N*', *N*'-dimethylcarbamoyl)ethyl-*N*-[3-tris(trimethyl siloxy)silylpropyl]acrylamide (SiDAAA) was synthesized according to Scheme 3-1-1. First, *N*-2-(*N'*,*N'*-dimethylamide)ethyl-*N*-3-tris(trimethylsiloxy)silylpropylamine (SiDAAm) was synthesized. SiPAm (5.01 g, 14.2 mmol) and DMA (1.47 g, 14.8 mmol) were combined in ethyl alcohol (15.1 mL). This solution was stirred for 4 days at room temperature, and no further change was confirmed by ATR-FTIR. After evacuation of the ethyl alcohol and residual DMA, distillation at reduced pressure was performed which gave 4.21 g of transparent liquid (boiling point 130^{o}C, 40 Pa).

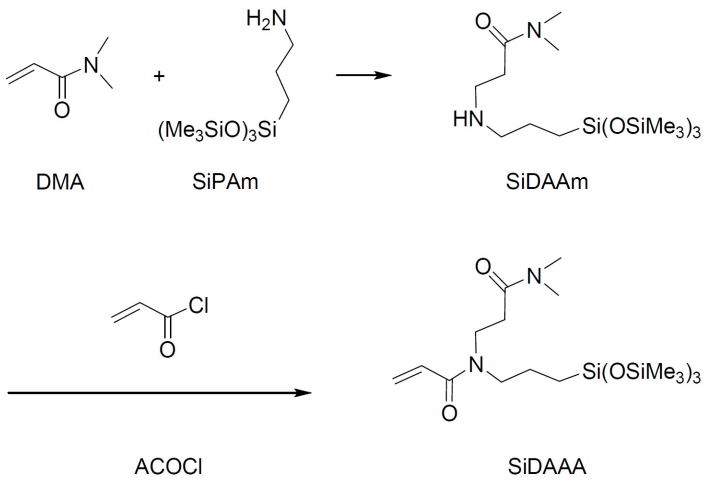

Scheme 3-1-1. Synthesis of SiDAAA.

As the second step, (SiDAAA) was synthesized. SiDAAm (3.35 g, 7.41 mmol), ethyl acetate(13.3 mL) and 1.38 N NaOH aqueous solution (6.20 mL) were combined and cooled to 5 ºC under stirring. After the drop-wise addition of acryloyl chloride (ACOCl) (0.724 g, 8.00 mmol) to this mixture with stirring, the solution was stirred 1 hr at 5 ºC and 2 hr at room temperature. After the phase separation, the ethyl acetate phase was washed with NaOH aqueous solution for 1 hr and then dried with sodium sulfate anhydride. The evacuation of ethyl acetate was followed by purification with silica gel

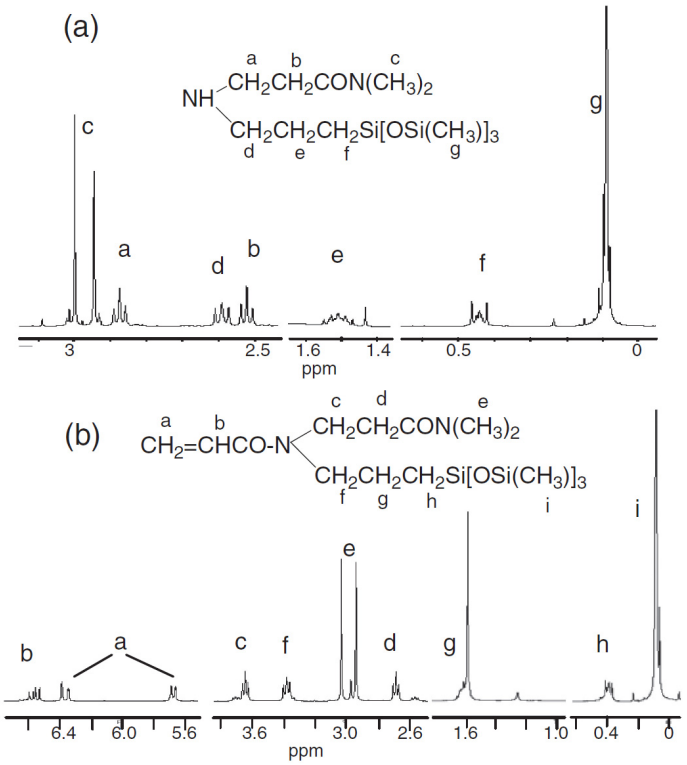

Figure 3-1-1. ^{1}H NMR spectra of SiDAAm (a) and SiDAAA (b).

column chromatography and 1.85 g of colorless liquid was obtained. Detailed information from the analysis of SiDAAA is as follow;

FT-IR (cm^{-1}): 1649, 1614, 1250, 1043, 837, 754.

Elemental Analysis: Calcd. for $C_{20}H_{46}O_5N_2Si_4$: C, 47.40; H, 9.10; N, 5.50%. Found: C, 47.13; H, 8.93; N, 5.53%.

FAB-MS: $[M+1]^+ = 507$

^{1}H NMR spectra of SiDAAm and SiDAAA are shown in Figure 3-1-1.

Hydrogel preparation

For the preparation of the silicone hydrogel, TRIS or SiDAAA as a silicone-containing monomer, DMA or HEMA as a hydrophilic monomer, 3G as the

crosslinker plus V-65 and V-40 as the initiator were combined according to the required balance, and degassed. The solutions were injected between a glass plate and a PTFE film separated with a silicone gasket (0.2 mm thickness) under a nitrogen atmosphere. The polymerization was then carried out by elevating the temperature from 50 ºC to 110 ºC according to the predetermined temperature profile program. After polymerization, the PTFE film and silicone gasket were removed, followed by immersion of the polymer gel in water heated to 60^{o}C for the required time. Finally, the recovered gels were repeatedly washed with ultrapure water.

3.1.3 Results and Discussion

Compatibility with hydrophilic monomer

To confirm the good compatibility and miscibility of SiDAAA with various types of hydrophilic monomers, DMA, HEMA, and HEAA were chosen as typical hydrophilic monomers, and the miscibility between these monomers and SiDAAA was studied. Both SiDAAA and TRIS showed good miscibility with DMA and HEMA. However, there was a big difference in the case of HEAA as shown in Figure 3-1-2. SiDAAA was very miscible with HEAA (Figure 3-1-2a), whereas the combination of TRIS and HEAA showed phase separation (Figure 3-1-2b). This suggests that a wide variety of hydrophilic monomers can be used with SiDAAA for silicone hydrogel preparation.

Figure 3-1-2. Comparison of miscibilities between SiDAAA and HEAA (a), and between TRIS and HEAA (b).

Appearance of hydrogel

Next, I compared the appearance of hydrogels. The results from the silicone hydrogel preparation using TRIS, SiDAAA, DMA, and HEMA are shown in Table 3-1-1. The conventional silicone monomer, TRIS, gave an opaque hydrogel when it was

Table 3-1-1. Preparation and appearance of hydrogel [a]

Run	Silicone monomer		Hydrophilic monomer		Appearence
	SiDAAA	TRIS	DMA	HEMA	
1	60	0	40	0	transparent
2	60	0	0	40	transparent
3	0	60	40	0	transparent
4	0	60	0	40	opaque

a: Weight ratio of monomers. Monomer/3G = 1/1 (wt/wt) and monomer/initiator = 1/0.2 (wt/wt).

copolymerized with HEMA, although it was transparent after copolymerization with DMA. On the other hand, the novel monomer, SiDAAA, produced transparent hydrogels by copolymerization with HEMA, as well as with DMA. These results imply that the additional amide group in the SiDAAA monomer supports good miscibility during hydrogel preparation. The appearance of the hydrogels is shown in Figure 3-1-3.

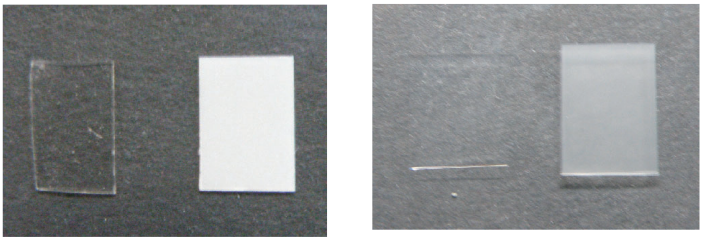

(a) (b) (c) (d)

Figure 3-1-3. Comparison of appearance of hydrogel. (a) dry polymer film from SiDAAA and HEMA, (b) dry polymer film from TRIS and HEMA, (c) hydrogel from SiDAAA and HEMA in water, and (d) hydrogel from TRIS and HEMA in water.

As expected from the miscibility test, SiDAAA gave a transparent polymer both before and after hydration of the hydrogel (Figures 3-1-3a and 3-1-3c). The difference in appearance between the TRIS and SiDAAA hydrogels may be due to the difference between the number and types of polar groups in each molecular structure, and this supports the validity of my approach to monomer design.

3.1.4 Conclusions

A novel silicone monomer bearing two amide groups (SiDAAA) was designed and synthesized. The design concept of this monomer was to improve its compatibility with various hydrophilic monomers, and thus two amide groups were introduced into the molecular structure. This monomer showed good miscibility with hydrophilic monomers bearing hydroxy group such as HEMA and HEAA. Furthermore, the hydrogel from SiDAAA and HEMA had good transparency. These results contrasted with those from hydrogel made with TRIS, conventional silicone monomer, and validated my monomer design concept.

3.1.5 References

1) Spaeth, E.E. and Friedlander, S.K. *Biophys. J.* **1967**, *7*, 827.
2) Kniazeva, T., Hsiao, J.C., Charest, J.L. and Borenstein, J.T. *Biomed. Microdevices* **2011**, *13*, 315.
3) Fakes, D.W., Newton, J.M. Watts, J.F. and Edgell, M.J. *Surf. Interface Anal.* **1987**, *10*, 416.
4) Ho, C.P. and Yasuda, H. *Polym. Mater. Sci. Eng.* **1987**, *56*, 705.
5) Tanaka, T., Sato, E., Hirokawa,Y., Hirotsu, S. and Petermans, J. *Phys. Rev. Lett.* **1985**, *55*, 2455.
6) Yoshida, R., Uchida, K., Kaneko, Y., Sakai, K., Kikuchi, A., Sakurai, Y. and Okano, T. *Nature* **1995**, *374*, 240.

7) Juodkazis, S., Mukai, N., Wakaki, R., Yamaguchi, A., Matsuo, S. and Misawa, H. *Nature* **2000**, *408*, 178.

8) Ono, T., Sugimoto, T., Shinkai, S. and Sada K. *Nat. Mater*. **200**7, *6*, 429.

9) Baker, R. "Controlled Release of Biologically Active Agents", Wiley: New York, **1987**.

10) Willis, S.L., Court, J.L., Redman, R.P. Wang, J.-H., Leppard, S.W., O'Byrne, V.J., Small, S.A., Lewis, A.L., S.A. Jones, S.A. and Stratford, P.W. *Biomaterials* **2001**, *22*, 3261.

11) Nicolson, P.C. and Vogt, J. *Biomaterials* **2001**, *22*, 3273.

12) Wang, J. and Li, X. *J. Appl. Polym. Sci.* **2010**, *116*, 2749.

13) Ohnishi, M., Uno, T., Kubo, M. and Itoh, T. *J. Polym. Sci. Part A: Polym. Chem*. **2009**, *47*, 420.

14) Ohnishi, M., Taguchi, N., Gotoh, J., Uno, T., Kubo, K. and Itoh, T. *Polym. Bull*. **2009**, *62*, 761.

3.2 The Role of Amide Groups in Vinyl Monomers Containing Siloxane Groups for Highly Oxygen Permeable Hydrogels

3.2.1 Introduction

Hydrogels are commonly used in the medical field[1–9] because of their soft and elastic properties as well as the progress in production technology of their shaped articles. Moreover, silicone-containing hydrogels (silicone hydrogels) have been receiving much attention for decades, and the poor gas permeability of the original hydrogel characteristics have been improved according to the progress in the research on the importance of oxygen permeability for the corneal health. For this purpose, it is typical that a small modification of PDMS is carried out with a PEG chain to cover the hydrophobic and lipophilic silicone character, in addition to the introduction of a radically polymerizable group into the PDMS.[10,11] However, this type of siloxane constituent (PDMS macromer) is compatible with only a limited number of hydrophilic monomers, resulting in the lack of tuning on the physical variety of these products.

To overcome the problems of PDMS macromers, I had made new approach to the silicone constituent for silicone hydrogel as stated in Section 3.1.[12] Considering the wide applications of silicone hydrogels, copolymerization with commercially available vinyl monomers could be an important approach, such as DMA, HEMA and so on. From this point of view, the design and synthesis of a novel vinyl monomer, *N*-2-(*N'*, *N'*-dimethylcarbamoyl)ethyl-*N*-[3-tris(trimethylsiloxy)silylpropyl]acrylamide (SiDAAA) had been reported which had one organosiloxanyl group and two amide groups, thus taking advantage of the high hydrophilicity of the amide group and the high activity for the vinyl polymerization of the acrylamide group.[12] SiDAAA has shown good compatibility with hydrophilic monomers like HEMA and HEAA.

In addition to the abovementioned SiDAAA which has a tris(trimethylsiloxy)silyl group, a novel monomer bearing two amide groups and a methylbis(trimethylsiloxy)silyl group, *N*-2-(*N',N'*-dimethylcarbamoyl)ethyl-*N*-

{3-[methylbis(trimethylsiloxy)silyl]propyl}acrylamide (SiDAAA2) was synthesized, to evaluate the influence of the number of Si–O–$SiMe_3$ bonds in the organosiloxanyl group on the polymer properties. The radical polymerization of SiDAAA and SiDAAA2 were carried out, and the properties of the resultant polymers were analyzed by differential scanning calorimetry (DSC) and thermogravimetry analysis (TGA).

Furthermore, their silicone hydrogels were evaluated by their appearance, water content, swelling ratio with various solvents, $P(O_2)$, and lysozyme uptake. Herein, I report that the novel monomers SiDAAA and SiDAAA2, which can provide good biomedical materials for applications such as contact lenses, showed good transparency with stable physical characteristics, as well as a high $P(O_2)$.

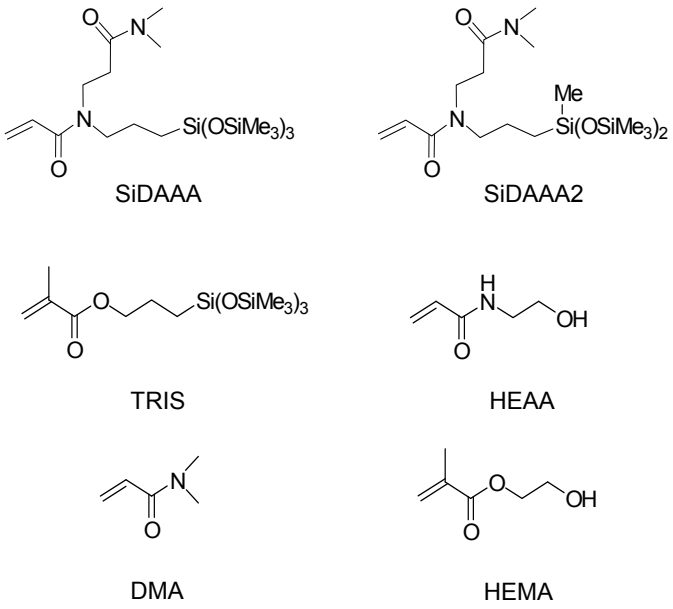

Figure 3-2-1. Chemical structures of used monomers.

3.2.2 Experimental Section

Materials

In addition to the materials described in Section 3.1.2, 3-aminopropylmethylbis (trimehylsiloxy)silane (SiPAm2) from Gellest (USA) was used. All materials were used as received. Chemical structures of used monomers are shown in Figure 3-2-1.

Measurement

The ^{1}H NMR spectra were recorded on a JEOL (Japan) ECS400 spectrometer using $CDCl_3$ as the solvent at room temperature. ATR-FTIR spectrum was obtained with a Spectrum 100 FT-IR spectrometer (Perkin-Elmer). The mass spectra were recorded on a JEOL JSM-700 mass spectrometer.

DSC and TGA were performed with a SEIKO Instruments EXSTAR 6000 series, DSC 6120, and TG/DTA 6200 under a nitrogen atmosphere. The heating rate was 5 ºC/min for DSC and 10 ºC/min for TGA.

The molecular weights of the homopolymers were estimated by SEC on a JASCO LC-2000 Plus series equipped with a TOSOH TSK gel GMH_{XL} and a TSK gel SuperH4000 at 40 ºC using tetrahydrofuran (THF) as the eluent at a flow rate of 0.6 mL/min, and PMMA standards for calibration.

$P(O_2)$ of the silicone hydrogel material was measured in water at 35 ºC with a polarographic method using a film oxygen transmissibility measurement apparatus made by Tsukuba Rikaseiki (Japan). The light transmittance of the silicone hydrogel and the absorbance at 562 nm of the bicinchoninic acid (BCA) assay solution was measured with a HITACHI U-3010 spectrophotometer. The silicone hydrogel samples were immersed in ultrapure water in a quartz cell for the light transmittance measurements.

Synthesis

SiDAAA2 was synthesized with the same scheme as previously reported, using SiPAm2 instead of SiPAm.[12)] Twenty grams of SiPAm2 (72.2 mmol) and 7.29 g of DMA (73.5 mmol) were combined in ethyl alcohol (31.9 mL). This solution was stirred for 4 days at room temperature, and no further change was confirmed by ATR-FTIR. After evacuation of the ethyl alcohol and any residual DMA, distillation at a reduced pressure was performed which gave 18.56 g of transparent liquid (boiling point 130 ºC,

40 Pa) at a 69% yield (SiDAAm2). Next, SiDAAm2 (18.56 g, 49 mmol), ethyl acetate (74 mL) and 1.38 N NaOH aqueous solution (42 mL) were combined and cooled to 5 ºC under stirring. After the drop-wise addition of acryloyl chloride (5.29 g, 58 mmol) to this mixture with stirring, the solution was stirred for 1 h at 5 ºC and for 5 h at room temperature. After the phase separation, the ethyl acetate phase was washed with NaOH aqueous solution for 1 h and then dried with sodium sulfate anhydride. The evacuation of the ethyl acetate was followed by purification using silica gel column chromatography and the mixture of ethyl acetate and hexane as an eluent, and 16.2 g of colorless liquid was finally obtained at 76% yield (SiDAAA2).

^{1}H NMR ($CDCl_3$, 400MHz), δ: 0.01 (s, 3H, Si–C*H*$_3$), 0.08 (s, 18H, O–Si–C*H*$_3$), 0.40 (t, *J* = 8.6Hz, 2H, CH_2–C*H*$_2$–Si), 1.54–1.62 (m, 2H, CH_2–C*H*$_2$–CH_2), 2.68 (t, *J* = 7.3Hz, 2H, CH_2–C*H*$_2$–CO), 2.94 (s, 6H×0.517, C–N–C*H*$_3$), 2.97 (s, 6H×0.108, C–N–C*H*$_3$), 3.00 (s, 6H×0.375, C–N–C*H*$_3$), 3.38 (t, *J* = 7.9 Hz, 2H, N–C*H*$_2$–CH_2–CH_2–), 3.65 (t, *J* = 7.3Hz, 2H, N–C*H*$_2$–CH_2–CO), 5.67 (d, *J* = 10.4Hz, 1H, C*H*$_2$=CH–C), 6.35 (d, *J* = 16.8 Hz, 1H, C*H*$_2$=CH–), 6.53 (dd, *J* = 16.9Hz, 1.04Hz, 1H, CH_2=C*H*–).

FT-IR(cm^{-1}): 1648, 1613, 1251, 1039, 836, 792, 753.

Elemental Analysis: Calcd. for $C_{18}H_{40}O_4N_2Si_3$: C, 49.95; H, 9.32; N, 6.48%. Found: C, 48.81; H, 9.16; N, 6.27%.

CI-MS: $[M+1]^+$ = 433.

The additional monomer bearing the siloxanyl group and two amide groups, SiDAAA was synthesized according to the previously reported method.[12)]

Polymerization

Silicone-containing monomers such as TRIS, SiDAAA and SiDAAA2, plus AIBN as the radical initiator, and *tert*-amyl alcohol as a solvent were combined in a recovery flask equipped with a three-way valve at a monomer concentration of 2 mol/L and an AIBN concentration of 0.1 mol/L. The monomer mixture was degassed by five

repeated cycles of freeze-thaw under nitrogen, and then sealed. It was placed in an oil bath controlled at a constant temperature (60 ºC) for 24 h. After polymerization, THF was added to the reaction mixture, and it was then precipitated and washed with methyl alcohol followed by drying at 70 ºC, 40 h *in vacuo*. The polymerization conversion was calculated from the recovered polymer weight and the monomer weight.

Hydrogel preparation

Hydrogel preparation was carried out with the same method as described in Section 3.1.2 using TRIS, SiDAAA or SiDAAA2 as a silicone-containing monomer, and DMA, HEMA or HEAA as a hydrophilic monomer.

The swelling ratio (S.R.) of obtained hydrogel in various solvents was estimated by the following equation: S.R. = $(W_w - W_d)/W_d$ where W_d is the weight of the hydrogel after drying at 40 ºC for 16 h *in vacuo* and W_w is the weight of the gel swollen in the solvent for 24 h.

Oxygen permeability coefficient

The $P(O_2)$ of the hydrogel was evaluated as follows. Experimentally, a series of several samples of different thicknesses were employed to obtain the $P(O_2)$ (P_m) from the following formula with a polarographic method.[13–15)]

$$(P_s \cdot N \cdot F \cdot A)/i_\infty = l_b/P_b + l_m/P_m + l_e/P_e \qquad (2)$$

where l represents the thickness, suffix $_b$, $_m$ and $_e$ represent the boundary layer, membrane (hydrogel sample), and electrolyte layer, respectively. P_s, N, F, A and i_∞ represent the oxygen pressure (760 mmHg), 4 (number of electrons), Faraday constant, the area of the Pt electrode, and the observed electric current, respectively. Thus, the $P(O_2)$ (P_m) was derived from the inverse of the slope.

Protein uptake

Lysozyme uptake was evaluated by the BCA assay[16,17] using a Micro BCA Protein Assay Kit from Thermo Scientific (USA) with lysozyme from egg white from WAKO. The BCA assay is based on the protein-induced reduction of Cu^{2+} in alkaline medium, and the formation of a chelate complex from the resultant Cu^{1+} and BCA, which has a strong absorbance at 562 nm. The calibration curve was prepared from the absorbance of the reacted solution from a pure lysozyme solution and the BCA assay solution, which was measured with a HITACHI U-3010 spectrophotometer. After immersion of the hydrogel films in a lysozyme solution at 35 ºC for 20 h and rinsing in a boric acid buffer solution, the lysozyme was extracted and the reaction with the BCA assay solutions was carried out. The lysozyme uptake was calculated from the absorbance and calibration curves.

3.2.3 Results and Discussion

Monomer synthesis, polymerization reactivity and evaluation of homopolymer

In addition to evaluating the introduction of two amide groups on the polymer and hydrogel properties, the influence of the balance between silicone-containing groups and amide groups in the monomer molecule was also evaluated. Furthermore, in order to evaluate the effect of the structure of the silicone-containing groups on the polymer properties, the synthesis of the novel monomer SiDAAA2, having two amide groups and methylbis(trimethylsiloxy)silyl group, was carried out in two steps according to the procedure shown in Scheme 3-2-1. The difference in molecular structure between SiDAAA and SiDAAA2 is the number of Si–O–Si–Me_3 groups and resultant volume occupied by siloxanyl groups as shown in Figure 3-2-1.

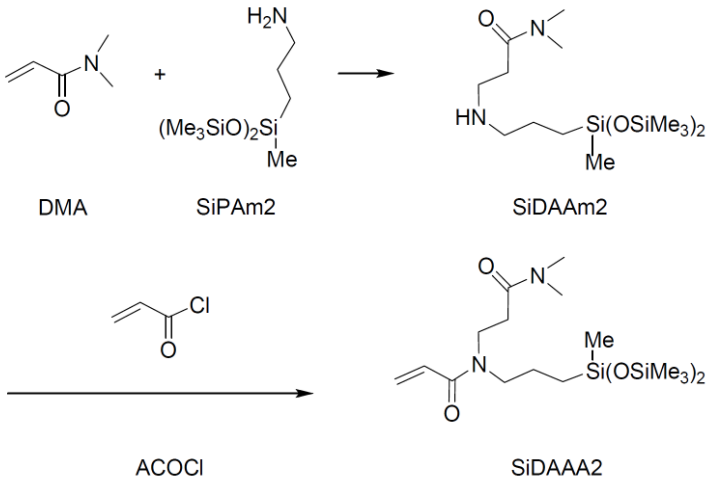

Scheme 3-2-1. Synthesis of SiDAAA2.

The molecuar weights of the homopolymers are summarized in Table 3-2-1. The degree of polymerization calculated from the M_n for poly(TRIS), poly(SiDAAA) and poly(SiDAAA2) was 90, 70, and 60, respectively. Considering that the values of conversion from homopolymerization were similar values (from 87 to 90% as shown in Table 3-2-1), it was recognized that these monomers had almost the same radical homopolymerization reactivity. This could be one of the merits of SiDAAA and SiDAAA2 for applications to the preparation of copolymers such as hydrogels.

Since both SiDAAA and SiDAAA2 have acrylamide groups and one more amide group (dimethylcarbamoyl group), which came from dimethylacrylamide and had a similar structure as dimethylformamide, it could be expected that poly(SiDAAA) and poly(SiDAAA2) had better miscibility with the solvents than poly(TRIS). The results from the miscibility test with various solvents are also shown in Table 3-2-1, implying that poly(SiDAAA) was miscible with 2-propanol which had polar charactreristics, as the result of the incorporation of another amide group.

Another effect of the amide groups in SiDAAA and SiDAAA2 on their homopolymer properties could be the high glass transition temperature (T_g) because of

Table 3-2-1. Properties of homopolymers

Run	Material	conversion (%)	SEC			Miscible solvents [a]
			$M_n(\times 10^4)$	$M_w(\times 10^4)$	M_w/M_n	
1	poly (TRIS)	90	3.8	1.8	4.8	THF, Toluene, $CHCl_3$
2	poly(SiDAAA)	87	3.5	2.3	6.4	2-PrOH,THF, Toluene, $CHCl_3$
3	poly(SiDAAA2)	87	2.6	1.4	5.3	—

a: Miscibility was tested with 1 mg of polymer and 1 mL of following solvent; H_2O, MeOH, EtOH, 2-propanol (2-PrOH), tetrahydrofuran(THF), acetone, DMSO, toluene and $CHCl_3$.

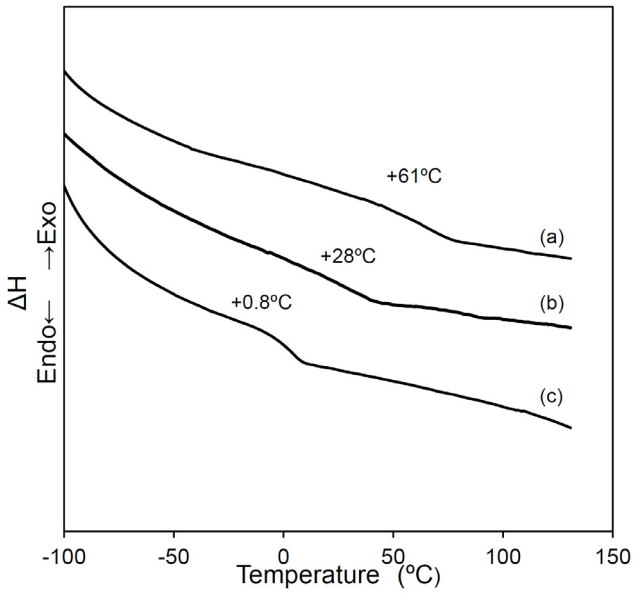

Figure 3-2-2. DSC traces of poly (SiDAAA) (a), poly (SiDAAA2) (b), and poly (TRIS) (c).

the highly polar characteristics. The results from DSC measurements are shown in Figure 3-2-2. A comparison between the methacrylate (Figure 2c, +0.8 ºC) and acrylamide with the same tris(trimethylsiloxy)silylpropyl group (Figure 3-2-2a, +61 ºC) showed about a 60 ºC difference in T_g as expected. In addition, a comparison between the acrylamide derivatives with different siloxane-containing groups showed that the methylbis(trimethylsiloxy)silyl group (Figure 3-2-2b, +28 ºC) led to about a 30 ºC lower

T_g than the tris(trimethylsiloxy)silyl group (Figure 3-2-2a). Thus the amide group had a larger influence on the T_g than the organosiloxanyl group. According to Kawakami and co-worker,[18] the T_g of poly[4-tris(trimethylsiloxy)silylstyrene] and poly{4-[methyl bis(trimethylsiloxy)silyl]styrene} was +114 ºC and +52 ºC, respectively. This difference of T_g due to the difference in silicone-containing groups showed good correspondence to our results. In other words, the T_g of the polymer from the silicone-containing monomer was determined by the polymerizable group, and the degree of branching in the siloxane-containing group. This relatively high T_g of poly(SiDAAA) and poly(SiDAAA2) could lead to good mechanical properties, such as enhanced elasticity of the hydrogel and a high modulus of rigidity of the copolymers.

Similar to the case of the T_g, good thermal stability could be expected from the intermolecular interactions between the amide groups in SiDAAA and SiDAAA2. Thus I conducted the TGA measurement, and the results are shown in Figure 3-2-3. Poly (SiDAAA) (Figure 3-2-3a) showed 5% weight loss at 354 ºC and it was more stable than that of poly(TRIS) (Figure 3-2-3c) at 291 ºC, and the difference in decomposition temperature was about 60 ºC. This difference showed a good correspondence to the difference in the T_g. In contrast, poly(SiDAAA2) (Figure 3-2-3b) showed a lower 5% weight loss temperature at 257 ºC than poly(TRIS) (Figure 3-2-3c), nevertheless the former showed a higher T_g value than the latter. Furthermore, poly(SiDAAA2) showed some residue. These observations could be correlated with the difference in thermal stability between the methylbis(trimethylsiloxy)silyl group and the tris(trimethylsiloxy)silyl group. In relation to this, I discovered that it was possible to have scission of the Si–C, Si–O–Si and C–H bonds and the recombination of these fragments in a silicone hydrogel under Ar gas plasma.[19] Therefore, this suggests the possibility of scission of the siloxane bond and the formation of a crosslinked silicate structure under the TGA measurement high temperature conditions for poly(SiDAAA2).

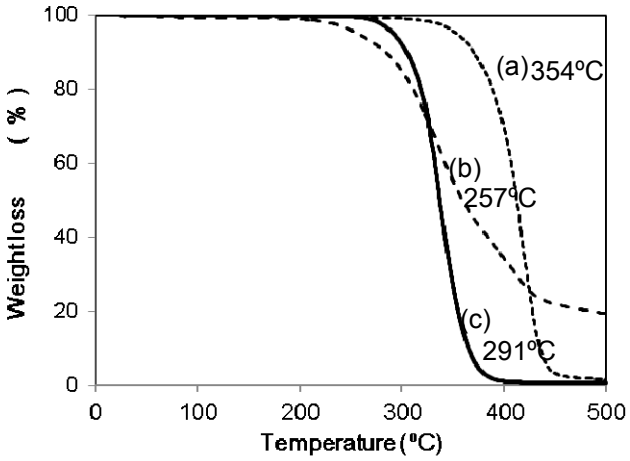

Figure 3-2-3. TGA analyses of poly (SiDAAA) (a), poly (SiDAAA2) (b), and poly(TRIS) (c).

Properties of Silicone Hydrogels

Transparency

Next, silicone hydrogels were prepared from SiDAAA, SiDAAA2, and TRIS as silicone group bearing monomers, DMA, HEAA, and HEMA as the hydrophilic monomer, and 3G as the crosslinker. The properties of these silicone hydrogels are summarized in Table 3-2-2. The transparency of the hydrogels was confirmed by their appearance in Figure 3-2-4, and by the light transmittance of hydrogels of 0.2 mm thickness in Figure 3-2-5. In addition to our previous report on the opaque appearance of a hydrogel from the combination of TRIS and HEMA,[12] I measured the light transmittance at 400 nm, and found that it was about 26% as shown in Figure 3-2-5**(**d**)**. With regard to TRIS and HEAA, they were immiscible with each other[12]. In contrast, SiDAAA gave a transparent hydrogel with DMA and HEMA (Table 3-2-2, entries 4–6, and 10). In the case of HEAA, even though the HEAA rich hydrogel (HEAA 60 weight parts) had a slightly hazy appearance (Table 3-2-2, entry 9 and Figure 3-2-4(c)), the SiDAAA rich hydrogels were transparent as shown in Figure 3-2-4 (a) (SiDAAA/HEAA (60/40)) and Figure 3-2-4 (b) (SiDAAA/HEAA (50/50)). The light

transmittance at 400 nm was about 98% for SiDAAA/HEAA(60/40) in Figure 3-2-5 (a), 88% for SiDAAA/HEAA (50/50) in Figure 3-2-5(b), and 45% for SiDAAA/HEAA (40/60) in Figure 3-2-5(c). A comparison of the data from Figure 3-2-4 and Figure 3-2-5 leads to the conclusion that 88% light transmittance is practically acceptable. The reason for the low light transmittance of the HEAA rich hydrogel could be coagulation of the hydroxy groups due to the numerical imbalance between the hydroxy groups and amide groups. It is noteworthy that the molecular design was based on introducing one more amide groups into the monomer to enable the silicone-containing polymers to improve their characteristics. Thus, SiDAAA can generate silicone hydrogels from various hydrophilic monomers with transparency, which is a very important property for applications in optical materials, such as contact lenses.

Table 3-2-2. Physical properties of silicone hydrogel [a]

Entry	Silicone-containing monomer		Hydrophilic monomer		Water content (%)[b]		Lysozyme uptake	Appearance
	Type	Weight	Type	Weight	25 ºC	35 ºC	μg/cm^2	
1	TRIS	60	DMA	40	33.6±0.6	32.7±0.3	5.4 ±0.8	transparent
2	TRIS	50	DMA	50	46.1±0.8	45.2±0.4	9.4 ±0.8	transparent
3	TRIS	40	DMA	60	54.3±2.0	52.9±2.1	13 ±8.8	transparent
4	SiDAAA	60	DMA	40	52.4±3.9	49.6±2.2	12 ±3.4	transparent
5	SiDAAA	50	DMA	50	63.8±2.6	60.9±2.1	4.3 ±2.7	transparent
6	SiDAAA	40	DMA	60	67.3±2.1	64.1±1.1	4.2 ±2.5	transparent
7	SiDAAA	60	HEAA	40	50.7±2.3	49.0±2.0	3.9 ±2.3	transparent
8	SiDAAA	50	HEAA	50	60.8±0.1	59.1±0.1	8.2 ±5.0	transparent
9	SiDAAA	40	HEAA	60	70.9±0.3	68.9±1.1	4.5 ±0.5	hazy
10	SiDAAA	60	HEMA	40	12.8	—	—	transparent[d]
11	SiDAAA2	60	DMA	40	66.7±0.6	65.7±0.1	1.5 ±0.1	transparent
12	SiDAAA2	50	DMA	50	75.1±1.3	74.4±0.6	8.0 ±2.1	transparent
13	SiDAAA2	40	DMA	60	N.A.[c]	N.A.[c]	N.A.[c]	transparent
14	TRIS	60	HEMA	40	—	—	—	opaque[d]
15	—	—	HEMA	100	36.2	—	21 ±2.5	transparent

a: All hydrogel composition contains 1 weight part of 3G as crosslinker.

b: Water content was calculated from following formula; $(W_w - W_d)/W_w \times 100$, where W_w and W_d show the wet weight and dry weight of hydrogel, respectively. $n = 3$.

c : too fragile to handle.

d : reference 12.

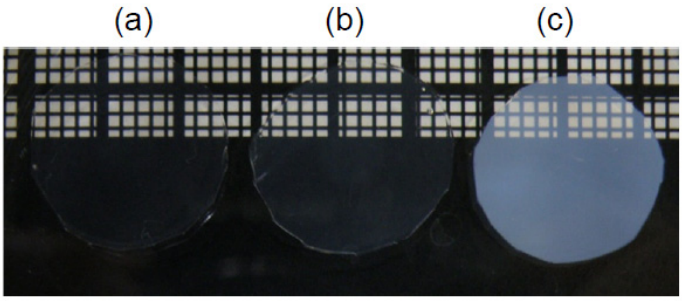

Figure 3-2-4. Appearance of silicone hydrogel with SiDAAA/HEAA (60/40) (Table 3-2-2, entry 7) (a), SiDAAA/HEAA (50/50) (Table 3-2-2, entry 8) (b), and SiDAAA/HEAA (40/60) (Table 3-2-2, entry 9) (c).

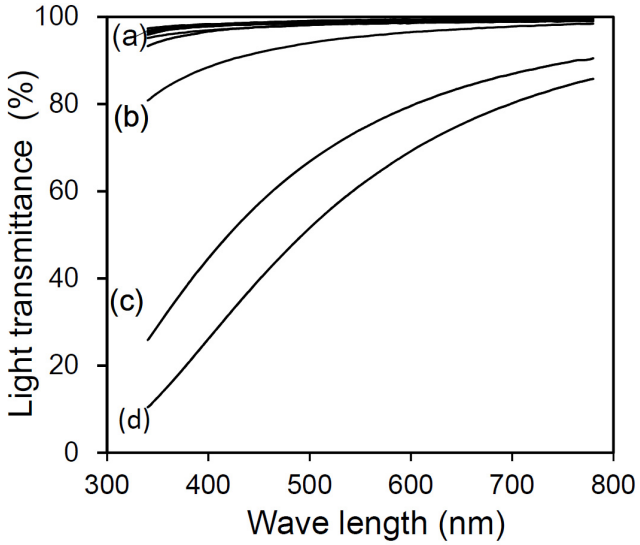

Figure 3-2-5. Light transmittance of silicone hydrogel with SiDAAA/HEAA (60/40) (Table 3-2-2, entry 7) (a), SiDAAA/HEAA (50/50) (Table 3-2-2, entry 8) (b), and SiDAAA/HEAA (40/60) (Table 3-2-2, entry 9) (c). (d) represents light transmittance of TRIS/HEMA (60/40) (Table 3-2-2, entry 14).

Water content

The water content of the prepared silicone hydrogels are depicted in Figure 3-2-6. In all cases, a higher temperature (35 ºC) caused the lower water content than a lower temperature (25 ºC) (Table 3-2-2). It was recognized that the contribution of HEAA to the water content was similar to that of DMA. The SiDAAA/DMA hydrogel had a more than 10% higher water content than the TRIS/DMA hydrogel of the same silicone monomer content (weight), due to the presence of two amide groups in

SiDAAA. Similarly, the SiDAAA2/DMA hydrogel showed a more than 10% higher water content than the SiDAAA/DMA hydrogel of the same silicone monomer content. Thus, both amide groups and the trimethylsiloxysilyl group could influence the water content, and the water content of a transparent silicone hydrogel could be controlled by using SiDAAA with various hydrophilic monomers, including hydroxy group bearing monomers.

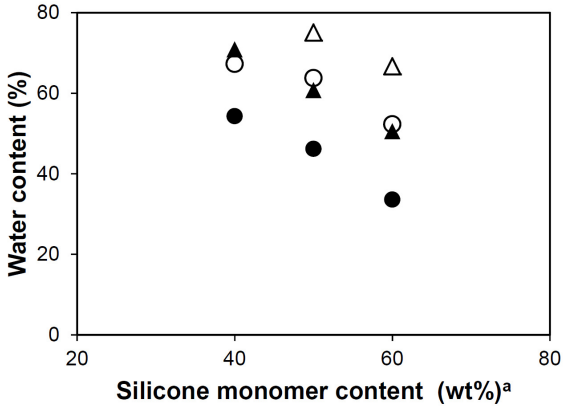

Figure 3-2-6. Water content of silicone hydrogels at 25 ºC. Closed circle, open circle, closed triangle, and open triangle represent hydrogel composition of TRIS/DMA, SiDAAA/DMA, SiDAAA/HEAA and SiDAAA2/DMA, respectively.
a : Hydrogel composition is silicone monomer/hydrophilic monomer/3G = x/(100–x)/1 (in weight).

Swelling Ratio

Since the silicone hydrogels synthesized thus far have both hydrophobic and hydrophilic moieties, the hydrophilicity could be evaluated by the swelling ratio (S.R.) when immersed in various solvents, including water, alcohols, polar solvents and non-polar solvents.[13] The results from the S.R. measurements are shown in Figure 3-2-7. It was clear that the HEMA-containing hydrogel (entry 10 in Table 3-2-2, 12.8% water content) showed a high S.R. in THF, DMSO, EtOH and $CHCl_3$ but a low S.R. in H_2O and toluene. In contrast, the HEAA hydrogel (entry 7 in Table 3-2-2, 50.7% water content) showed similar values for all solvents except for acetone and toluene, demonstrating an improvement in the hydrophilicity of the hydrogel material. Thus,

when a silicone group and two amide group-bearing monomer (SiDAAA) was used, even though the SiDAAA content was kept constant, changing the type of hydrophilic monomer enabled us to control the S.R.

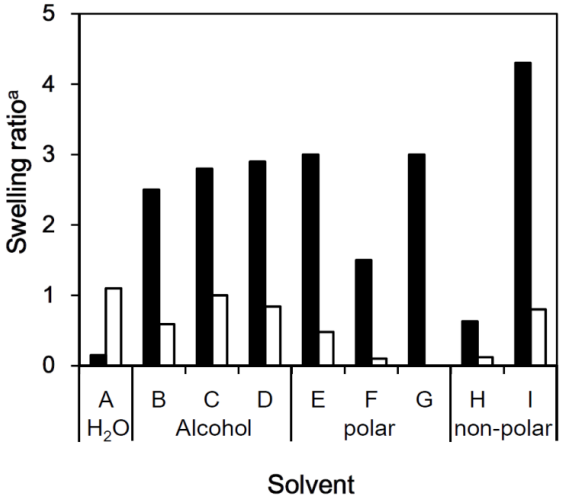

Figure 3-2-7. Swelling ratio of silicone hydrogels with various solvents. Open stick and closed stick represent the silicone hydrogel composition of entry 7 (SiDAAA/HEAA/3G =60/40/1, 50.7% of water content), and entry10 (SiDAAA/HEMA/3G = 60/40/1, 12.8% of water content) in Table 3-2-2 respectively. A, B, C, D, E, F, G, H and I show H_2O, MeOH, EtOH, 2-Propanol, THF, $(CH_3)_2CO$, DMSO, Toluene, and $CHCl_3$, respectively.
a: Swelling ratio was calculated with following formula; $(W_w–W_d)/W_d$, where W_w is weight with solvent and W_d is the weight of dried hydrogel.
b; Swelling ratio for DMSO of open stick could not be obtained because the gel was too fragile to handle.

Oxygen Permeability Coefficient

Experimentally, a series of several samples of different thicknesses were employed to obtain the $P(O_2)$ (P_m) from formula (1) using a polarographic method.[13–15] Thus, the $P(O_2)$ (P_m) is derived from the inverse of the slope as shown in Figure 3-2-8. The results from the oxygen permeability measurements are shown in Figure 3-2-9, and all silicone hydrogels from various silicone-containing monomers suggested the same relationship between the $P(O_2)$ and water content. It was clear that the water content (or silicone content) of the hydrogel influenced the $P(O_2)$ and lowered the water content (or increased the silicone content), increased the oxygen permeability in the measured water

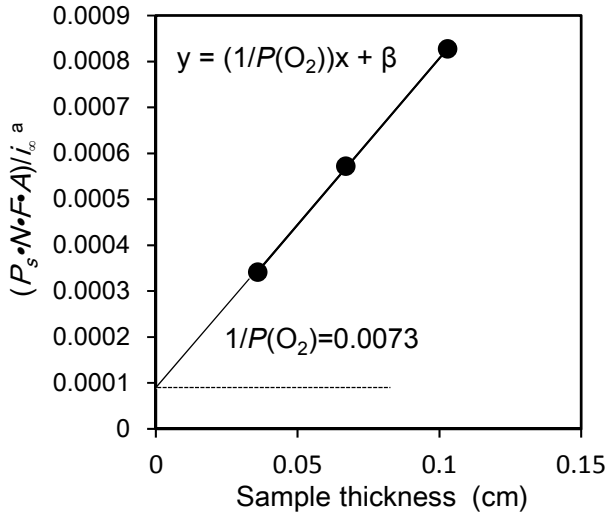

Figure 3-2-8. Example of plot of $(P_s \cdot N \cdot F \cdot A)/i_\infty$ vs sample thickness to calculate oxygen permeability coefficient ($P(O_2)$). Silicone hydrogel composition is the entry 2 in Table 3-2-2. [a] : $\times 10^{-11}$ml(STP)$\cdot$cm/(cm$^2\cdot$sec$\cdot$mmHg).

content range. It is well known that $P(O_2)$ of conventional hydrogel generally increases under increased water content. However, obtained $P(O_2)$ of silicone hydrogel showed an opposite tendency because silicone possesses a much higher $P(O_2)$ value than water and works as main oxygen permeation paths. With regard to the critical oxygen transmissibility ($P(O_2)/L$), where L represents the average thickness) needed to avoid corneal edema with extended wear of contact lenses, which is the most important factor in ensuring corneal safety for a contact lens wearer, Holden and coworker reported a value of 87.0 ± 3.3×10^{-9}(cm×mlO_2) /(sec×ml×mmHg).[20] Assuming that the average thickness is 0.1 mm and the safety margin for $P(O_2)$ is 20%, a $P(O_2)$ of $100\times10^{-11}\times$ml(STP)$\cdot$cm/(cm$^2\cdot$sec$\cdot$mmHg) or 100 barrer would be the target value. This $P(O_2)$ corresponded to a value of about 60% water content. Thus, it was confirmed that the hydrogels with the silicone-containing monomers which bear two amide groups, have sufficient oxygen permeability for applications as medical devices and a similar value as the silicone hydrogel contact lens available in the commercial market[21] at a lower than 60% water content.

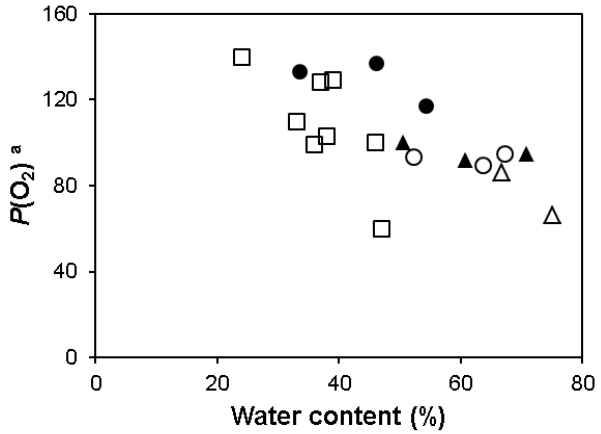

Figure 3-2-9. Oxygen permeability coefficient and water content of silicone hydrogel at 35ºC. Closed circle, open circle, closed triangle, open triangle, and open square represent hydrogel composition of TRIS/DMA, SiDAAA/DMA, SiDAAA/HEAA, SiDAAA2/DMA, and silcone hydrogel lenses in market ($P(O_2)$ value by manufacturer), respectively. a : $\times 10^{-11}$ml(STP)$\cdot$cm/(cm$^2\cdot$sec$\cdot$mmHg).

Lysozyme Uptake

Lysozyme uptake by the silicone hydrogel was measured by the BCA assay, and the results are also shown in Table 3-2-2. The lysozyme uptake was 1.5–13 μg/cm^2 and had no dependence on the silicone hydrogel composition, type of silicone monomer, type of hydrophilic monomer, or water content. The lysozyme uptake by a typical soft contact lens material like poly(HEMA) was found to be 21 ± 2.5 μg/cm^2 (n = 3) (Table 3-2-2, entry 15). A similar value (23.5 μg/cm^2) was previously reported with the same experimental conditions for a nonionic hydrogel from poly(HEMA) and poly (HEMA-*co*-DMA) material, in addition to the higher value (100–250 μg/cm^2) for a methacrylic acid containing ionic hydrogel.[22] These results suggest that lysozyme uptake is determined by hydrogel characteristics such as ionicity, the presence of non-polar or hydrophilic groups, and was not influenced by water content. Thus it was clear that these two amide groups and silicone bearing monomer resulted in a novel silicone hydrogel with transparency and a smaller interaction with the typical tear film constituent lysozyme than poly(HEMA) or ionic materials.

3.2.4 Conclusions

The novel monomers SiDAAA and SiDAAA2 which have two amide groups and an organosiloxane group to improve the compatibility with a hydrophilic monomer to induce transparency and high $P(O_2)$, were synthesized and examined for their radical polymerization reactivity and homopolymer properties. The polymerization reactivity of these monomers, which had a number average degree of polymerization of 60–70, was comparable to the conventional silicone monomer (TRIS) due to the acrylamide group. The miscibility of poly(SiDAAA) in 2-propanol, which was not miscible in poly(TRIS), was improved due to the two amide groups, and a higher (about 60 ºC) T_g and higher (about 60 ºC) 5% weight loss temperature due to strong intermolecular forces were confirmed. In addition, the silicone hydrogel from these silicone-containing monomers showed good transparency; the light transmittance at 400 nm exceeded 88%, in comparison with various hydroxy group bearing hydrophilic monomers such as HEMA and HEAA, which showed an opaque appearance or 26% of light transmittance at 400 nm, or immiscibility when used in conventional TRIS. This could be explained by the contribution of the two hydrophilic amide groups in the novel monomers preventing the coagulation of the hydroxy groups. Furthermore, these novel silicone hydrogels showed an about 10% higher water content than hydrogels from conventional TRIS due to the two amide groups. In addition, a comparable $P(O_2)$ for the hydrogel from SiDAAA and SiDAAA2 as silicone hydrogel contact lenses in the market was observed, and furthermore the lysozyme uptake was found to be less than one-half of the value for a poly(HEMA) nonionic material, which is important for a soft contact lens material. Since TRIS is an important constituent in commercially-available silicone hydrogels, the introduction of two amide groups into a silicone monomer in biomedical materials such as contact lenses results in improved transparency (more than 60 point improvement in light transmittance from 26% to 88%), comparable high oxygen permeability as commercially available silicone hydrogel lenses, and better thermal

stability (more than 60 ºC).

3.2.5 References

1) Tanaka, T., Sato, E., Hirokawa,Y., Hirotsu, S. and Petermans, J. *Phys. Rev. Lett.* **1985**, *55*, 2455.
2) Yoshida, R., Uchida, K., Kaneko, Y., Sakai, K., Kikuchi, A., Sakurai, Y. and Okano, T. *Nature* **1995**, *374,* 240.
3) Juodkazis, S., Mukai, N., Wakaki, R., Yamaguchi, A., Matsuo, S. and Misawa, H. *Nature* **2000**, *408*, 178.
4) Ono, T., Sugimoto, T., Shinkai, S. and Sada K. *Nat. Mater.* **2007**, *6*, 429.
5) Fukushima, T., Asaka, K., Kosaka, A. and Aida, T. *Angew. Chem. Int. Ed.* **2005**, *44*, 2410.
6) Haraguchi, K., Takehisa, T. and Fan, S. *Macromolecules* **2002**, *35*, 10162.
7) Gong, J.P., Katsuyama, Y., Kurokawa, T., Osada, Y. *Adv. Mater.* **2003**, *15*, 1155.
8) Okumura, Y. and Ito, K. *Adv. Mater.* **2001**, *13*, 485.
9) Heller, H. *Adv. Drug. Delivery Rev.* **1993**, *10*, 163.
10) Nicolson, P.C. and Vogt, J. *Biomaterials* **2001**, *22*, 3273.
11) Wang, J. and Li, X. *J. Appl. Polym. Sci.* **2010**, *116*, 2749.
12) Yokota, M., Nakamura, M., Ajiro, H. and Akashi, M. *Chem. Lett.* **2011**, *40*, 858.
13) Erdodi, G. and Kennedy, J.P. *J. Polym. Sci., Part A: Polym. Chem.* **2005**, *43*, 4965.
14) Hosaka, S., Adachi, Y. and Tanzawa, H. *Membrane (Maku)* **1980**, *5*, 245.
15) Karunakaran, R. and Kennedy, J.P. *J. Polym. Sci., Part A: Polym. Chem.* **2007**, *45*, 308.
16) Smith, P.K., Krohn, R.I., Hermanson, G.T., Mallia, A.K., Gartner, F.H., Provenzano, M.D., Fujimoto, E.K., Goeke, N.M., Olson, B.J. and Klenk, D.C. *Anal Biochem.* **1985**, *150*, 76.
17) Soltys-Robitaille, C.E., Ammon Jr., D.M., Valint Jr., P.L. and Grobe III, G.L.,

Biomaterials **2001**, *22*, 3257.

18) Kawakami, Y. and Sugisaka, T. *J. Membr. Sci.* **1990**, *50*, 189.

19) Yokota, M., Shimoyama, N., Fujisawa, K., Nakamura, M., Ajiro, H. and Akashi, M. *Chem. Lett.* **2011**, *40*, 1297.

20) Holden, B.A. and Mertz, G.W. *Invest. Ophthalmol. Vis. Sci.* **1984**, *25*, 1161.

21) Menzies, K.L. and Jones, L. *Optom. Vis. Sci.* **2010**, *87*, 387.

22) Shirogane, T., Saito, N., Uno K. and Kanai, A. *J. Jpn. Contact Lens Soc.* **1999**, *41*, 113.

Chapter 4
Novel Method for Surface Modification of Silicone-Containing Hydrogel Using Addition Reaction

4.1 Introduction

Surface properties of hydrogels are very much important because it contacts with others such as tear layer or blood and so on.[1)] Accompanying the progress in the research on the silicone-containing hydrogels (silicone hydrogels), surface properties of silicone hydrogels have been receiving much attention for decades, because the hydrophobic nature of silicone constituents cause poor surface wettability of silicone hydrogels.[2–9)]

For the improvement of wettability of silicone material or silicone-containing material, many efforts have been reported such as oxidative plasma discharge treatment,[10)] low-temperature inert gas plasma processing,[11)] plasma polymerization,[12,13)] plasma-induced polymerization or graft polymerization,[14)] combination of plasma polymerization and graft reaction.[15)] However, there are still some points to be improved such as durability of wettability.[16)] The combination of introducing reactive groups by plasma polymerization and subsequent reaction between PEG chain and the reactive group, is widely used.[15)] However, as the reactive group exists only on the surface of plasma polymerized film, the density of the PEG chain might be insufficient, resulting in unsatisfactory performance. Albertsson and co-workers reported Ar microwave plasma treatment and subsequent hydrosilylation grafting based on the assumption of –SiH group formation.[17)] However, they used silicone elastomer instead of silicone hydrogel and made the speculation on –SiH formation indirectly from XPS data. Furthermore, they supplied hydrogen after microwave plasma treatment and used a fluorine containing allyl compound leading to no change in contact angle.

My main concern is reducing the contact angle with PEG derivatives and to confirm the mechanism of hydrosilylation without special apparatus such as microwave plasma at 2.45GHz or active gas such as hydrogen. Thus, I designed novel surface modification methods for direct introduction of PEG chain to siloxanyl groups by hydrosilylation.

4.2 Experimental Section

Materials

DMA from KOHJIN (Japan), 2-propanol from Wako Pure Chemical Industries (Japan), both-end capped with methacryloyloxypropyl PDMS (M_n = 1,000, FM7711) from Chisso (Japan), methacryloyloxypropyl end capped PDMS (M_n=1,000, FM0711) from Chisso, 3-glycidoxypropylmethylbis(trimethylsiloxy)silane, methacryloyloxypropyltrimethoxysilane and dimethylchlorosilane, all from Shin-Etsu Chemical (Japan), trichlorosilane, ethyleneglycol monoallylether and methoxytrimethylsilane, all from Tokyo Chemical Industries (Japan), hydrogen hexachloroplatinate (IV) hexahydrate from Wako, 3G from Shin-Nakamura Chemical Co., Ltd (Japan) and triethylamine from Tokyo Chemical were used without further purification. Methacryloylchloride from Tokyo chemical was used after distillation. 2-Hydroxy-2-methyl-1-phenyl-2-propanone (Darocur 1173) from BASF Japan, PEG monoallylether with molecular weight (M_W) of 400 and 1,500, methoxypolyethyleneglycol monoallylether with M_W of 400 and 1,500, both from NOF corporation (Japan), ethyleneglycol dimethylether, butylacetate, both from Tokyo Chemical were used without further purification.

As –SiH group containing monomer, 3-methacryloyloxypropyltris (dimethylsiloxy) silane (TRIS-3H) was prepared according to the previously reported method.[18] 3-(2-Methacryloyloxy-ethoxy)propyltris(trimethyl-siloxy)silane (SiOEMA), which was used as comonomer of TRIS-3H, was prepared referring to the previously

reported method using trimethylmethoxysilane instead of chlorodimethylsilane.[19] 3-(2-Hydroxy-3-methacryloyloxypropyloxy)propylmethylbis(trimethylsiloxy)silane (SiMAA2), which was used for the preparation of the silicone hydrogel material for plasma treatment, was prepared according to the previously reported method.[20] Used monomers are summarized in Figure 4-1.

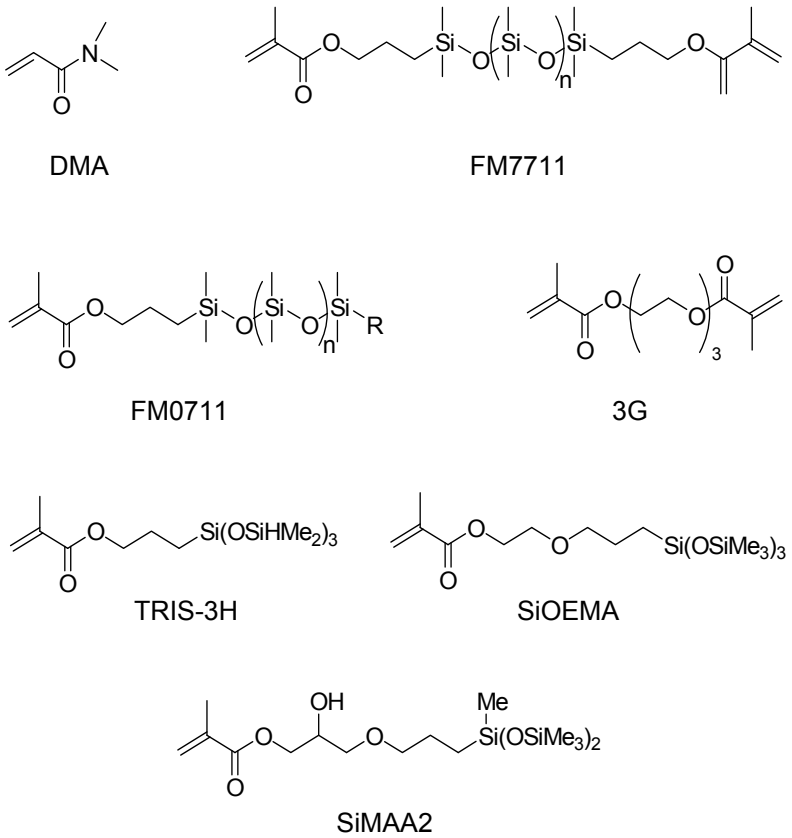

Figure 4-1. Structure of used monomers.

Preparation of Silicone Hydrogel

The combination of TRIS-3H and SiOEMA, or that of SiMAA2 and FM0711 was used for –SiH containing hydrogel, or plasma treated hydrogel, respectively. Silicone-containing monomer, DMA, crosslinker (3G or FM7711), polymerization solvent (diethyleneglycol dimethylether) and photopolymerization initiator (Darocur 1173) were mixed according to the specific balance in the test tube followed by the degassing under nitrogen gas atmosphere. The resultant monomer mix was inserted into

the spaces made by plastic molds in the glove box under nitrogen atmosphere, and the photopolymerization was conducted using the lamp having peak wave length at 350 nm with the light intensity of 1 mW/cm^2 and 30 minutes.

After polymerization, plastic molds were immersed in IPA aqueous solution heated to 60ºC for specific time, and separated from each other. The immersion of the gel into water was followed by repeated water replacement and hydration of the gel at the sterilization condition (120 ºC, 30 min).

Hydrosilylation Reaction between Silicone Hydrogel having –SiH group and Allylether having PEG Compounds

20 g of 0.5 mol/L diethyleneglycol dimethylether solution of allylether having PEG compounds, 1.6 mg of hydrogen hexachloroplatinate (IV) hexahydrate was added into sample bottle having 25 mL volume, followed by the addition of the hydrogel having –SiH group which was vacuum dried beforehand and immersed in reaction solvent. The temperature was kept at 60ºC for specific time to carry out the hydrosilylation reaction. After the reaction, hydrogel was transferred into water, followed by the repeated water replacement, immersion in boric acid buffer solution (pH is 7.1 to 7.3), hydration by the sterilization condition (120 ºC, 30 min).

Plasma treatment of the Silicone Hydrogel having no –SiH group

Silicone hydrogel having no –SiH group was vacuum dried and was plasma treated using Yamato Scientific (Japan) PR-41 plasma reactor and argon gas with specific gas flow rate, electric power and specific time.

Evaluation of Physical Properties

Tensile strength

ORIENTEC (Japan) RTM100 TENSILON tester was used for the

measurement of tensile strength, elongation at break, and modulus in the environment of 23 ºC and 50% humidity with 100 mm/min elongation speed. Sample shape is modified dog bone type having 2 mm of minimum width and 15 mm of length.

Water content

After conditioning at 20 ºC circumstance, hydrogel weight was measured as wet weight followed by the measurement of hydrogel dry weight after vacuum drying at 40ºC, 16 hr. Water content was calculated according to the following formula.

Water content (%) = 100 × (wet weight – dry weight)/wet weight

Dynamic contact angle

Rhesca Corporation (Japan) WET-600 apparatus was used for the measurement of dynamic contact angle in the environment of 25 ºC and 50% humidity. Liquid for immersion was boric acid buffer solution with 5 mm of sample width and the moving speed was 0.1 mm/min for 7 mm length.

FTIR-ATR Measurement

Thermo fisher Scientific (USA) AVATAR360 apparatus was used for the measurement of ATR spectrum of vacuum dried sample.

Accelerated shelf life study

This study was carried out keeping the samples at 120 ºC for 30 hrs.

4.3 Results and Discussion

Introduction of PEG chain to overall hydrogel

At first, the preparation of crosslinked copolymer from –SiH group bearing monomer and hydrophilic monomer followed by hydrosilylation were conducted. The

scheme of this process is shown in Scheme 4-1. This was expected to allow the uniform introduction of PEG chain into all over the hydrogel. For this approach, –SiH group

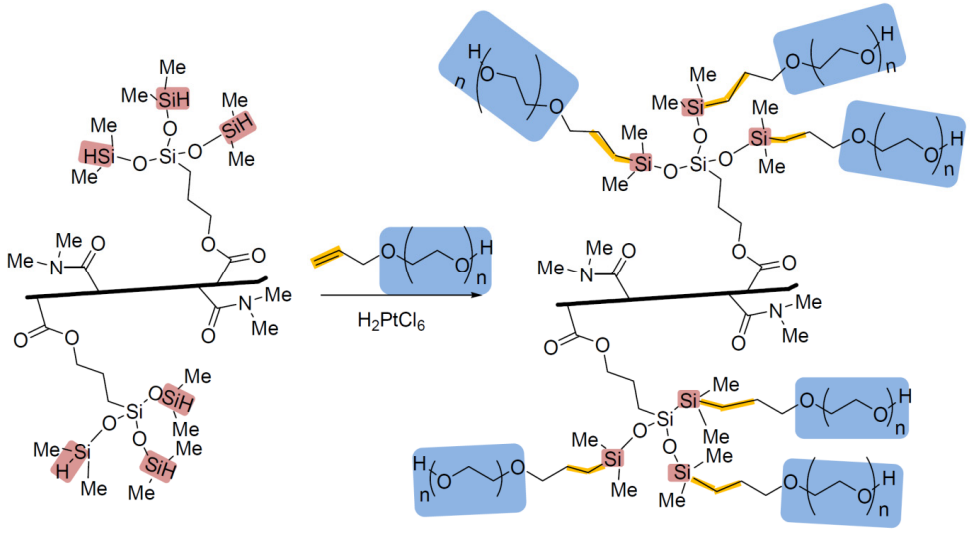

Scheme 4-1. Introduction of PEG chain to overall hydrogel.

bearing silicone hydrogel was prepared and hydrosilylation reaction between resultant gel and PEG monoallylether having two M_ws, was carried out. As shown in Table 4.1, it was found that the contact angle could be effectively reduced and simultaneously water content increased. This increase of water content suggests the progress of hydrosilylation reaction between –SiH group and PEG monoallylether as it had survived the 120ºC, 30 min pretreatment in water before measurement.

Table 4-1. Characteristics of hydrogels from overall hydrosilylation of silicone gel [a]

Entry	PEG M_n	Contact angle (º) [b]	Water content[c] (%)
1	none	91	26
2	400	79	42
3	1,500	66	43

[a] Gel composition :TRIS-3H/SiOEMA/DMA/3G=10/55/35/1 (weight).
[b] Hydrogel sample was pretreated with 120 ºC, 30 min in water before water content measurement.
[c] Water content was calculated from following formula; $(W_w - W_d)/W_w \times 100$, where W_w and W_d show the wet weight and dry weight of hydrogel, respectively.

Introduction of PEG chain to near the surface

The other approach is to restrict the place of hydrosilylation reaction to only near the surface in hydrogel cross section. My second concept could be achieved by using the dry process with conventional high frequency (13.56 MHz) plasma treatment, in which diffusion of gas plasma into inside of the hydrogel is expected to be low because of the short processing time. Furthermore, Ar gas was selected for its

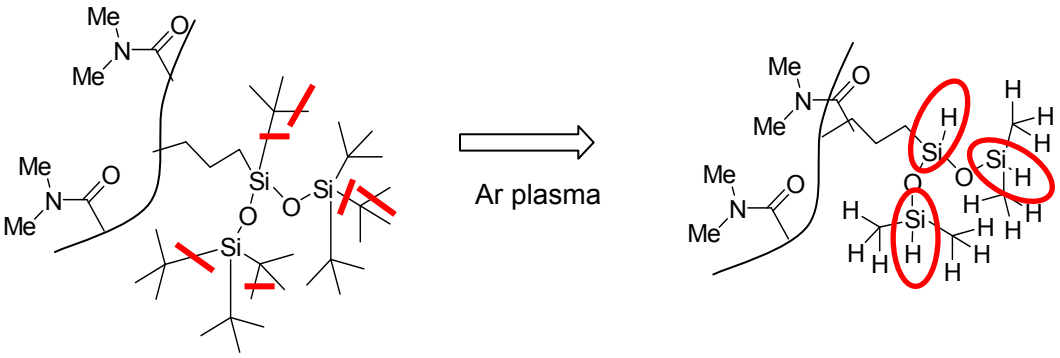

Scheme 4-2. Expected reaction scheme of Ar gas plasma treatment.

non-oxidative action, scission of chemical bond and recombination which could lead to the formation of –SiH group on the surface. Thus the combination of plasma treatment and hydrosilylation reaction is examined as the second method as shown in Scheme 4-2.

To confirm the effectiveness of this approach, silicone hydrogel bearing no –SiH group was prepared from 3-(2-hydroxy-3-methacryloyloxy)propylmethylbis (trimethylsiloxy)silane (SiMAA2), methacryloyloxypropyl single end capped PDMS (M_n = 1,000, FM0711), DMA and methacryloyloxypropyl both end capped PDMS (FM7711). After dried and Ar gas plasma treated, hydrosilylation reaction was carried out with and without hydrogen hexachloroplatinate (IV) hexahydrate as catalyst. The contact angles at each step of this process are shown in Table 4-2.

Table 4-2. Contact angle of silicone hydrogel[a] at each step of high frequency Ar gas plasma treatment and hydrosilylation process

None	After plasma	after immersion in PEG [b] solution	
		without H_2PtCl_6	with H_2PtCl_6
87 º	78 º	75 º	57 º

[a] Silicone hydrogel composition : SiMAA2/FM0711/DMA/FM7711 = 31/31/38/2.6.
[b] PEG M_w = 400.

It shows that Ar gas plasma treatment alone is insufficient, furthermore, the addition of hydrogen hexachloroplatinate (IV) hexahydrate has a great influence on the obtained contact angle. This suggests the formation of functional group such as –SiH group in silicone component which can undergo the hydrosilylation reaction with PEG monoallylether. This –SiH group formation was also suggested by FTIR-ATR measurements shown in Figure 4-1. With regard to the plasma treatment and hydrosilylation, various change of absorption band was observed. The decrease of intensity at 1,260 cm^{-1}($Si–CH_3$ deformation in $SiMe_n$) and 842 cm^{-1} ($Si–CH_3$ deformation in $SiMe_3$) were recognized. The intensity of the peak around 1,040 cm^{-1} (Si–O stretching in Si–O–Si group) also decreased, while the peak at 798 cm^{-1} increased which was assigned to $Si–CH_3$ deformation in $SiMe_2$ group. Also, the intensity change of the band at around 2,960 cm^{-1} (C–H stretching in CH_3) suggests the scission of C–H bond. Furthermore, there exists a band at 900 cm^{-1} which is considered to correspond to –SiH bond (Si–H deformation).[21] So this is one of the proof of the formation of –SiH bond by high frequency plasma treatment and thus the expected scheme in Scheme 4-2 could be confirmed. This could be also supported by the results from XPS measurements which described the decomposition of some hydrocarbon and siloxane bonds under plasma bombardment.[11] From FTIR-ATR spectra, the formation of PEG chain layer was confirmed by the existence of the band at around 1,400 cm^{-1} (O–H deformation in alcohol), around 1,140 cm^{-1}(C–O–C stretching in ether), and 1,000 cm^{-1} (C–O stretching in alcohol). Keeping the same hydrosilylation condition

as that in Table 4-2, obtained relationship between the plasma treatment conditions and hydrogel properties were shown in Figure 4-2. It is noteworthy to point out that nevertheless the contact angle showed greatly reduced value, water content showed almost constant value. This suggests that introduction of PEG chain is restricted to near the hydrogel surface as expected in my process design concept.

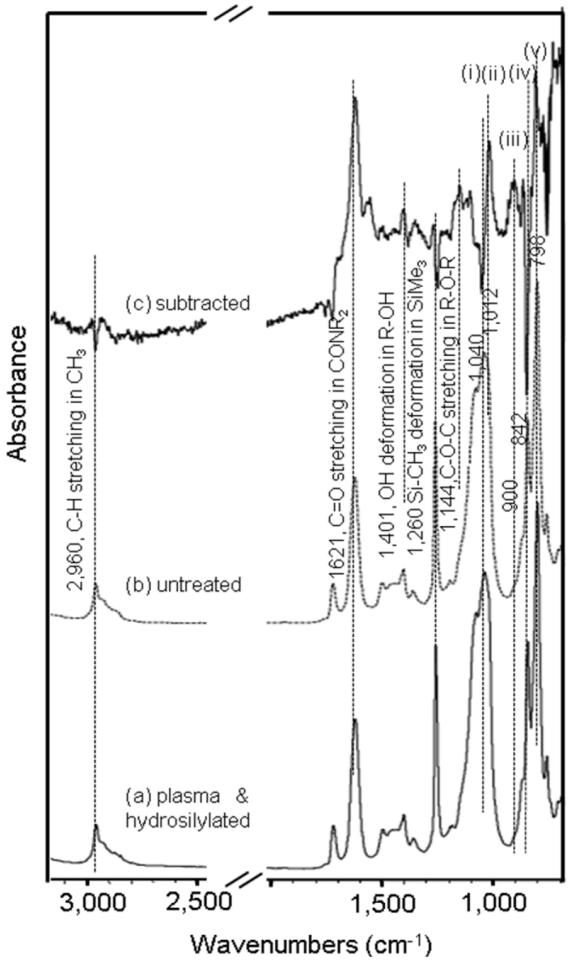

Figure 4-1. FTIR-ATR spectra of (a) high frequency plasma treated and hydrosilylated hydrogel, (b) untreated hydrogel and (c) subtracted spectrum from (high frequency plasma treated and hydrosilylated silicone hydrogel – untreated one). Composition is same as that in Table 2. (i), (ii), (iii), (iv), and (v) show Si–O stretching in Si–O–Si (1040 cm^{-1}), C–O stretching in R–OH (1012 cm^{-1}), Si–H deformation in $SiHCH_3$ (900 cm^{-1}), $SiCH_3$ deformation in $SiMe_3$ (842 cm^{-1}), and $SiCH_3$ deformation in $SiMe_2$ (798 cm^{-1}) respectively.

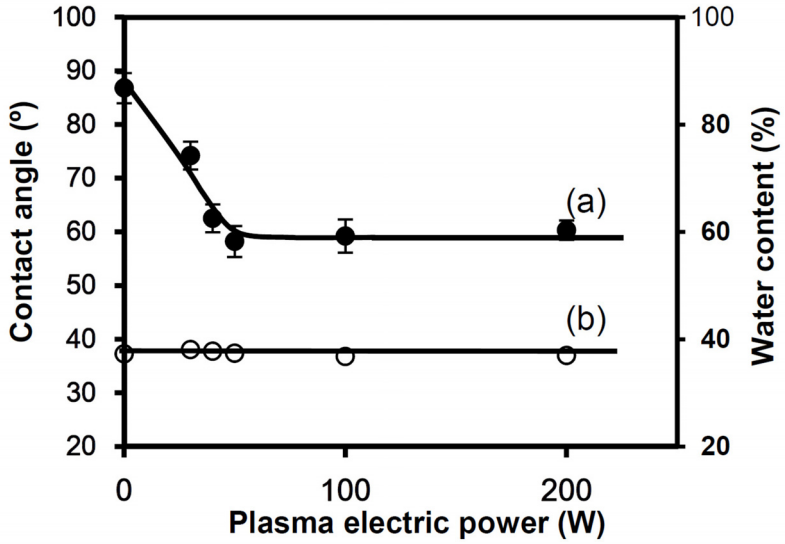

Figure 4-2. Relationship among plasma electrical power, contact angle, and water content of high frequency plasma treated and hydrosilylated silicone hydrogel. (a) and (b) show contact angle and water content, respectively.

4.4 Conclusions

Novel surface modification methods of shaped articles from silicone-containing hydrogel were designed and carried out. The design concept of this method was to introduce –SiH group into silicone component and conduct hydrosilylation reaction between this –SiH group and allyl group bearing PEG to improve contact angle of silicone hydrogel shaped article. Both of copolymerization of –SiH group bearing monomer and high frequency Ar gas plasma treatment were effective for the hydrosilylation and contact angle reduction. From the effect of using hydrogen hexachloroplatinate (IV) hexahydrate to hydrosilylation reaction and FTIR-ATR spectra, the formation of –SiH group by Ar gas plasma was suggested. This finding may develop novel application of plasma process combined with other chemical reaction.

4.5 References

1) Lee, J.H., Kopecek, J. and Andrade, J.D. *J. Biomed. Mater. Res.* **1989**, *23*, 351.

2) Bowers, R.W.J. and Tighe, B.J. *Biomaterials* **1987**, *8*, 83.

3) Maldonado, C., Morgan, P.B., Efron, N. and Canry, J.C. *Optom. Vis. Sci.* **2004,** 81, 455.

4) Cheng, L. Susan, J. and Radke, C.J. *Current Eye Res.* **2004**, *28*, 93.

5) Kheirandish, S. and Jabbari, E. *Colloid. Polym. Sci.* **2006**, *284*, 1411.

6) Lorentz, H. and Jones, L. *Optom. Vis. Sci.* **2007**, *84*, 286.

7) Maldonado, C. and Morgan, P.B. *J. Biomed. Mater*. Res. **2007**, *83A*: 496.

8) González-Méijome, J. M., López-Alemany, A., Almeida, J.B. and Parafita, M.A. *J. Biomed. Mater. Res. Part B: Appl. Biomater.* **2009**, *88B*, 75.

9) Menzies, K.L. and Jones, J. *Optom. Vis. Sci.* **2010**, *87*, 387.

10) Fakes, D.W., Newton, J.M., Watts, J.F. and Edgell, M.J. *Surf. Interface Anal.* **1987**, *10*, 416.

11) Yin, S., Wang, Y., Ren, L., Zhao, L., Kuang, T., Chen, H. and Qu, J. *Appl. Surf. S*ci. **2008**, *255*, 483-485.

12) Ho, C.P. and Yasuda, H. *Polym. Mater. Sci. Eng.* **1987**, *56*, 705-709.

13) Yasuda, H. and Matsuzawa, T. *Plasma Process Polymer* **2005**, *2*, 507-512.

14) Yao, K., Huang, X-D., Huang, X-J. and Xu, Z-K. *J. Biomed. Mater. Res. Part A* **2006**, *78A*, 684.

15) Kingshott, P., Thissen, H. and Griesser, H. *Biomaterials* **2002**, *23*, 2043.

16) Thissen, H. Gengenbach, T., du Toit, R., Sweeney, D.F., Kingshott, P., Griesser, H.J. and Meagher, L. *Biomaterials* **2010**, *31*, 5510.

17) Olander, B., Wirsén, A. and Albertsson, A.-C. *Biomacromolecules* **2002**, *3*, 505.

18) Zenbayashi, M., Kurita, O. and Sato, N. Jpn Patent Publication No. 60-166691, **1985**.

19) Nakamura, M., Morikawa, Y. and Yokota, M. Jpn Patent 4,524,838B, **2010**.

20) Nakamura, M., Shimoyama, N. and Yokota, M. Jpn Patent 4,123,648B, **2008**.

21) For example, FT-IR spectrum of tris(dimethylsilyloxy)methyl silane: “The Aldrich Library of FT-IR Spectra”, 2nd Ed. Sigma-Aldrich Co. LLC., Milwaukee, **1997**, Vol.3, p4386C.

Concluding Remarks

This thesis deals with the creation of the material, which has high gas permeability coefficient and high transparency for the use as mainly medical devices, especially in the anterior eye circumstances. As the typical medical device material in this field, RGP material and silicone-containing hydrogel material have been attracting much attention, because these material have still various challenging issues to attain the ideal target. Thus, I focused on the design of internal structure or novel compound, the preparation of rigid copolymer or silicone-containing hydrogel, resultant correlation between the physical properties and systematically changed composition as well as components, and the verification of the material design concept.

In Chapter I, I tried to use microheterophase structure as RGP material to obtain good breakage strength. This is because that in homogeneous structure, the fragility issue has arisen from high content of silicone-containing monomer with low intermolecular force. In order to understand the relationship among the physical properties such as T_g, light transmittance, $P(O_2)$ (or Dk), Vickers hardness, and polymer composition and components, copolymers from both ends methacryloyl group capped PDMS macromer, acrylic monomers such as MMA and TFEMA, and crosslinker, were fabricated with systematically changed composition and components.

DSC measurements of the T_g showed that PMMA or PTFEMA and PDMS were insoluble in each other. The transparency of MMA/PDMS crosslinked copolymer depended on the PDMS M_n; a higher M_n (partly 3,300, 4,700, and 7,800 g/mol) caused an opaque appearance**,** but copolymerizing with TFEMA instead of MMA induced a drastic improvement in transparency. This could be the result of reduced light scattering due to a reduced difference of refractive index between PDMS and poly(acrylic monomer), and the copolymerization of *t*-BuMA supported this hypothesis. In the low PDMS M_n range (1,700 and 3,300 g/mol), the $P(O_2)$ was proportional to $[M_n]^{2/3}$, and

domain size ratio in this range was found to be 1.6. This is the first proof of the relationship between domain size and the PDMS [M_n] in a crosslinked copolymer.

Copolymerization with TFEMA instead of MMA gave a surprisingly large increase in the $P(O_2)$. A calculation of the relationship among the morphology models, PDMS volume fraction and $P(O_2)$, implied that a morphology change to the parallel model occurred at a low PDMS volume fraction, and was caused by some properties such as the solubility parameter and so on. This was supported by the additional $P(O_2)$ measurements on the copolymer using *t*-BuMA and HFIPMA.

Thus, the copolymerization of a fluorine-containing acrylic monomer was found to lead to a transparency improvement, a $P(O_2)$ increase, and therefore, fluorine-containing monomers could be expected to develop further applications in various fields.

In the second Section in Chapter 1, we conducted ^{13}C solid-state CP-MAS NMR measurements to investigate the molecular-level relationship between the physical properties and systematically changed composition and components of copolymer. T_1^H and $T_{1\rho}^H$ data suggested that a larger PDMS M_n value resulted in a higher molecular mobility of $-OSi(CH_3)_2-$, and the high mobility could be correlated to a higher gas permeability. In addition, the copolymers with PDMS M_n of 1,700 and 4,700 were found to have a homogeneously dispersed structure with a diameter of approximately 3 nm and tens of nm, respectively. This result could be correlated to the appearance of the copolymer. T_1^H, $T_{1\rho}^H$ and $T_{1\rho}^C$ suggested the difference in the morphology of MMA copolymers and TFEMA copolymers. Furthermore, larger $T_{1\rho}^C$ value in TFEMA copolymer than that in MMA copolymer implied the amplified molecular motion was related to the mechanism of increased oxygen permeability. Herein, the efficiency of ^{13}C solid state CP-MAS NMR for the study on the relationship between microstructure, molecular mobility and bulk properties, was revealed.

In the third Section in Chapter 1, TEM observation was carried out and the

microstructure of these copolymers depended on the PDMS content, the PDMS M_n, and the type of methacrylate comonomer. First, at low PDMS content, all of the specimens showed an "isolated domain" morphology with "islands" or isolated domains of methacrylate polymer dispersed throughout a "sea" like surrounding area. Moreover, since many small PDMS domains were also found dispersed in these islands, this morphology had a multilevel structure. At higher PDMS contents, a different morphology was observed, which consisted of a continuous phase of methacrylate polymer and more homogeneously dispersed PDMS domains. Second, the size and area of these "islands" as well as their homogeneity in the dispersion of PDMS domains depended on the PDMS M_n. A larger PDMS M_n caused a larger "island" size and greater inhomogeneity in the dispersion of PDMS domains, and also caused a higher PDMS content necessary for the formation of a homogeneous structure. Third, in addition to the PDMS M_n, the employment of TFEMA instead of MMA affected the morphology, such as a different island surrounding area phase composition or structure, and a more homogeneous structure suggestive of better solubility or compatibility between the TFEMA or PTFEMA and the other components.

In addition, observations at 100,000-fold magnification revealed that the specimens had a "fundamental" common morphology, and it was a co-continuous one. From measurements of this domain size, the PDMS M_n was concluded to influence this PDMS "fundamental" domain size. Thus, studies using the observation of two microstructures could be a novel tool for evaluating the relationship between morphology and physical properties. Based on those findings, many bulk properties could be predicted by morphology, such as T_g, transparency, and oxygen permeability.

In Chapter 2, to examine the fragility issue of RGP materials, I have developed new methods of evaluating the physical properties of RGP materials in order to be able to predict clinical performance. Tests of ball impact breakage strength and flexural breakage strength were made, in addition to the study of the physical microstructure of

various RGP materials by TEM.

The breakage resistance of various RGP materials was evaluated and found not to correlate with the *Dk* value of the material including my material which was developed with the design concept described in Chapter 1, and had microheterophase structure. By combining the impact and flexural strength test results, I predicted properly the incidence of lens breakages found in clinical studies. Furthermore, from observation of the microstructure of RGP materials, I understood why breakage resistance did not depend on the *Dk* of the material. In other words, breakage strength depends on the type of microstructure of the material. Thus I believe that the efficacy of my material design concept was verified. In addition, a relationship between the physical microstructure of RGP materials and their deposit resistance is suggested.

In the first Section in Chapter 3, a novel silicone monomer bearing two amide groups (SiDAAA) was designed and synthesized for silicone hydrogel use. The design concept of this monomer was to improve its compatibility with various hydrophilic monomers, and thus two amide groups were introduced into the molecular skeleton. This monomer showed good miscibility with hydrophilic monomers bearing hydroxy group, such as HEMA and HEAA. Furthermore, the hydrogel from SiDAAA and HEMA had good transparency. These results contrasted with those from hydrogel made with TRIS, conventional silicone monomer, and verified my monomer design concept.

In the second Section in Chapter 3, the novel silicone-containing homopolymer and novel silicone hydrogels were prepared from SiDAAA and novel SiDAAA2 monomer which has two amide groups and an organosiloxane group with different ratio of (amide group)/(trimethylsiloxy group) from SiDAAA. The aim is the improvements of the compatibility with wide range of hydrophilic monomers for high transparency, to give the high radical polymerization reactivity, and to provide the resultant silicone-containing hydrogel with controllable swelling ratio, high oxygen permeability, high thermal stability and low lysozyme uptake.

The polymerization reactivity of these monomers was comparable to the conventional silicone monomer (TRIS) due to the acrylamide group. The miscibility of poly(SiDAAA) in 2-propanol, which was not miscible with poly(TRIS), was improved due to the two amide groups, and a higher (about 60 ºC) T_g and higher (about 60 ºC) 5% weight loss temperature due to strong intermolecular forces were confirmed.

In addition, the silicone hydrogel from these silicone-containing monomers showed good transparency with various hydroxy group bearing hydrophilic monomers such as HEMA and HEAA, and furthermore, about a 10% higher water content than hydrogels from conventional TRIS due to the two amide groups. In addition, these hydrogel showed a reduced lysozyme uptake which was found to be less than one-half of the value for a poly(HEMA) nonionic material, which is an important material for soft contact lens. Thus, I believe that the material design concept was verified.

In Chapter 4, novel surface modification methods of shaped articles from silicone-containing hydrogel were designed and performed. The design concept of these methods was to introduce –SiH group into silicone component and conduct hydrosilylation reaction between this –SiH group and allyl group bearing PEG to improve contact angle of silicone hydrogel shaped article. Both of copolymerization of –SiH group-bearing monomer and high frequency Ar gas plasma treatment were effective for the hydrosilylation and contact angle reduction. From the effect of using hydrogen hexachloroplatinate (IV) hexahydrate to hydrosilylation reaction and FTIR-ATR spectra, the formation of –SiH group by Ar gas plasma was suggested. This finding may develop novel application of plasma process combined with other chemical reaction.

List of Publication

Chapter 1

1) **Mitsuru Yokota**, Hiroharu Ajiro and Mitsuru Akashi, "Effect of Copolymerizing Fluorine-Bearing Monomers on the Relationship among Internal Structure, Gas Permeability, and Transparency in Copolymer Networks Composed of Methacrylates and Siloxane Macromers". *J. Appl. Polym. Sci.* in press (DOI: 10.1002/app.37813).

2) **Mitsuru Yokota**, Yuko Miwa, Hiroharu Ajiro and Mitsuru Akashi, "The systematic study of the microstructure of crosslinked copolymers from siloxane macromonomers and methacrylates by changes in composition and components". *Polymer J.* **2012**, *44*, 301-305[Featured Article].

3) **Mitsuru Yokota**, Hiroharu Ajiro and Mitsuru Akashi, "Transmission Electron Microscopic Observations of the Multilevel Microstructure of Crosslinked Copolymers with Methacrylates and Siloxane Macromers by a Radically Polymerizable Tuning Approach". *J. Appl. Polym. Sci.* in press (DOI: 10.1002/app.37764).

Chapter 2

4) **Mitsuru Yokota**, Tsutomu Goshima, Shin Itoh, "The Effect of Polymer Structure on Durabiliy of high *Dk* Rigid Gas-Permeable Materials". *J. Brit. Contact Lens Assoc.* **1992**, *15*, 125-129.

Chapter 3

5) **Mitsuru Yokota**, Masataka Nakamura, Hiroharu Ajiro and Mitsuru Akashi, "Synthesis of a Novel Silicone Monomer Bearing Amide Groups to Improve Compatibility with Hydrophilic Vinyl Monomers", *Chem. Lett.* **2011**, *40*, 858-859

6) **Mitsuru Yokota**, Hiroharu Ajiro and Mitsuru Akashi, "The Role of Amide Groups in Vinyl Monomers Containing Siloxane Groups for Highly Oxygen Permeable

Hydrogels", *Bull. Chem. Soc. Jpn.* **2012**, *85*, 584-591[Selected Paper].

Chapter 4

7) **Mitsuru Yokota**, Naoki Shimoyama, Kazuhiko Fujisawa, Masataka Nakamura, Hiroharu Ajiro and Mitsuru Akashi, "Novel Method for Surface Modification of Silicone-containing Hydrogel Using Addition Reaction", *Chem. Lett.* **2011**, *40*, 1297-1299.

Other Publication

Hideki Kenjyo, **Mitsuru Yokota**, Minoru Ueda and Jyun Torikai, "Coulometric Method of Measuring Dk of Gas-Permeable Hard Contact Lenses Using the Zirconia Oxygen Detector", *J. Jpn. Contact Lens Soc.* **1989,** *31*, 319-324.

Acknowledgements

This study was performed at Advanced Materials Research Laboratories, Toray Industries, Inc, from 1980 to 2006, and also at the Department of Applied Chemistry, Graduate School of Engineering, Osaka University from 2010 to 2012. This work was partially supported by Showahokokai, and Shorai Foundation for Science and Technology.

I would like to express my sincere gratitude to Professor Mitsuru Akashi of Osaka University for his continuous guidance and invaluable encouragement through the course of the study at Osaka University. Especially, I would like to express appreciation and thank Specially Designated Associate Professor Hiroharu Ajiro of Osaka University for his continuous encouragement, helpful suggestions, and invaluable discussions during the study at Osaka Universiy.

I would like to express gratefully acknowledgements to Dr. Hiroshi Kiuchi, Dr. Zenji Izumi, Mr. Syunro Kataoka, Mr. Keisuke Ohshima, Dr. Masaru Kurihara, and Dr. Takashi Taniguchi for their continuous guidance, encouragement and kind discussions through the course of research work at Advanced Materials Research Laboratories, Toray Industries Inc.,

I would like to express my appreciation to Dr. Toshihide Inoue, Dr. Tetsuya Gotoh, Dr. Hiroyuki Sugaya, and Mr. Masataka Nakamura of Toray Industries Inc., for their kind permissions to submit the articles and this thesis. I would like to express my grateful acknowledgments to Dr. Yuko Miwa of Toray Research Center for the arrangement and measurement with solid state CP-MAS NMR, and invaluable discussions. Also, I would like to express my appreciation to Mr. Masato Shimagami, Mr. Hiroki Suzuta and Mr. Kazumi Saigo of Toray Industries Inc., for the measurement of Vickers hardness and the light transmittance.

I would like to express my grateful acknowledgments to Mr. Masataka

Nakamura, Mr. Tsutomu Goshima. Mr. Naoki Shimoyama, Dr. Nobuo Saitoh, Mr. Kazuhiko Fujisawa, Ms. Yukie Morikawa, Ms. Kaoru Yanagida, Dr. Takehiro Kohara, Mr. Shin Itoh, Mr. Yoshihiro Kawabe, Mr. Akira Kohama and Mr. Teiji Kawano for their kind cooperation at Advanced Materials Research Laboratories, Toray Industries Inc.,

I would like to express my heartful acknowledgments to Dr. Michihiko Tanaka, Mr. Masumi Fujiura, Mr. Hideki Kenjyo, Mr. Kazushige Komaki, Mr. Fujio Gotoh, Mr. Takashi Nomura, Mr. Kiyokazu Ikenouchi, Mr. Hirotake Ohtsuji, and Mr. Shin-ichi Yamamoto for their kind encouragement and cooperation through the course of development work at Toray Industries Inc.,

I would like to express my appreciation and thanks to Associate Professor Toshiyuki, Kida, Specially Designated Associate Professor Takami Akagi, Assistant Professor Michiya Matsusaki and all members of Akashi laboratory of Osaka University, for their valuable discussions, hearty support, and kind help. I would like to express acknowledgment to Professor Hirotaro Mori and Mr. Toshiaki Hasegawa of Research Center for Ultra-High Voltage Electron Microscopy, Osaka University for their arrangement and measurement with TEM.

Finally, I would like to express sincere appreciation to my family for their continuous encouragement and support.

September 2012

Mitsuru Yokota